Seasonal Energy Storage

An optimized district heating system for solar thermal operation in combination with seasonal heat storage

G.L.A. Wolbert

Sustainable Energy Technology
Student number 4233913
Supervisor TU Delft: C.A. Infante Ferreira

ISBN 000-00-0000-000-0

TU Delft

Seasonal Energy Storage

An optimized district heating system for solar thermal operation in combination with seasonal heat storage

by

G.L.A. Wolbert

to obtain the degree of Master of Science
at the Delft University of Technology,
to be defended publicly on Friday August 28, 2020 at 10:00.

Student number:	4233913	
Project duration:	March 1, 2019 – August 28, 2020	
Thesis committee:	Dr. Ir. C.A. Infante Ferreira,	TU Delft, supervisor
	Dr. O. Moultos,	TU Delft
	Dr. Ir. R. Pecnic,	TU Delft

This thesis is confidential and cannot be made public until August 28, 2025.

An electronic version of this thesis is available at `http://repository.tudelft.nl/`.

TU Delft

HoSto
HOT COLD STORAGE

Acknowledgements

I wish to express my sincere gratitude to Gerda and Rene Geerts for providing me an opportunity to conduct my thesis at HoCoSto and allowing me to work on their exciting new energy storage solution.

Also, I would like to thank prof. Carlos Infante Ferreira from the technical university of Delft for his effort and assistance as a daily supervisor.

Last but not least, special thanks go to my friends Bram ter Meulen and Patriek Brouwer for keeping me motivated throughout the project.

G.L.A. Wolbert
Delft, August 2020

Abstract

This study aims to find ways to optimize the district heating network side of a high temperature community heating system powered by decentralised solar collectors and seasonal thermal energy storage (STES). Since the development of such systems is rapidly emerging in the Netherlands, the importance of gaining knowledge on the optimization of the distribution side has abruptly become significant.

After a review of literature, six network configurations are conceived which have the potential to improve system performance compared to a base scenario. The base scenario consists of a 2-line network with a fixed supply temperature where the decentralised solar collectors feed in over the heating network. The six alternative network configurations all aim to improve system performance by lowering the temperature of consumed and/or produced heat. Lowering the temperature in the heating network reduces heat losses and decreases heat pump utilization. Lowering the operational temperature of the solar collectors increases their efficiency. The strategies explored by the different configurations include variable supply temperatures, a 4-line network (where the solar collectors do not feed into the heating network), and ways to mitigate temperature constraints imposed by domestic hot water production regulations.

As a case study, the neighborhood 'Karwijhof' in the village Nagele is used. In this neighborhood, 24 consumers will make the switch to a solar+storage district heating system with a revolutionary STES design proprietary to the company HoCoSto. They will be frontrunners in the city Nagele, which is to become one of the greenest cities in the Netherlands as part of a government-funded pilot program.

In order to assess their performance, all six configurations and the base scenario are modelled in a Matlab/Simulink environment. The system performance is measured in terms of levelised cost of heat (LCOH) and seasonal coefficient of performance (SCOP). Additionally, they are compared to a scenario where the dwellings are outfitted with individual high temperature air to water heat pumps instead.

Apart from directly trying to find ways to optimize the district heating side of the system, a key objective of this study is also to construct an elaborate model of a STES+distributed solar district heating system. The study shows that alterations to the network side can lead to lower overall costs of a district heating network with decentralised solar collectors and seasonal energy storage. Two measures were found to be effective. Making the supply temperature variable (and dependent on the ambient temperature) reduces pipeline thermal losses and reduces heat pump utilization. The transition from a 2-line network to a 4-line network where the solar collectors are connected to the buffer using a separate network was found to significantly increase solar collector efficiency, especially in winter. The combination of these two measures reduces the LCOH by 4.5 %. In a situation where an additional constraint is applied, which is that the SCOP should be at least 5, the combination of these two measures still achieves the lowest LCOH. An important observation is that slightly oversizing the buffer volume and solar area significantly increases the SCOP while having a very small impact on LCOH.

When comparing the improved community solar heating system with a scenario where every house is heated with an individual heat pump instead, it is found that the community solar system achieve a 15.7 % lower LCOH while having a SCOP of 4.4 compared to just 2.75 for the heat pump scenario. In the development of future community solar plus storage heating systems, it is recommended that the solar collectors should not feed in to the heating network, but are to be con-

nected to the STES through a dedicated network instead. Additionally, having a variable supply temperature in the network is adviced. When ecological aspects are considered important, slightly oversizing the buffer and amount of solar collectors are key in increasing the SCOP.

Contents

Nomenclature

The next list describes several abbreviations and symbols that will be later used within the body of the document

Abbreviations

AOI	Angle of incidence
CAPEX	Capital Expenditure
COP	Coefficient of Performance
DHI	Diffuse horizontal irradiance
DHS	District Heating System(s)
DHW	Domestic Hot Water
DIN	Deutsches Institut für Normung, a German normalisation institute
DN	Nominal Diameter
DNI	Direct normal irradiance
GHI	Global horizontal irradiance
HHV	Higher heating value
KNMI	Koninklijk Nederlands Meteorologisch Instituut, or Royal Netherlands Meteorological Institute
LCOH	Levelized Cost Of Heat
NEN	Nederlandse Norm, a Dutch normalisation institute
OEM	Original Equipment Manufacturer
OPEX	Operational Expenditure
PE	Polyethylene
PUR	Polyurethane
SCOP	Seasonal Coefficient Of Performance
STES	Seasonal Thermal Energy Storage
UTC	Coordinated Universal Time
WACC	Weighed Average Cost of Capital
XPS	Extruded polystyrene

Subscripts

0	Refers to steady state zero loss efficiency
1	Bottom of buffer
$2.5m/s$	Refers to fluid velocity of 2.5 $\frac{m}{s}$
50	Refers to 75/65/20 operation of radiators
a	Asymetrical
amb	Ambient
$auxiliary$	Auxiliary
B	Beam radiation
$bathroom$	Bathroom
$boilerB$	Refers to DHW concept B
$boilerC$	Refers to DHW concept C
bot	Bottom of buffer
$buffer$	Buffer
$Carnot$	Carnot, refers to operation at Carnot COP
D	Diffuse radiation
$demand$	Demand
DHI	Diffuse horizontal irradiance
DHW	Domestic hot water
$elec$	Electric
$evaporator$	Evaporator
$flow$	Charge and discharge flow through buffer
g	Soil
HE	Heat Exchanger
$heating$	Heating
$house$	House
HP	Heat pump
i	Insulation of pipe
in	Inlet
ini	Initial

$inner$	Inner, refers to diameter
$jacket$	Jacket of a twin pipe
$kitchen$	Kitchen
L	Longitudinal
m	Mean
$mixing$	Mixing flow, from cold side of network to supply
$network$	Network
$nodes$	Nodes of buffer
out	Out
$outer$	Outer, refers to diameter
PE	Polyethylene
$peak$	Peak
$pumpedannual$	Annually pumped
PUR	Polyurethane
$return$	Return
s	Symmetrical
$shell$	Shell of building
$side$	Side of buffer
$solar$	Solar
$solarloop$	Solar loop, the separate network
$steel$	Steel
$supply$	Supply
T	Transverse
top	Top of buffer
win	Window

Greek Symbols

α	Thermal Diffusivity [$\frac{m^2}{s}$]
β	Parameter describing the insulation of the pipes [-]
η	Efficiency [-]
κ	Solar collector tilt from horizontal [^{0}]

λ	Heat transfer coefficient [$\frac{W}{m*K}$]
ϕ	Solar collector azimuth (clockwise, south being 0) [^{0}]
σ	Stefan-Boltzmann constant [-]
$\tau\alpha$	Effective transmittance-absorptance product [-]
τ	Window transmittance [−]
θ	Angle between collector surface and beam irradiance [^{0}]

Roman Symbols

ΔT	Temperature difference [K]
$\dot{m}$	Massflow [$\frac{kg}{s}$]
$\dot{Q}$	Thermal conductive power [W]
A	Surface area [m^2]
a	Length of the buffer [m]
b	Width of the buffer [m]
C	Electricity consumption expenditures [€]
C_p	Heat capacity [$\frac{J}{kg*K}$]
D	Half the distance between supply and return pipes in ground [m]
d	Diameter [m]
f	Shading factor [-]
F'	Solar collector efficiency [-]
G	Irradiance on surface [$\frac{W}{m^2}$]
H	Burial depth of district heating pipelines [m]
h	Heat loss factor for heat loss problems [-]
$head$	Head [m]
I	Irradiance on horizontal surface[$\frac{W}{m^2}$]
K	Incidence angle modifier [-]
M	Operation & maintenance expenditures [€]
mc	Thermal heat capacity [$\frac{J}{K}$]
P	Power[W]
q	Heat loss in the problem of pipe losses [$\frac{W}{m}$]
r	Radius [m]

s	Insulation thickness $[m]$
T	Temperature $[K]$
u	Wind speed in $[\frac{m}{s}]$
UA	Heat transfer coefficient $[\frac{W}{K}]$
X	Investment expenditures [€]

1 Introduction

In the fight against climate change, the Dutch government has vowed to replace current natural gas-based heating systems in buildings for more environmentally friendly alternatives.

The need to convert hundreds of thousands of buildings annually, and its accompanying incentives, have sparked a pursuit for low carbon heating systems. A system relatively novel to the Netherlands, is one where solar thermal energy is used to provide the built environment with its heating needs.

When such a system is to provide a large portion of the total heating load, energy storage is needed in order to cope with the seasonal mismatch between supply and demand. Until recently, few of these projects were developed due to prohibitively high costs of the high temperature seasonal thermal energy storage (STES). However, the introduction of a new STES design by the company HoCoSto has diminished costs to a point where economic feasibility is achieved for a variety of projects.

While HoCoSto's solar-plus-storage concept has been tried and tested for several use cases such as individual houses, sport accommodations and schools, arguably the most promising application is the combination with small district heating systems (DHS). In such a system, several consumers would be connected to a central STES by a DHS. This study focuses on decentralised generation, where the consumers generate thermal energy with solar collectors on their own roofs.

The concept of having a solar heating network with high temperature STES, offers the appealing benefit that the DHS could operate at a relatively high temperature, mitigating the need to convert participating buildings to be suited for low temperature heating (as is the case for many other low carbon heating concepts). However, having high temperatures in the network has three major downsides:

- Heat losses in the DHS increase
- Higher supply temperatures means more exergy needs to be generated by a heat pump (when the buffer temperature is below the supply temperature, a heat pump needs to supply exergy)
- The solar collectors have to operate at higher temperatures, decreasing their efficiency

This study aims to improve the performance of decentralised solar+storage district heating systems while maintaining the possibility to work with high temperature heating systems. The performance of the system is measured in LCOH, or levelised cost of heat. LCOH takes into account all costs, discounted for the weighed average cost of capital (WACC), divided over the discounted consumption. The result is an energy cost expressed in $\frac{€}{kWh}$. Chapter 5 further elaborates on the LCOH.

The improvements potentially leading to a lower LCOH will be sought in (partially) mitigating one or more of the three issues enumerated above. After careful examination of current literature in Chapter 2, several possible mitigation options are laid out in Chapter 3. In total, seven different network configurations are considered. The general design and layout of these systems are elaborated on in Chapter 4.

In order to compare the different configurations based on LCOH, they are simulated for several years in a Matlab/Simulink environment. Chapter 5 discusses the model and its components, and Chapter 6 covers how the technical performance is translated into an LCOH.

Additionally, to compare how the systems financially hold up to alternative heating systems, they are compared to a scenario where the houses are heated by individual air to water heat pumps. A simple model of a single house and heat pump is introduced in chapter 7.

Finally, the comparison between the systems is made in Chapter 8. First, the systems are scaled based on buffer size and solar area for the lowest LCOH. Additionally, all systems are also sized for the lowest LCOH with the additional constraint that the SCOP must be at least 5. This is done because it is reasonable to assume that ecological constraints will be applied in the adoption of such systems. The SCOP, or seasonal coefficient of performance, is defined as the ratio between the annual consumed thermal energy by the consumers and the total electricity consumption by the entire system. The SCOP is assumed to be a good measure of ecological impact of the system.

The most promising configurations will be further elaborated on. For these systems, a breakdown of the LCOH is given, and special attention will be paid to the differences in heat losses, electricity consumption and solar collector efficiency.

As a test case, the neighborhood Karwijhof in the village Nagele is evaluated. This village has been assigned by the Dutch government to be a showcase area for innovative sustainable energy solutions. As a part of that project, a solar plus storage district heating network is under consideration for the Karwijhof.

While pursuing a low LCOE, social acceptance is strongly taken into account throughout the research. High comfort levels are to be guaranteed to consumers, while physical space occupation and work required inside dwelling is to be minimized.

Limitations regarding the presented approach include:

1. The networks are projected on a quite specific demand and network layout scenario, other scenarios might yield different outcomes
2. The resulting LCOH are highly dependent on component pricing (e.g. the price per m^3 of buffer), which is subject to future changes and potentially errors in estimates
3. Some Simulink submodels will have to be simplified, e.g. the thermal stratification in the storage buffer
4. The study is made without taking subsidies into account. These can obviously quickly shift the economics of various configurations and systems.

Research Goals

Summarizing the section above, the main question is: "How can a district heating network be optimized for operation with decentralised solar collectors and seasonal thermal energy storage?"

The answer to this general question is sought by resolving the following research questions:

- What changes could be made to the district heating system which can potentially lower the total cost of energy?
- For a base scenario and every possibly improved system, what is the optimal sizing of the solar collectors and buffer volume to achieve the lowest cost of energy?
- Which of the compared systems actually achieves the lowest cost of energy?

- Why does this system achieve lower costs and what is the cost breakdown?
- Can this system compete on cost with individual air to water heat pumps?

The research questions above are solved only with reducing the cost of energy in mind. Additionally, a scenario is also considered where the system has to have a SCOP of at least 5. For this scenario, the research questions above are answered again, while imposing the constraint of having to reach the SCOP of 5.

2

Literature Review

This research aims to optimize the distribution network side of solar based district heating systems (DHS) with seasonal heat storage. This chapter aims to identify the most relevant research done on this subject. In section 2.1, research on DHS in general is covered, while in section 2.2 research on solar based DHS is explored. In section 2.3, the modelling of DHS systems is examined, and finally, in section 2.4 the heat consumption of dwellings is attended to.

2.1. District Heating Systems

District heating systems serve the purpose of delivering heat to consumers for space heating and domestic hot water (DHW) preparation. It typically consists of three components: An energy source, a distribution network, and more than one end-user. DHS have been deployed globally, with some systems dating back several centuries. Due to the urge to replace fossil fuel based boilers, the deployment of these systems is currently gaining momentum in several countries.
Over the past decades supply temperatures have seen a downward trend, with the most recent (4th generation) DHS boasting supply temperatures well below 100 $^{\circ}C$. According to Ecofys & Greenvis [32], lower supply temperatures offer three advantages to conventional DHS: Firstly, it lowers heat losses in the network; Secondly, it allows for the use of a wider range of materials; and finally it enables higher energy source efficiencies. However, there are two constraints regarding lower supply temperatures: Firstly, the network has to be able to supply enough heat to keep the residences warm, secondly, a sufficient supply of domestic hot water (DHW) has to be secured while complying with legionella laws.
Most studies done on DHS focus on low temperature networks. Elmegaard et al. [8] compare energy and exergetic efficiency and annual heating costs for low temperature DHS which utilize electricity for supplementary heating of DHW (direct electric heating as well as heat pump solutions). The lowest annual costs were achieved for conventional solutions at lowest possible temperatures. Individual booster heat pumps turned out not to be cost effective.
A study done by Yang & Svendsen [36] compares return temperatures for different DHW preparation methods. It found that houses with supplementary direct electric heaters achieved lower return temperatures than houses which utilize storage tanks. The difference found was 7.8 $^{\circ}C$ in winter and 5.8 $^{\circ}C$ in summer. Another study, also done by Yang & Svendsen [35], compares the LCOE of different supplementary heating configurations for low temperature DHS. Configurations with storage tanks, direct heat exchangers, and booster heat pumps were compared and the authors found the most optimal configuration to be the one displayed in figure 2.1.

In this configuration, the DHW is heated by the district heating network to 40 °C using a plate heat exchanger, and used directly for sanitary purposes. The DHW needed for kitchen use (which

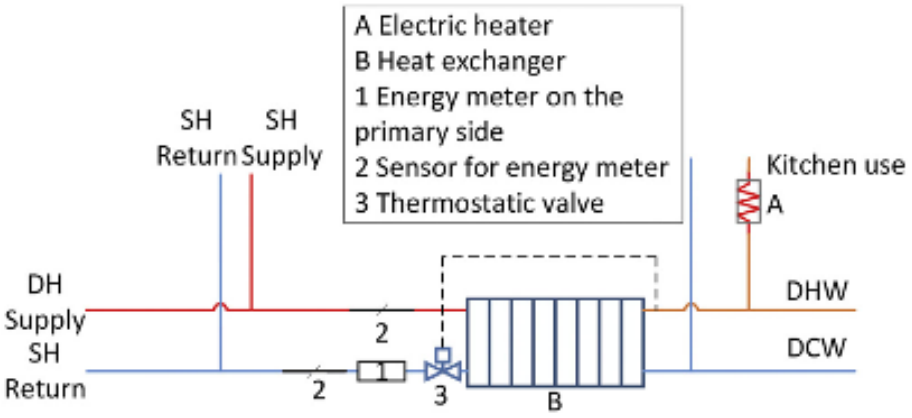

Figure 2.1: Substation 4 [35]. DCW is domestic cold water, DH is district heating, SH is space heating

accounts for just 12.6% of the DHW volume demand according to Yang & Svendsen [35]) is heated from 40 to 45 $^{\circ}C$ using an in-line electric heater. This configuration was not only found to yield the lowest overall LCOH, but also results in low electricity peak loads since the flow and ΔT of DHW flow is low at 0.1 L/s and 5 K, respectively. The only restriction to this configuration, is that the minimum supply temperature at the consumer level should be 45 $^{\circ}C$, since the ΔT over the heat exchanger is approximately 5 K. If the supply temperature at the consumer side can drop below 45 $^{\circ}C$, the DHW for sanitary purposes is also to be heated by the electrical heater.

Note that these studies originate from Denmark which generally has less strict legionella laws, therefore, certain configurations may not be allowed in the Netherlands.

2.2. Solar District Heating

Some DHS use solar thermal panels to harvest solar energy as an energy source. Several studies have covered the feed in of solar energy into a DHS. However, most studies focus on systems where solar energy is responsible for a small fraction of the total supplied energy. Faninger [12] concludes that small solar fractions can be quite easily achieved in Austrian district heating networks, mainly to cover DHW demand in summer. He argues that the main barrier for high solar fractions is the lack of low cost high temperature seasonal energy storage options. He also finds that low supply and return temperatures are beneficial to the solar fraction, mainly because solar collectors are more efficient at lower temperatures.

Van Miltenburg [31] underwrites the need for thermal energy storage in order to achieve substantial solar fractions. By running simulations in Simulink of district heating networks with solar feed-in, several aspects of the system are evaluated. Many aspects of the solar based DHS such as the solar collectors, pipelines, pumps etc. are thoroughly covered. While van Miltenburg's research models the distribution network to be a classic two-line network, it does note that a three-line network could offer advantages to the system. The potential benefits of a three-line network to solar based DHS are underlined by a report from Ecofys & Greenvis [32] as well as by Averfalk & Werner [5], who point out that by using a three-line network the solar collectors can operate at higher efficiencies, and that the heat storage buffer can be discharged to lower temperatures.

A paper by Sibbitt et al. [24] investigates the performance of a solar based DHS combined with seasonal borehole heat storage in Canada, the Drake landing solar community. The DHS supplies up to 97% of the space heating demand of 52 detached homes with solar energy. In this system, the solar collectors are connected to the STES through separate pipelines in order to allow the collectors to operate at ideal temperatures. Also, the supply temperature of the DHS is made dependent on

the ambient temperature.

2.3. Modelling

This research aims to optimize the distribution side of a solar DHS with STES, and it aims to do so by simulating and evaluating different systems. This section will cover the literature on the modelling of DHS.

Most studies seem to use TRNSYS for modelling of district heating networks: It is used by Sibbitt et al. [24] to model the Drake Landing solar community, as well as by Flynn & Siren [13], who use simulations to show that seasonal storage combined with thermal solar collectors can provide solar fractions above 95% at various locations throughout Europe. Also, Urbaneck et al. [29] use TRNSYS to conclude that low solar fractions (of around 10%) can be achieved easily in existing DHS throughout Germany.

Another example of modelling software often used for district heating networks, is Modelica. It is used for example by Rama et al. [23], who highlight the advantages such as being open source, and having a large community-built library with a large selection of sub models.

While these software packages are very suited to model standard district heating networks, they are less suited for applications where non-standard components are to be modelled. Since this thesis explores adaptations in district heating networks which are not common, using a blackbox modelling software package might not be optimal.

A more suited approach is to model the DHS based on physical models in general simulation software, like Miltenburg [31] did with Simulink. Therefore, this approach is chosen.

Within this software, not every component has to be modelled from the ground up. Some components can be based on existing MATLAB/Simulink libraries such as CARNOT (Conventional and Renewable Energy systems Optimization Toolbox) as used by Stephan & Schebeck [26]. They argue that CARNOT is well suited to study complex DHS due to the wide range of user definable components as well as the possibility to develop own components through its open source design. Wemhoner et al. [34], who simulate a solar thermal system in Simulink using CARNOT, argue that a large advantage compared to TRNSYS is that variable step sizes can be used, making it suited for both long time simulations, as well as for very short simulations.

2.4. Domestic Heat consumption

The amount of energy consumed for building heating depends greatly on building properties such as shell insulation, ventilation rate and window area and orientation. Fabriek [11] found that in multi-zone models, compared to single-zone models, heating demand can vary up to 10% due to different air couplings. It also states that internal heat gains, while very important for well insulated houses, is less relevant in poorly insulated houses. Fabriek, as well as Purdy & Beausoleil-Morrison [22] stress the importance of air infiltration, since small leaks can lead to large increases in heating loads, especially in high-wind conditions.

Apart from building characteristics, energy demand for space heating also depends on the number of occupants and their behaviour. According to research by both Santin [15] as well as Fabriek [11], space heating demand depends greatly on behaviour such as thermostat temperature settings.

The total heating load consists not only of space heating, but also of the production of domestic hot water (DHW). According to Fuentes et al. [14] and van Vliet et al. [32], the share of DHW production in the total heat demand of dwellings has been increasing for the past years due to higher frequency and longevity of showers and reductions in space heating consumption (because of improvements in insulation). Fuentes et al. [14] thoroughly explore DHW consumption profiles, and offer an extensive literature summary on the differences in DHW consumption between demographic groups.

2.4.1. Legislation on hot water supply

In the Netherlands, legislation is in place for the production and distribution of domestic hot water. In order to comply with the 'bouwbesluit' and 'drinkwaterbesluit', tap water installations have to be designed and installed according tot NEN 1006 (General design guidelines for potable water installations). These guidelines are published by the Dutch normalisation institute (NEN). The practical consequences of this design code, are elaborated on in the 'waterwerkbladen', published by KIWA [17].

For the concept choice of domestic hot water preparation in a DHS, the most relevant points are given in the following subsections.

Supply Temperature

The KIWA [17] command minimum temperatures at tap locations, which are as follows:

1. WB4.4A-2.1: The supply temperature at tap locations in dwellings without circulation has to be at least 55 $^{\circ}C$.
2. WB4.4A-2.2: The supply temperature at tap locations in dwellings with circulation has to be at least 60 $^{\circ}C$.
3. WB4.4A-2.3: The return temperature of DHW installations with circulations has to be at least 60 $^{\circ}C$.
4. WB4.4A-2.7: The temperature at the tap locations can be lower than specified in WB4.4A-2.1 and WB4.4A-2.2 if the following conditions are met:
    - The DHW preparation device is a heater without an internal hot water supply.
    - The water volume from the device to the furthest tap location is less than 1 L.
    - The geyser supplies one space, or several spaces destined for the same consumer.
    - The tap locations are meant for personal hygiene.

Waiting times

1. WB4.4A-4.1 states that the maximum waiting time for DHW is 35 seconds. This requirement holds for all tap points except for a bath or (dish)washing machine. The standard device waiting time is set at 15 seconds.

Separation of primary medium and DHW

The production of DHW is done through a heat exchanger. The heat exchangers have to comply to design code KIWA BRL-K656 [6]. Furthermore, heat exchangers meant for DHW preparation in a system where the total nominal heating capacity exceeds 45 kW should have a double separation between the primary medium and tap water according to KIWA WB4.4B-9/10 [17].

In practice, every DHS will have a nominal capacity far exceeding 45 kW, thus the heat exchangers will have to be doubly separated.

DHW buffers

For DHW buffers which are not continuously at a uniform temperature of at least 55 $^{\circ}C$ (60 $^{\circ}C$ for systems with circulation), a thermal disinfection is required at 60 $^{\circ}C$ for at least 20 minutes per week (shorter times are allowed at higher disinfection temperatures).

Also, if the minimum supply temperatures (according to WB4.4A-2.1-3) cannot be met, an extra heater will have to be installed to guarantee these minimum temperatures. The required buffer volume and heater power can be calculated according to WB2.1E [17].

3

System Configurations

Typical district heating systems (DHS) consist of three main components: An energy source, a distribution network, and more than one end-user. This thesis examines solar-based DHS with an additional component: Seasonal thermal energy storage (STES). In the village Nagele, 24 buildings will be connected to a small district heating network powered by decentralised solar thermal energy. At the center of this system rests a large seasonal thermal energy storage buffer supplied by the company 'HoCoSto'.

The aim of this study is to optimize the district heating part of the system for operation in conjunction with solar and storage. The performance of the system is measured in LCOH.

In order to optimize the distribution network for operation with energy storage and decentralised solar collectors, several network configurations are dynamically modelled and compared. This section gives an overview of the different network configurations.

Three main approaches are considered to improve overall system performance; Firstly, the implementation of a four-line network so that the solar collectors do not feed into the heating network, but have their own dedicated network instead; Secondly, an approach where the DHW systems of consumers are altered in order to allow lower supply temperatures; Finally, the introduction of a variable supply temperature based on the ambient temperature.

In total, seven different combinations are compared:

- 0-A: Base case, fixed supply temperature, 2-line network, DHW system A
- I-A: Variable supply temperature, 2-line network, DHW system A
- I-B: Variable supply temperature, 2-line network, DHW system B
- I-C: Variable supply temperature, 2-line network, DHW system C
- II-A: Variable supply temperature, 4-line network, DHW system A
- II-B: Variable supply temperature, 4-line network, DHW system B
- II-C: Variable supply temperature, 4-line network, DHW system C

All of these configurations have their advantages and disadvantages, this study aims to conclude which one achieves the lowest overall costs while maintaining a high consumer comfort level.

Section 3.1 gives a general overview of the 2-line and 4-line configurations. Section 3.2 covers fixed and variable supply temperatures, after which it goes on to explore three DHW supply methods (concepts A, B and C) and their characteristics.

3.1. Two-line and four-line networks

In this study, two main pipeline configurations are considered, both of which are shown in figure 3.1. In both configurations, three heat exchangers per consumer are used to achieve hydraulic separation between the network on one side, and the solar collectors, heating system, and DHW system on the other side.

In system I, there are just two pipelines to which every consumer is connected. Through these pipelines, heat is delivered from the buffer to the consumers, but also the solar energy generated by the solar collectors is transported from the dwellings to the buffer. The biggest benefit of this system is its simplicity and the resulting reduced installation costs since only two pipelines have to be used. System II is unique in the way that it uses a separate network for the solar collectors, much like the Drake Landing solar community in Canada as described by Sibbitt et al. [24]. The main presumed benefit of this system is an increase in efficiency of the solar collectors since they can operate at lower temperatures. Also, it eliminates the need of one circulation pump per consumer. Of course, overall thermal losses from the pipelines would be higher as more pipelines are required. The additional pipelines would also add to material and installations costs.

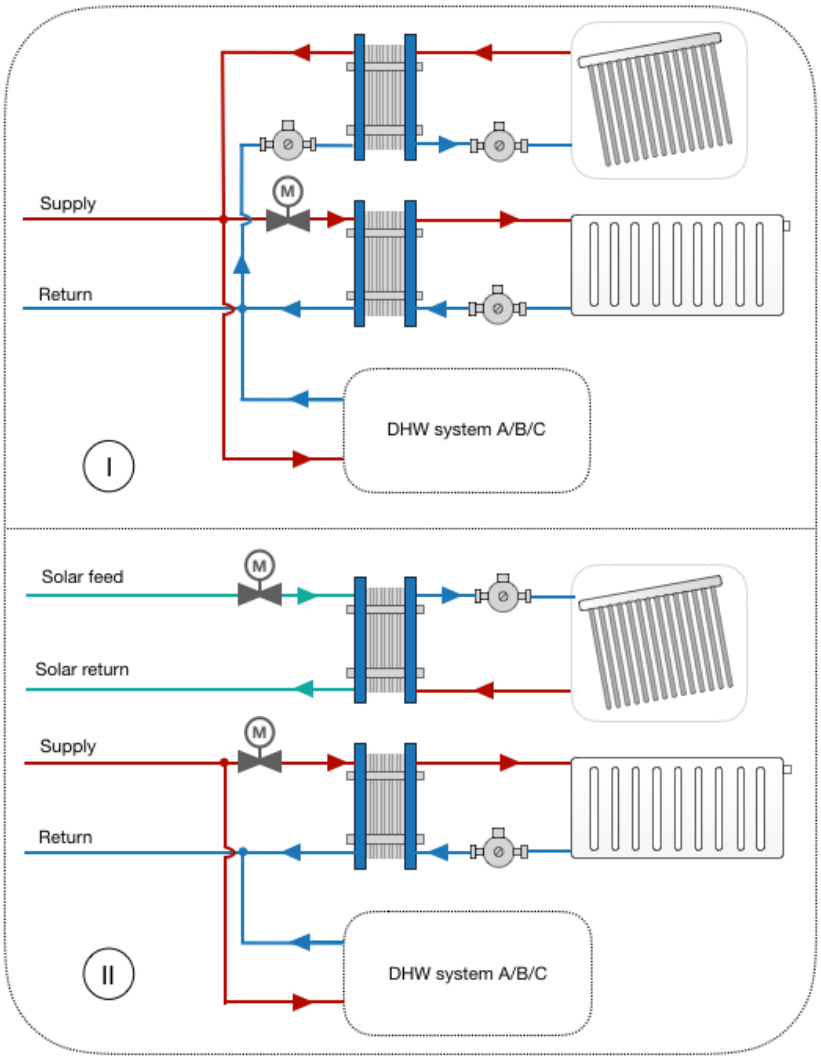

Figure 3.1: Two main network configurations. In configuration II, the solar collectors feed in to their own dedicated network. In configuration I, the solar collectors feed in to the heating network, mitigating the need for this dedicated network for the solar collectors.

3.2. Supply Temperatures

As pointed out in chapter 1, the system benefits from low supply temperatures, as it results in decreased heat losses and lower electricity consumption by the heat pump. Also, low supply temperatures allow for the use of a wider range of materials and it results in lower return temperatures, which lead to higher solar collector efficiencies.

The supply temperature is constrained by several factors: It needs to be sufficiently high to provide enough capacity for space heating, it needs to be high enough to produce DHW according to Dutch legislation, and it is influenced by outlet temperature of the solar collectors.

The houses in Nagele are suited so that a supply temperature of 70 $^{\circ}C$ is sufficiently high to provide enough space heating power year round. However, required space heating power obviously is greatly dependent on weather conditions and is therefore not equal throughout time. Because of that, the supply temperature could be made weather dependent: For higher ambient temperatures, the supply temperature could be lower than the 70 $^{\circ}C$ needed at low outdoor temperatures. As a result, average network temperatures can be reduced, yielding the advantages listed above. Note that the 70 $^{\circ}C$ stated above is the temperature needed at the heating system level. Since heat exchangers are used between the consumer heating systems and the district heating network (to protect the DHS from fouling and to limit the negative effects of a potential leak), an additional ΔT has to be added. The heat exchangers will be scaled so that the ΔT at maximum power will be 3 K. Obviously, this ΔT will be smaller for lower powers.

The main constraint in lowering supply temperatures, is the preparation of DHW, since minimum temperatures need to be achieved in order to provide enough comfort and mitigate Legionella growth.

The most common method of DHW preparation in district heating networks, is direct preparation through a plate heat exchanger. This method is described by DHW concept A below. Two other concepts (B and C) are conceived which aim to reduce the minimum network supply temperature.

3.2.1. DHW concept A

DHW concept A is the preparation concept used in most district heating systems. A single heat exchanger provides all hot water using the heating network as the sole energy source.

As discussed in detail in chapter 2, the minimum DHW supply temperature at tapping locations is 55 $^{\circ}C$ for non-sanitary purposes, while DHW for sanitary purposes can have temperatures below that. The DHW will have to be prepared by a heat exchanger which is (according to regulations) doubly walled. Therefore, a mean temperature difference over the heat exchanger of 5 K is assumed (based on research by Yang & Svendsen [35]). Also, there will be (small) thermal losses in the pipelines between the heat exchanger and tapping location. All and all, it is assumed that the supply temperature of the network will have to be at least 6 K higher than the DHW temperature. This would mean that the minimum network temperature at the heat exchanger is 61 $^{\circ}C$.

A simple system like this is shown in figure 3.2, concept A. Summarizing, if this DHW preparation concept were to be used, the supply temperature of the network (at consumer level) would, depending on ambient temperatures, vary between 61 and 73 $^{\circ}C$.

The main advantages of this method are the simplicity (thus low costs), low physical space occupation, and unlimited DHW tapping. The main downside is that a relatively high supply temperature is required year-round.

3.2.2. DHW concept B

Most of the time, ambient temperatures would allow the minimum supply temperature to be lower than 61 $^{\circ}C$. Since this constraint is set by the minimum DHW temperatures, methods are explored to break this constraint.

As laid out in chapter 2.1, the temperature of DHW for sanitary purposes (which makes up 87.4%

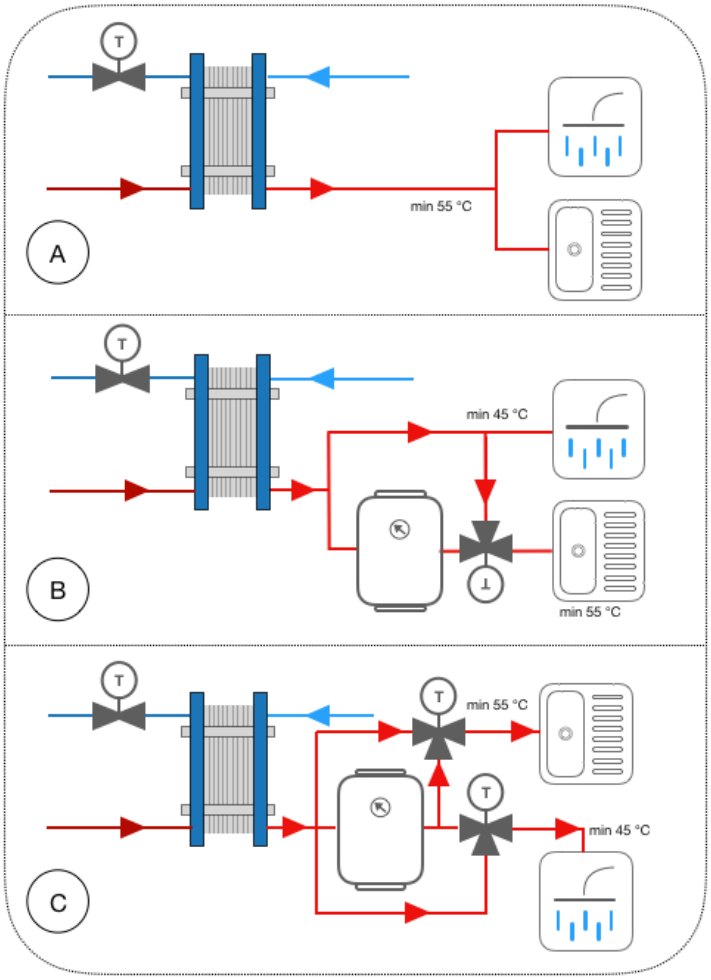

Figure 3.2: Three DHW preparation concepts. Concept A uses only a heat exchanger, requiring the outlet temperature of the heat exchanger to be at least 55 °C. Concept B uses an electric heater to reheat the DHW for kitchen use, reducing the required temperature at the outlet of the heat exchanger to 45 °C. Concept C uses an electric heater to reheat the DHW for all purposes, further reducing the required temperature at the outlet of the heat exchanger. Thermostatic valves are added to limit the outlet DHW temperature to the required level.

of total DHW demand) is allowed to be below 55 °C in residential environments. Concept B, shown in figure 3.2, makes use of this exception by using an in-line heater to heat non-sanitary water to the 55 °C level. The minimum temperature for sanitary DHW is chosen to be 45 °C, as this seems to be the highest temperature at which consumers shower/bathe.

One important component of this concept, is the thermostatic mixing valve after the electric boiler. This allows the hot water tapping temperature to remain constant also for higher boiler temperatures. This is important in Nagele, since space comes at a premium. By using the mixing valve, the boiler temperature can be higher, which increases the stored energy. If the mixing valve was not to be used, and mixing would be done at the tap, electrical energy consumption would be higher.

A downside to this concept is that the DHW tapping volume in the kitchen at 55 °C is limited. However, kitchen tap water volumes are usually low, and tap water of at least 45 °C has unlimited availability. Another downside is that electrical energy is used to heat DHW at times when the supply temperature of the network is low. However, this is not the case year-round, and only the DHW for non-sanitary purposes needs to be heated (by a maximum of 10 K). The advantage is that network temperatures can decrease for relatively high ambient temperatures. Taking into account the same heat exchanger ΔT's and pipeline losses as discussed above, the network supply temperature (at

consumer level) can vary between 51 and 73 $^{\circ}C$. The additional costs compared to DHW concept A are low, since only a small boiler (in the order of 10-15 L) is needed.

3.2.3. DHW concept C

Much like DHW concept B, concept C aims to decrease the minimum network supply temperature needed to satisfy DHW needs. Concept B is constrained by the 45 $^{\circ}C$ temperature needed for sanitary purposes. This is resolved in concept C (shown in figure 3.2), where the sanitary water is also heated by the boiler to reach the minimum service level. Again, thermostatic valves are used in order to maximise the amount of energy taken from the network, and minimize the consumption of electrical energy.

While theoretically there is no minimum network temperature for this concept since all DHW energy can be supplied by the boiler, this would incur high electricity consumption. Also, there is not enough physical space available at the consumers in Nagele to place sufficiently large boilers. Therefore, the minimum DHW exit temperature of the heat exchanger is chosen to be 35 $^{\circ}C$. The reason being that, in combination with a relatively small 40 L boiler at 85 $^{\circ}C$, 200 L of 45 $^{\circ}C$ DHW can be produced, which is assumed to be a very comfortable amount for the consumers (the only exception being a multi-purpose building, which can be outfitted with a larger boiler).

This concept goes further than concept B in achieving lower network temperatures at the cost of higher electrical energy consumption at the consumer level and slightly higher costs of installation. Electrical consumption will be higher when network temperatures are low, but lower average network temperatures have their benefits. In such a configuration, the network supply temperature (at consumer level) can vary between 41 and 73 $^{\circ}C$.

3.2.4. Supply temperatures of all systems

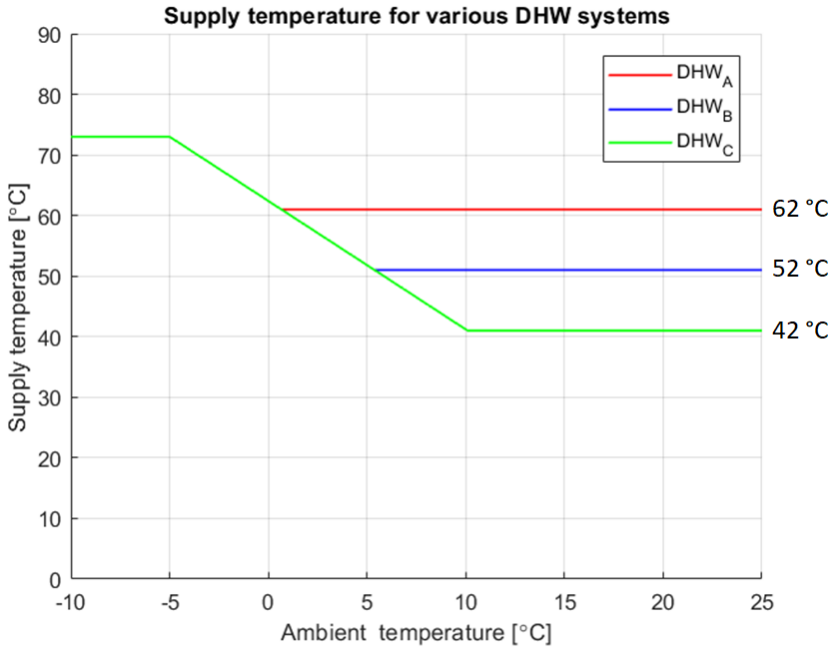

Figure 3.3: Supply temperatures for all DHW concepts as a function of ambient temperatures

DHW systems B and C are conceived in order to reach lower network temperatures than system A allows. In figure 3.3, the supply temperatures of all three concepts are shown. It is clear that for concepts B and C, the system can operate at lower supply temperatures. Note that these temperatures are supply temperatures at the consumer level, therefore, upstream temperatures will have to

be slightly higher in order to reach this.

In figure 3.4, the simulated supply temperatures for the year 2008 is shown for all three concepts. Ambient temperature data from the KNMI [18] for the location Marknesse is used. Marknesse is roughly 13 km from Nagele. When looking at the graph, it can clearly be seen that the peak supply temperature of 73 $^{\circ}C$ is rarely reached. While it appears that network B and C operate at much lower temperatures most of the time, note that the temperatures displayed are the supply temperatures assumed necessary to properly heat the buildings and provide their DHW. It is the minimum temperature needed in the supply lines of the network at the consumers. Therefore, in the two-line network where the solar collectors feed in over the same pipelines, the actual supply temperatures will be higher at times. Especially at the end of summer when buffer temperatures (and thus solar inlet temperatures) are high, the outlet temperatures of the solar collectors will be significantly higher than the service level temperatures.

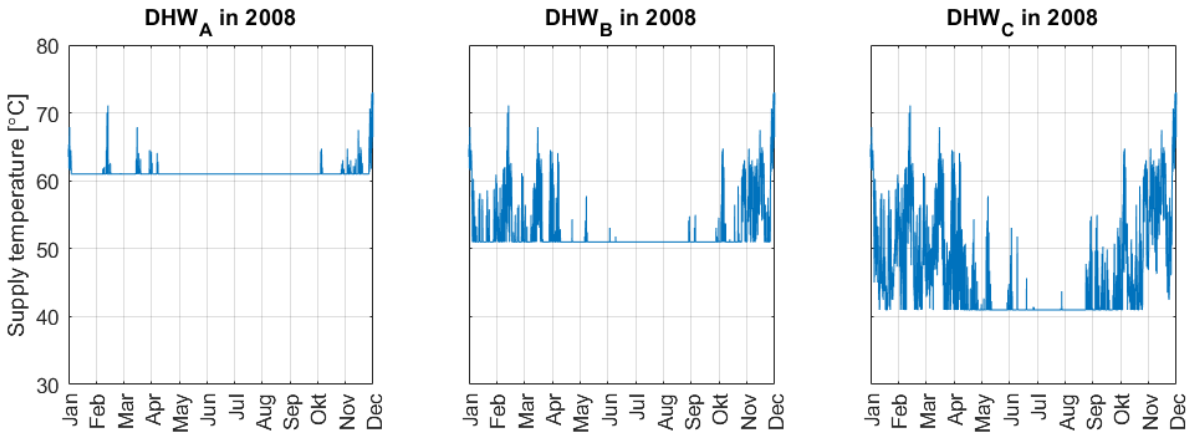

Figure 3.4: Simulated supply temperatures for all DHW concepts for the year 2008

4

System Design

In this research, seven different district heating network configurations are conceived and simulated in order to conclude which system achieves the lowest overall costs. Chapter 3 gives a quick overview of the seven systems. This Chapter elaborates further on the layout and components of how the systems could be installed in Nagele, the testcase location. Chapter 5 gives a more detailed view of how the system is modelled.

4.1. Layout

In figure 4.1, the 24 participating consumers are shown as well as the space available for pipelines and the buffer. The consumers can roughly be divided into three groups:

- Consumers 1-8: Smaller terraced houses as shown in figure 4.2.
- Consumers 9-23: Detached houses, some relatively small (as seen in figure 4.4), and some larger (figure 4.5).
- Consumer 24: A former primary school (shown in figure 4.3) which currently functions as a multipurpose community building (a children's daycare among others).

Several layouts exist for district heating grids. The most common layouts are branched and looped grids, both shown in figure 4.6. According to Li et al. [20], looped networks increase system reliability at the expense of a higher investment. Hybrid layouts, or 'branched-looped networks' as shown in figure 4.6, are also possible. Pipeline topology directly affects the construction cost, heat loss and pressure differentials of the system.

Due to the restricted nature of the project, which is clearly displayed in figure 4.1, there is not much room for design alterations. The only possible network layout is branched, and the most optimal buffer location is location no. 2, since that results in the lowest total pipeline length.

4.2. Consumer characteristics

In table 4.1, the annual gas consumption and roof area available for solar collectors is shown. Since the dataset was not complete, some values for gas consumption were to be estimated. For the eight terraces houses only the gas consumption for no.4 was available. The annual consumption of no.4 is 1355 m^3 while the average for this type of dwelling is 1350 m^3 according to Essent [1]. Since no.2 to 7 are all exactly the same, their annual gas consumption is assumed to be equal. No.1 and No.8 have more exterior wall area and are therefore assumed to have an annual consumption of 1600 m^3, which is the average for this type of dwelling according to Essent [1]. No. 9, 11 and 21 are unique detached houses. However, since they were built in the same period and style as the adjacent houses, it is assumed that the building characteristics are roughly equal. Therefore, their

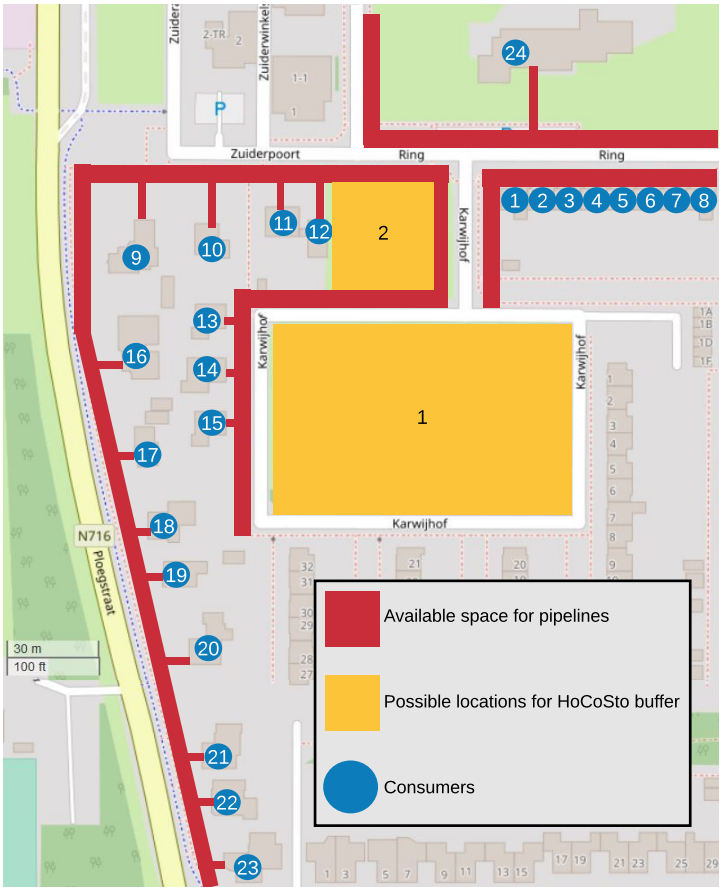

Figure 4.1: Participating consumers for the testcase project in Nagele [25], consumers 1-8 being smaller terraced houses, 9-23 detached houses, and 24 a school

Figure 4.2: Consumers 1-8

Figure 4.3: Consumer 24

Figure 4.4: Typical smaller house of group 9-23

Figure 4.5: Typical larger houses of group 9-23

consumption was estimated based on the consumption of the other detached houses of similar size and shape. The annual gas consumption of most buildings is in line with average numbers

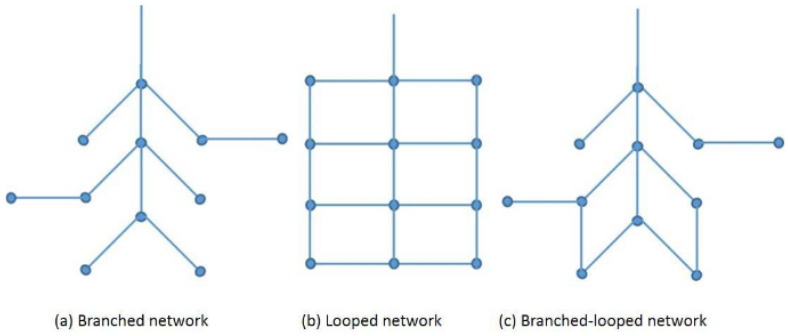

Figure 4.6: Different types of district heating layouts [20]

according to Essent [1], with the exception of No.12, 16, 20 and 24, which have an exceptionally high gas consumption. These dwellings will be recommended to improve their insulation. As a result, it is assumed that their consumption will decrease by 20%. Additionally, buildings 1 to 8 will get improved rooftop insulation, which is assumed to decrease consumption by 10%.

The houses, and especially the terraced ones, are quite limited in terms of physical interior space. Therefore, the space occupied by indoor installations should be limited as much as possible. This is especially relevant for the placement of domestic hot water (DHW) buffers. Therefore, the largest indoor installations considered in this study, are those of DHW concept C, where a 40 L electric boiler is required. The physical space occupation for such a boiler is roughly equal to the gas boilers which are to be removed.

4.2.1. Heat delivery

In district heating networks, delivery kits are used to deliver the heat from the network to the heating systems and DHW of the consumers. A schematic of a typical delivery kit is shown in figure 4.7. These delivery kits have several tasks: Handling pressure differences between the distribution network and space heating system, preparing DHW, regulating the ΔT (through the flow), and metering the consumption.

The preparation of DHW is done through a doubly walled plate heat exchanger. While delivery kits exist without hydraulic separation between the DHS and space heating system (as is the case in figure 4.7), the project in Nagele will use heat exchangers between the systems. There are two reasons why hydraulic separation is implemented: Firstly, it prevents contamination and fouling between the two systems (the old heating systems in Nagele will undoubtedly contain rust particles); Secondly, it greatly reduces potential damages and downtime in case of fluid leakage at the consumer side. This is a serious concern, since system fluid leakages occur frequently in older heating systems. If hydraulic separation were not to be implemented, a single leak could theoretically drain the entire system, resulting in serious downtime.

The heat delivery kit also includes a metering system which is used to measure the consumed energy, which is then billed to the consumers. Standard delivery kits will be used for the DHW and space heating needs. The solar feed-in will be done at the network side in front of the delivery kits.

4.3. Solar Collectors

The solar collectors which are to harvest the thermal energy for the system will be decentralised, meaning they will be scattered across the rooftops from where they will feed in energy to the district heating network. Only the solar collectors on the eight terraced houses (No. 1 to 8) will be coupled and connected together to the DHS. This is possible since they share a single roof, and done in order to simplify and reduce the costs of installation.

Table 4.1: Consumer characteristics

No.	Adress	Gas consumption [m³/year] (* estimated)	Gross unshaded roof area available for solar collectors [m²]
1	Ring 98	1600*	50
2	Ring 100	1355*	50
3	Ring 102	1355*	50
4	Ring 104	1355	0
5	Ring 106	1355*	55
6	Ring 108	1355*	55
7	Ring 110	1355*	55
8	Ring 112	1600*	55
9	Zuiderpoort 2	2000*	28
10	Zuiderpoort 4	1500	82
11	Zuiderpoort 10-low	1500*	0
12	Zuiderpoort 10-high	3500	0
13	Karwijhof 35	2100	20
14	Karwijhof 34	2000	50
15	Karwijhof 33	1500	100
16	Ploegstraat 7	4500	80
17	Ploegstraat 9	1933	40
18	Ploegstraat 11	2925	0
19	Ploegstraat 13	2442	70
20	Ploegstraat 15	4200	50
21	Ploegstraat 17	1258	100
22	Ploegstraat 19	1750	120
23	Ploegstraat 21	2000*	120
24	Ring 1 (former school)	11000	340
Total		57438	1570

4.3.1. Solar collector type

There are three main types of solar collectors on the market suitable for rooftop applications: Flat plate, evacuated tube, and honeycomb collectors. Flat plate collectors are often praised for their high annual gain and low costs, however, their output drops significantly for high temperature differences between the working fluid and ambient temperature. Since the system operates at high temperatures, the efficiency and thus gain of the plat plate collectors would be low, especially during cold periods when heat demand is high (at these times, energy comes at a premium). This would result in the need for both a large amount of solar collectors, as well as for a larger buffer.

Honeycomb solar collectors are a novel improved version of standard flat plate collectors. They promise higher annual yields through lower heat losses, and offer relative high efficiencies at high operating temperatures. However, these panels are prohibitively expensive for the project.

Therefore, the type of collector to be used in the project is the evacuated tube collector. The working principle of regular vacuum tube collectors is shown in figure 4.8: The inner tube contains a fluid which evaporates after being heated by the solar irradiance, the vapor then flows up and

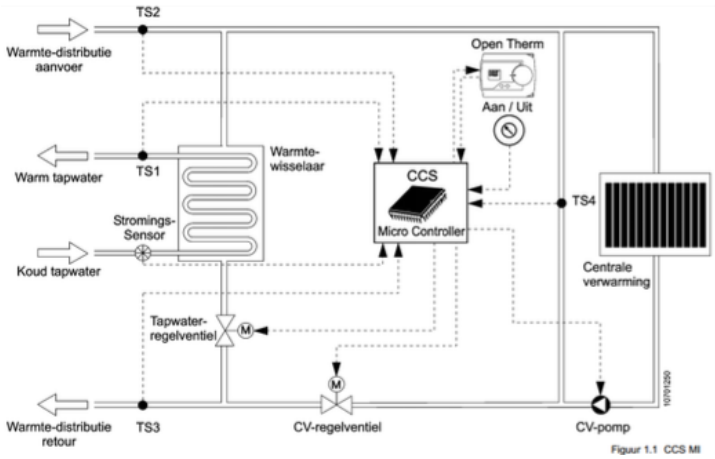

Figure 4.7: Typical unseparated consumer delivery kit for district heating systems [6]

transmits its thermal energy to the the header water by condensing in the heat pipe condenser after which the condensate flows down for the process to start over again. The tube consists of two glass layers, the inner and outer layer, between which there is a vacuum space which offers thermal insulation. While this is the most commonly used and best known type of evacuated tube collector, the type used in Nagele works slightly differently. A 'direct flow', or 'U-tube' collector is used. This type still consists of two glass layers with a vacuum in between, but no secondary fluid is used. Instead, the primary fluid flows directly through the tubes. The reason this type is used, is that regular heat pipes require a minimum installation slope of 30 degrees since the vapor inside the tubes must be able to flow upward. This minimum installation slope cannot be achieved in Nagele since (due to the historical nature of the town) the collectors are to be installed as flat as possible in order to preserve the architectural beauty of the town. Direct flow collectors have no minimum installation angle. Another advantage of direct flow vacuum tubes is the increased efficiency, since the temperature in the tubes can be lower because a ΔT between primary and secondary fluid is eliminated.

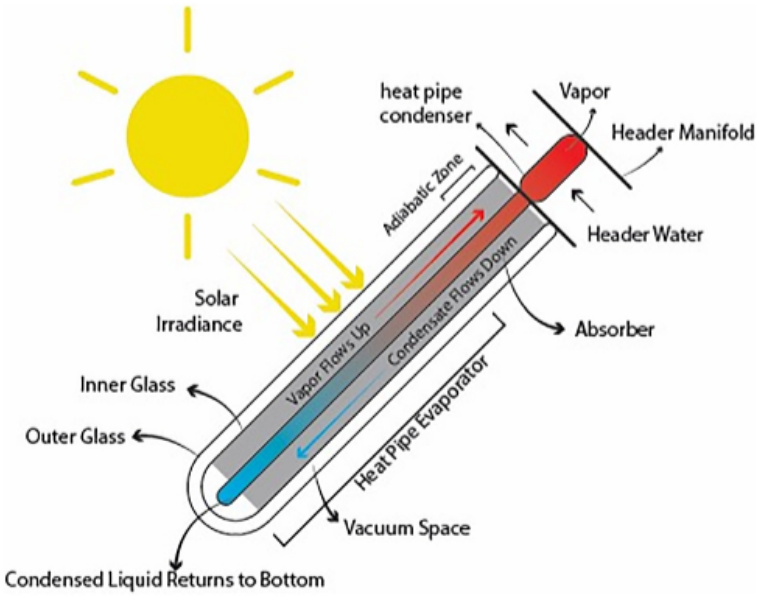

Figure 4.8: Working principle of a regular evacuated tube solar collector [9]

An evacuated tube solar collector consists of several evacuated tubes connected to a single header manifold. The specific type of collector assembly used is the Kloben industries ATON G1800 22-tube collector. This appears to be the most efficient high-temperature evacuated tube solar collector on the market. Efficiency at high temperatures is important since available rooftop area is constrained. There are several reasons why this collector achieves such high efficiencies: It utilises concentrating reflectors behind the tubes, uses a very wide vacuum (space between inner and outer tube), and is one of the few collectors with copper instead of steel tubes.

4.3.2. Installation

Since all rooftops are flat, the azimuth angle can be optimised. Therefore, the collectors will be installed facing directly south in order to maximise yield. Because the square rooftops in Nagele are aligned with wind directions, south facing collectors are aesthetically pleasing and result in high fill factors (the percentage of the roof which is covered). As mentioned above, the collectors should be visible as little as possible from the streets. For this reason, the zenith angle should be as low as possible. The minimum installation angle is 15 degrees. This is the minimum angle at which the concentrating mirrors at the back of the collectors get rinsed well during rain. The optimal zenith angle at the location is 35 degrees. While decreasing this angle to 15 degrees would only result in about 5% lower annual yield, the negative effects on the system will be larger. This has to do with the yield distribution over the year. Installing the collectors at a lower angle will significantly reduce yield during winter months, while slightly increasing yield during summer months. Therefore, lower installation angles result in an increase in necessary storage volume, increasing the system costs. When installation angles are free to be chosen, the optimum angle will be higher than 35 degrees, since winter yield comes at a premium to summer yield. Nonetheless, the highest acceptable zenith angle for this project is assumed to be 15 degrees.

In table 4.1, the available unshaded rooftop area of every consumer is given. Simple hand calculations show that collectors on the rooftops of the dwellings alone do not provide enough energy to cover the entire demand. Fortunately, consumer number 24 (a re-purposed school building), has a large unshaded roof and relatively low consumption. This can be used to compensate for the deficit of the other consumers.

It would be more cost efficient to maximise the installation on the school, and not outfit every dwelling with solar collectors, since large arrays are cheaper to install and maintain. But because the basis of the concept is that, if possible, every consumer generates at least a part of its own energy consumption, every consumers rooftop is outfitted with solar collectors. The solar array on the school building is scaled so that the remaining demand is covered.

Table 4.1 shows that some consumers do not have unshaded roof area available, this is because those buildings are already fully covered with solar PV panels. For the remaining buildings, the maximum fill factor of the rooftops is assumed to be 70%, meaning that the highest amount of solar collector area on every roof is 70% of the available gross area. Therefore, the maximum area of solar collectors which is to be installed, is 1100 m^2. At a fill factor of 70% and a relatively low zenith angle of 15%, it is assumed there is no self shading.

4.4. Heat Pump

As much energy as possible is delivered directly to the consumers, however, when the buffer temperature drops below the supply service level temperature, this is no longer possible. Therefore, a heat pump is used to increase the exergy at times when it is necessary. Behind the heat pump, a small secondary buffer is used to shave off peaks.

The heat pump is a water/water heat pump supplied by the company NRGTEQ. Because the heat pump has a piston compressor, it remains efficient over a wider operational range. Therefore, the heat pump is assumed to achieve 40% of Carnot efficiency at every operation point. The high

temperature range from NRGTEQ is able to consistently provide supply temperatures of up to 80 $^{\circ}C$.

Consideration has been given to the option to outfit every consumer with an individual heat pump instead of a single centralised heat pump. While decentralised heat pumps would allow for lower network temperatures at times when the buffer temperature is low, a centralised heat pump system is chosen for the following reasons:

- Large consumers of electricity pay significantly lower rates than small consumers, thus, electricity costs will be lower for a centralised system.
- The CAPEX of material and installation of a centralised heat pump system will be lower than 24 individual heat pumps.
- A central system contains less components and is easier to access, resulting in lower maintenance costs.
- Because a central system can be made redundant, uptime will most likely be higher.
- A large central heat pump system will likely achieve higher efficiencies than small decentralised pumps.
- Decentralised heat pumps would cause the need for more powerful grid connections.
- The implementation of decentralised heat pumps would complicate billing.
- Not every consumer has the physical space available required for a heat pump

The point about redundancy relates to the possibility of installing not a single, but several central heat pumps. For example, three central heat pumps could be installed. This would have two benefits: Firstly, a wide operational range can easily be achieved (e.g. 10% of power can be delivered by operating one heat pump at 33% power); Additionally, there would be redundancy in the system, lowering the possibility of downtime.

The aforementioned peak shaving buffer will be a standard cylindrical steel buffer in the central installation building. Its purpose is to assist the heat pumps in coping with short peak demands. These peak demands will most likely occur at the end of winter, when buffer temperatures are low, as are ambient temperatures. Especially in the evenings, when consumers turn up their heating and consume DHW, short demand spikes will be inevitable. An additional benefit of having a small buffer behind the heat pump is the prevention of short cycling at times when the heat pump has to operate below its minimum operational capacity. Short cycling does not only impair the performance of the heat pump, but also reduces its lifetime.

4.5. Pipelines

The distribution network has two tasks: Transport heat from the buffer to the consumers, and transport heat (generated by the solar collectors) back to the buffer. In this research, two different distribution network concepts are assessed: Firstly, a 2-line network where both tasks are carried out by the same network; Secondly, a double '4-line' network where 2 pipelines take care of the heating load, while 2 dedicated pipelines are used to transport heat from the solar collectors to the buffer.

4.5.1. Pipeline types

Typical district heating pipelines consist of three layers: An inner pipe with a surrounding insulation layer, and a protective shell pipe. According to Miltenburg [31], the most commonly used pipe is Steel-PUR-PE, with PUR being polyurethane and PE being polyethylene. However, according to Averfalk & Werner [5], it is becoming common practice for small diameter sections to use twin pipes. The single pipe is displayed by figure 4.9 (a), while the twin pipe is displayed by figure 4.9 (c). Figure 4.9 (b) displays a single pipe with additional vacuum panel insulation around the inner pipe. This type of pipe is not covered in this research due to the high material costs.

In the system, both Single Steel-PUR-PE pipelines as well as twin pipelines are considered. It is assumed that the twin pipelines are of the type MicrofleX, a pre-insulated underground flexible

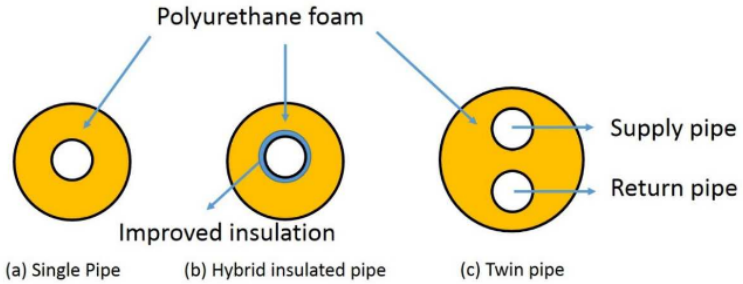

Figure 4.9: Different types of DHS pipes. (a) being a a classic single pipe encapsulated in PUR insulation, (b) resembles (a), but has improved insulation directly around the inner pipe, often in the form of vacuum insulation, (c) consists of both the supply and return pipe in a single jacket. All pipe types usually have a protective jacket, often made of PE

pipe system. The internal carrier pipes are stable, corrosion resistant, and can take continuous temperatures of up to 85 $^{\circ}C$, and up to 95 $^{\circ}C$ for short periods of time. The carrier pipes are made from PE-Xa, a high density, cross-linked polyethylene resistant to chemical corrosion, and with a non-permeable membrane to stop oxygen ingress [4]. The MicrofleX pipe system is available in a wide choice of diameters and layouts (e.g. also quad pipe systems are available). In figure 4.10, a quad pipe is shown.

Figure 4.10: Microflex quad pipeline [4]. Flexible pipe systems such as Microflex can reduce overall installation costs and speed. A quad pipeline for instance could be used to supply consumers with both their heating and DHW needs directly.

Since the exit temperature of the solar collectors can reach temperatures above the maximum allowed temperatures of the twin system pipelines, steel pipelines have to be used for the solar loop. In the first (two-line) network configuration, where the solar collectors feed from the return to the supply of the main network, both the supply and return will be steel-PUR-PE pipelines. In the 4-line network, where the solar loop is separated, the solar loop is steel-PUR-PE, and the heating network is made of Microflex twin pipelines.

4.5.2. Burial depth

The burial depth of the pipelines is decided based on local soil conditions. As can be seen in figure 4.11, the upper layer of the soil in Nagele consists of clay, with a layer of fine sand between 0.7 and 1.2 m depth. As the soil sample has been taken at the exact location of the project (Karwijhof), and the heating grid is relatively small, it can be assumed that the sample is representative for the entire heating grid.

In figure 4.12, the groundwater level of Nagele is show. It is clear that the groundwater level is quite high, thus it is assumed that the ground surrounding the pipes is saturated. Hamdhan

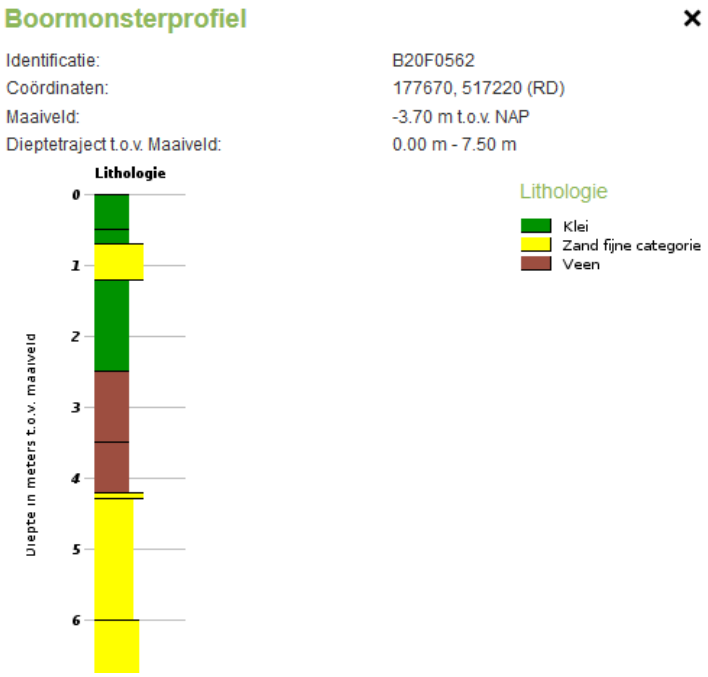

Figure 4.11: Ground composition in Nagele [28]. At the project location, the soil consists of a layer of clay up to 0.7 m depth, then a layer of fine sand up to 1.2 m, clay again till 2.5 m, and then peat till 4.2 m.

& Clarke [16] found thermal conductivity values of 1.52 $\frac{W}{m*K}$ for saturated (China) clay, and 2.75 $\frac{W}{m*K}$ for saturated fine sand. However, it is hard to pin an exact value for thermal conductivity to saturated clay and fine sand from literature due the vast amount of different specific types of clay and sand. For example, van der Hoeven & Lablans [30] list thermal conductivity values of 1.0 $\frac{W}{m*K}$ for clay and 2.0 $\frac{W}{m*K}$ for wet sand. Regardless, it can be said that clay in general has lower thermal conductivity. Thus, if possible, the pipelines should be laid above 0.7 m in order to minimize losses. Since typical burial depths of the distribution part of DHS is roughly between 0.6 and 1 m, a burial depth of 0.6 m is assumed.

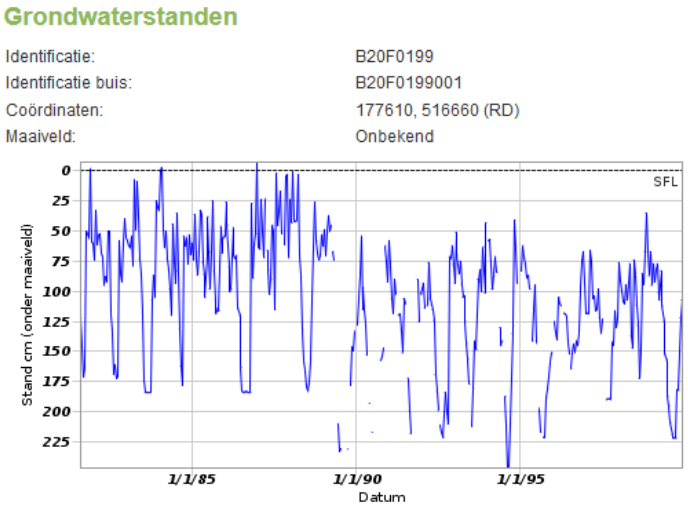

Figure 4.12: Ground water depth chart at the project location in Nagele [28], which shows the groundwater depth to typically be between 0 and 2.5 m depth.

4.5.3. Sizing

Energy in the network is transported from and to consumers through pipelines. The pipelines will have to be dimensioned to the appropriate diameter which balances costs, heat losses, and required pumping power. Generally, it can be said that CAPEX is directly related to the material, pipe diameter and the amount of insulation of the pipelines. Heat losses depend on pipe diameter, insulation, and soil conditions (depth, conductivity). The required pumping power is proportional to the pressure losses caused by friction. This friction is dependent on pipe inner diameter, fluid flow speed (which is proportional to the diameter) and surface roughness of the pipe.

For simplicity's sake, the pipelines are sized by imposing a limit on the fluid velocity. In picking an appropriate maximum fluid velocity, it is important to understand that peak power (and thus peak fluid velocity) only rarely occurs in the network. The average power is much lower. Therefore, the economic optimum peak fluid velocity will be relatively high. The pipelines are sized so that this peak fluid velocity does not exceed 2.5 $\frac{m}{s}$. Note that pipe diameters are rounded up to the nearest available diameter, so the real peak velocity will be much lower on most sections. The peak flow rates are of course directly related to the peak power and temperature differences, as expressed equation 4.1.

Two different network configurations are considered in this study: A steel 2-line heating network where the solar collectors feed in to the heating network, and a 4-line network consisting of 2 PE heating pipes and 2 steel solar pipes. The layout and sizing of the pipelines in these networks is discussed below.

$$\dot{m}_{peak} = \frac{P_{peak}}{C_p * \Delta T} \tag{4.1}$$

Two-line network (configuration I)

The two-line network consists of two steel pipelines. The total required pipe length is 691 m. In table 4.2, the available pipe diameters are shown. The table also shows the flow rate at a fluid velocity of 2.5 $\frac{m}{s}$.

The peak power at every section is determined by either the maximum heating load (space heating + DHW) during cold days, or by the maximum solar yield during hot sunny days, since the solar collectors feed in over the network. The ΔT between supply and return for space heating is assumed to be 20 K, while the ΔT for DHW preparation is assumed to be 50 K. The pump of every solar array is chosen so that it can provide enough flow to keep the ΔT at a maximum of 30 K during peak power. The DHW peak demand is assumed to be 1/4 th of the absolute peak, since not all consumers will consume DHW simultaneously.

In figure 4.13, the resulting pipeline topology and dimensions of network I are shown. In total, 185 m of DN32, 165 m of DN25 and 341 m of DN20 is needed. The peak solar power is leading in diameter selection on every section.

Table 4.2: Standard dimensions of pre-insulated steel-PE-PUR pipelines and calculated flow rates at 2.5 m/s [31]

DN	d_o [mm]	d_i [mm]	$\dot{m}_{2.5m/s}$ [kg/s]
20	90	21.7	11.99
25	90	28.5	20.66
32	110	37.2	35.21
40	110	43.1	47.27

Four-line network (configuration I)

The 4-line network consists of a PE heating network to satisfy space heating and DHW loads, and a steel pipeline network to transport the thermal energy generated by the solar collectors to the

Table 4.3: Standard dimensions of Microflex duo pipelines and calculated flow rates at 2.5 m/s [4]

d_o [mm]	d_i [mm]	d_{jacket} [mm]	$\dot{m}_{2.5m/s}$ [kg/s]
25	20.4	160	10.58
32	26.2	160	17.46
40	32.6	160	27.04
50	40.8	200	42.48

buffer. Since the solar yield was leading for diameter selection of the steel pipelines in the 2-line network, the steel network in the 4-line configuration wil be equally sized. Thus, the steel pipeline layout for the 4-line network is shown in figure 4.13.

In table 4.3, general data about the PE pipelines is given. Similar to scaling the steel network, the PE pipelines are scaled using the peak power in the network. The resulting topology is shown in figure 4.14. Concluding, 75 m of DN40, 200 m of DN32, and 416 m of DN25 are needed.

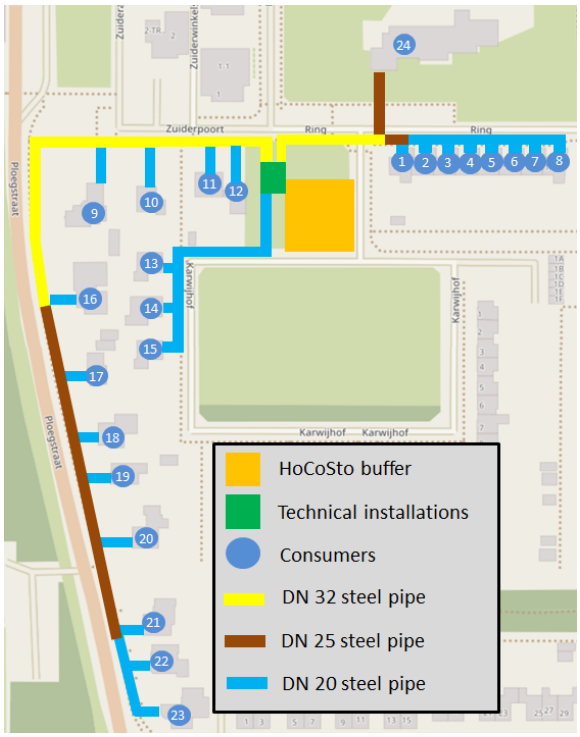

Figure 4.13: Layout of the steel pipe network which shows pipe diameters for every section.

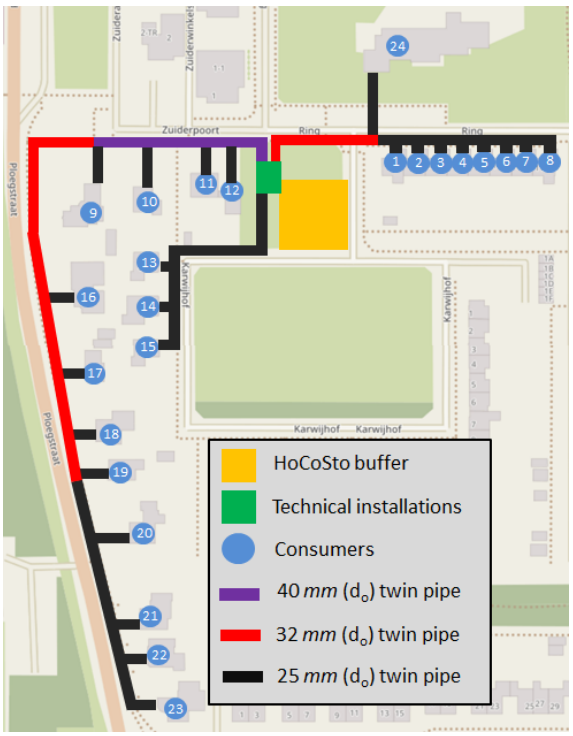

Figure 4.14: Layout of the flexible twin pipe network which shows pipe diameters for every section.

4.6. STES

The seasonal thermal energy storage (STES) to be used in the project in Nagele, is one supplied by the company HoCoSto. It is a pit type of storage, with water as a heat carrier medium. In figure 4.15, the structure of a STES is being placed. This patented aluminum frame allows HoCoSto to install buffers quickly, and cheaper than any other thermal storage solution. Since the frame can carry large loads, the space above the buffer can be used effectively, for example as a parking lot.

The space frame is constructed using aluminium tubes with an outside diameter of 25 mm and a wall thickness of 1.5 mm. The layer height is 600 mm.

In figure 5.3, the shape of the buffer is depicted. For the buffer, it is ideal to have as much height

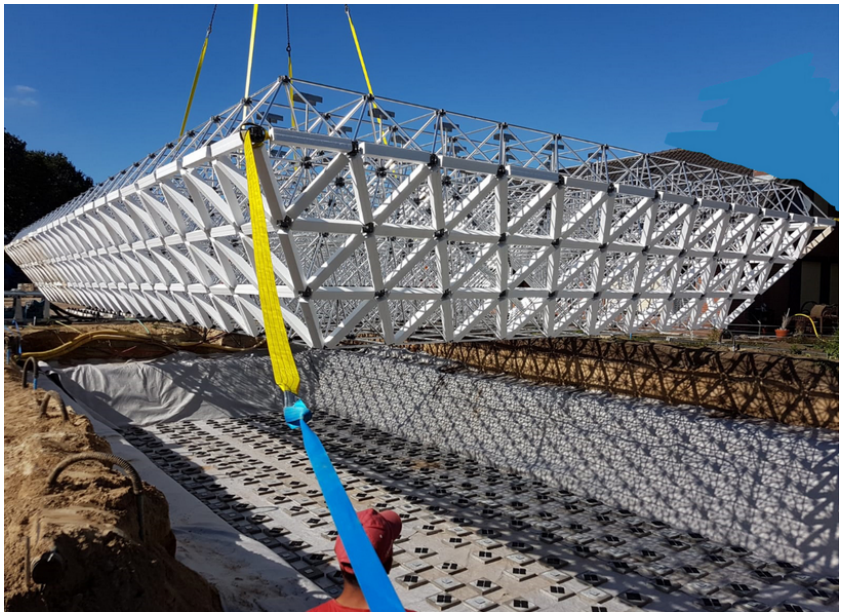

Figure 4.15: HoCoSto STES structure being placed

as possible since this will benefit the thermal stratification. However, due to the soil conditions in Nagele, digging deeper than about 4.5 m would incur large costs (large water pumps would be needed during construction). Since the layer height is fixed at 0.6 m, the total height h is fixed at 3.6 m to allow 0.9 m above the buffer for insulation and a covering layer of soil.

While it would be possible to place several buffers and take advantage of the possibility to keep them at different temperature levels, this is not the focus of this study.

Simple hand calculations show that the buffer size in Nagele will be about 1000-2000 m^3. The width has been fixed at 20 m, resulting in a length of roughly 20-40 m. The buffer will feature no heat exchangers. Instead the system is open, meaning that the fluid inside the buffer will circulate through the DHS. The reason a system without heat exchangers was chosen, is that there will always be a temperature difference over the heat exchanger resulting in a lower system efficiency. Discharging the buffer is done by extracting fluid from the top of the buffer and returning it to the bottom of the buffer. Charging is done the other way around.

The buffer system will be insulated on all sides using XPS (extruded Polystyrene) with a thermal conductivity of 0.035 $\frac{W}{m*K}$. The insulation thicknesses on the bottom, sides, and top will be 0.15, 0.25, and 0.4 m, respectively. Additionally, on top of the buffer there will be 0.5 m of soil. As per experiment, for the buffer in Nagele there will be a thin layer of Argon gas laying directly above the water level, however, the potential effects of this presumably insulating gas are not included in this study.

5

Matlab/Simulink Model

In order to assess which variations in the heating network will benefit the overall performance of the system, the entire system is modelled in a Matlab/Simulink environment.

Apart from answers to the research questions, a key deliverable of this research is an elaborate model of a district heating system with solar thermal generation and thermal energy storage. It is imperative to obtain such a model in order to properly optimize the entire system. For instance, the model could easily be utilized to quantify the benefits of additional pipeline insulation, additional storage volume, or more efficient solar collectors. The entire model is constructed in coordinated universal time (UTC). Note that UTC is not equal to Dutch time.

This chapter gives an overview of the model and its components. Section 5.1 covers the consumers, 5.2 the solar collectors, 5.3 the buffer, 5.5 the pipelines, 5.6 the heat pump and 5.7 the control.

In the model, weather data is present for the period from 01-01-2008 till 31-12-2016. The results presented in this study result from 5-year simulations run from 01-01-2008 till 31-12-2012. Because it is important to have realistic buffer temperatures at the start of the simulation, the first year is not used in the results.

5.1. Consumers

In order to simplify the model and reduce simulation times, the amount of consumers in the network has been reduced from 24 to 6. The consumers, as shown in figure 4.1, are grouped in clusters. The 6 clusters consist of:

- Cluster 1: Consumers 1 to 8
- Cluster 2: Consumers 9 to 12
- Cluster 3: Consumers 13 to 15
- Cluster 4: Consumers 16 to 20
- Cluster 5: Consumers 21 to 23
- Cluster 6: Consumer 24

The clusters are chosen to be as such based on the type and size of the dwellings, as well as their locations. For every cluster, all heat flows (space heating, hot water demand and solar generation) are simulated. As a result, the mass flow and inlet/outlet temperatures at every consumer level are calculated.

The annual energy consumption of the consumers has been derived from their gas consumption, given in table 4.1. After subtraction of presumed reductions due to further insulation, as mentioned in 4.2, the annual energy consumption is simply calculated by multiplying the annual gas consumption with the energy content of the natural gas, and the efficiency of a typical gas boiler.

The resulting annual energy consumption consists of the space heating demand and DHW energy demand.

Since the network is branched and bidirectional, fluid flows will occur directly between the solar collectors and the space heating and DHW heat exchangers. Therefore, it cannot simply be assumed that the inlet temperatures of the DHW and space heating heat exchangers are equal to the network supply temperature, and neither can it be assumed that the inlet temperature of the solar collectors is equal to the network return temperature. For that reason, the fluid temperatures at the consumer level are calculated for each timestep depending on the fluid flows (and their inlet/outlet temperatures) through each of the three heat exchangers at the consumers, and the flow to or from the network. For example, when the supply temperature of the network is 60 $^{\circ}C$, the solar collectors operate at an outlet temperature of 80 $^{\circ}C$ and 5 $\frac{L}{min}$, the DHW heat exchanger would have an inlet temperature of 70 $^{\circ}C$ at 10 $\frac{L}{min}$. This is especially relevant for the solar collector efficiency, since it is very dependent on the inlet temperature.

5.1.1. DHW consumption

The heating load consists not only of space heating, but also of the production of domestic hot water (DHW). According to Fuentes et al. [14] and van Vliet et al. [32], the share of DHW production in the total heat demand of dwellings has been increasing for the past years due to higher frequency and longetivity of showers and reductions in space heating demand due to improvements in insulation. Fuentes et al. [14] thoroughly explore DHW consumption profiles, and offer an extensive literature summary on the differences in DHW consumption between demographic groups. For example, household income is found to be strongly related to DHW usage profiles, while age and household size show strong positive correlations with DHW consumption.

Based on this research, demand profiles are generated for all consumer clusters. The demand is separated into three different categories: Showers, baths and tapping (kitchen etc.). The flow rates expressed in $\frac{L}{min}$ of 45 $^{\circ}C$ for showers and baths, and 55 $^{\circ}C$ for tapping. Variations are given between households in time of occurrence, longevity, and flow rate. The means are based on DIN 1988-300 [14], which indicates that the average flow rates for shower heads, baths and sinks are 7.5, 9 and 4 $\frac{L}{min}$, respectively. The average drawn volume per household per day is 80, 20 and 28 $\frac{L}{day}$ for showers, baths and sinks, respectively.

The heat exchangers for DHW production are scaled so that at maximum power, the temperature difference over the exchanger is 5 K. Since $P_{max} = UA * \Delta T_{max}$, UA (in $\frac{W}{K}$) is easily calculated. In reality UA will vary for different flow rates, however, since the flow rate over the DHW heat exchanger always operates in roughly the same order of magnitude, these differences are assumed to be negligible. The fixed UA value for every heat exchanger is used to calculate the mean temperature difference over the heat exchanger for every timestep (e.g. if a heat exchanger's UA is 500 $\frac{W}{K}$, and the power is 2 kW, the ΔT will be 4 K).

The heat loss in the pipelines of the consumers (between heat exchanger and tapping point) is assumed to be 1 K. The cold water inlet temperature is set equal to the ground temperature at 1 m depth, since the uninsulated water pipelines lay roughly at that depth and thus assume approximately the ground temperature. Hourly soil temperature data has been retrieved from the KNMI for the location Marknesse, which is about 13 km from Nagele. It is found that the temperature will vary roughly between 6 and 18 $^{\circ}C$. Finally, it is assumed that massflows on both sides of the DHW heat exchanger are equal.

In figure 3.2, the three different DHW concepts are shown. All three concepts are built into the

same model. By means of a multiport switch controlled from the Matlab workspace, a DHW concept can be chosen to model.

Boiler electricity consumption

One of the most important differences between DHW concepts, will be boiler electricity consumption. The energy consumption of the electric boilers consists of both energy delivered and heat losses. Since the boilers are kept at a constant temperature, the heat losses of the boiler are introduced as a fixed loss. The loss equals 20 W for the small boilers, and 35 W for the big boilers. The power delivered by the electric boilers is given by equation 5.1.

Equation 5.2 gives the power delivered by the boilers for DHW concepts B. This equation is based on equation 5.1. In this equation, T_{out} is set equal to the hot water temperature in the kitchen, $T_{kitchen}$.

The inlet temperature of the boiler is equal to the outlet temperature of the heat exchanger. Because the mass flows on both sides of the heat exchanger are equal, the outlet temperature of the DHW side of the heat exchanger is equal to the inlet temperature on the network side, $T_{HE_{in}}$, minus the mean temperature difference over the heat exchanger.

The power delivered by the boiler for DHW concept C is given by equation 5.3. The power delivered to the bathroom is calculated using the same approach as equation 5.2, and subsequently the power delivered to the kitchen is added with the term P_{boiler_B}

Note that the total power delivered is not equal to the electrical power consumption. Instead, the electrical energy consumption is equal to the total power delivered plus heat losses of the boiler.

$$P_{boiler} = \dot{m} * C_p * (T_{out} - T_{in}) \tag{5.1}$$

$$P_{boiler_B}(t) = \dot{m}_{kitchen}(t) * C_p * (T_{kitchen}(t) - (T_{HE_{in}}(t) - \frac{P_{HE}(t-1)}{UA_{DHW}})) \tag{5.2}$$

$$P_{boiler_C}(t) = \dot{m}_{bathroom}(t) * C_p * (T_{bathroom}(t) - (T_{HE_{in}}(t) - \frac{P_{HE}(t-1)}{UA_{DHW}})) + P_{boiler_B}(t) \tag{5.3}$$

DHW heat exchanger power and mass flow

The power delivered by the heat exchanger is equal to the total DHW power, $P_{DHW_{total}}$, minus the power delivered by the boiler, P_{boiler}. this is shown in equation 5.4. The total DHW power is defined by the temperature differences between the cold water inlet (equal to the soil temperature, as elaborated on above) and the hot water outlet.

The mass flow on the network side of the DHW heat exchanger is equal to the power P_{HE}, divided by the ΔT and Cp, shown in equation 5.5.

$$\begin{aligned} &P_{HE}(t) = P_{DHW_{total}}(t) - P_{boiler}(t) = \\ &((T_{kitchen}(t) - T_g(t)) * \dot{m}_{kitchen}(t) + (T_{bathroom}(t) - T_g(t)) * \dot{m}_{bathroom}(t)) * C_p - P_{boiler}(t) \end{aligned} \tag{5.4}$$

$$\dot{m}_{HE}(t) = \frac{P_{HE}(t)}{(T_{HE_{in}}(t) - \frac{P_{HE}(t)}{UA_{DHW}} - T_g(t)) * C_p} \tag{5.5}$$

5.1.2. Space Heating

For the component space heating, it is not only important to know the power required by the consumers, but also the mass flows and temperatures of these mass flows. Therefore, a heating system is modelled for every cluster. Figure 5.1 shows the energy balance which is made for the clusters.

For each time step, the room temperature is updated using the heat flows in and out of the house. Equation 5.6 represents this energy balance. The different components of this energy balance are elaborated on below.

$$T_{house}(t) = T_{ini} + \int_0^t \frac{P_{heating}(t) + \dot{Q}_D(t) + \dot{Q}_B(t) - \dot{Q}_{shell}(t)}{mc_{house}} dt \tag{5.6}$$

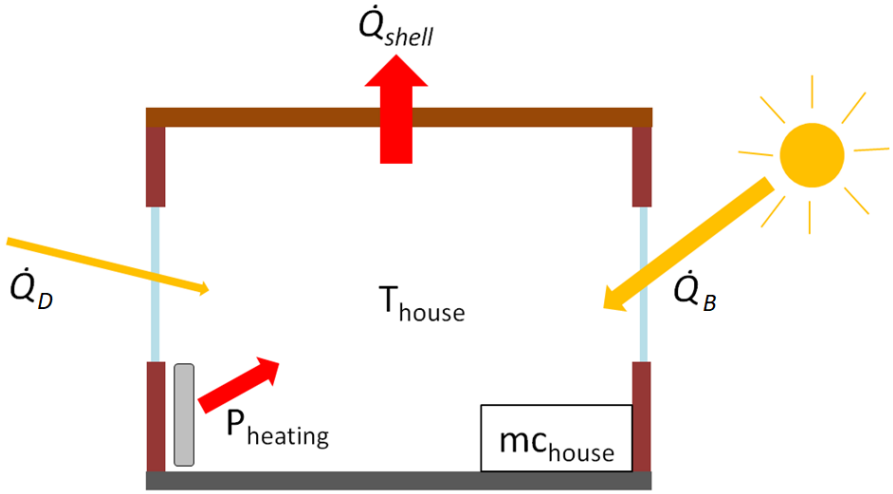

Figure 5.1: Energy balance of a consumer, with the beam and diffuse solar gains, heat losses through the shell and heating gains

Solar irradiance

In the Karwijhof in Nagele, all houses are aligned with wind directions, therefore, solar irradiance only has to be calculated for four directions: North, east, south and west.

The beam and diffuse solar gain through the windows are given by equations 5.7 and 5.8. The terms G_B and G_D are the beam and diffuse solar powers on the window surfaces in $\frac{W}{m^2}$. These terms are calculated for every wind direction using the solar model also used for the solar collectors, which is discussed in more detail in section 5.2. Subsequently, the total heat gain is calculated by multiplying these terms with the window surface A_{win}, transmittance τ_{win} and a shading factor $f_{shading}$. The window surface areas and shading per dwelling have been estimated using Google street view. The summed areas per cluster are shown in table 5.1.

Table 5.1: Window area for each cluster

Cluster	North facing [m²]	East facing [m²]	South facing [m²]	West facing [m²]
1	16	0	20	0
2	16	8	8	12
3	3	6	9	9
4	22	10	8	20
5	20	10	10	8
6	10	3	12	4

$$\dot{Q}_B(t) = f_{shading} * G_B(t) * A_{win} * \tau_{win} \tag{5.7}$$

$$\dot{Q}_D(t) = f_{shading} * G_D(t) * A_{win} * \tau_{win} \tag{5.8}$$

Shell heat losses

The shell heat losses are calculated using a linear heat loss coefficient UA, yielding a total heat loss through the shell of $Q_{shell} = (T_{house} - T_{amb}) * UA$.

The model itself is used to find a proper value of UA. Since the solar gains, heating power response and heat capacity of the house are defined, the only remaining variable leading to the annual energy consumption is the heat loss through the shell. The annual energy consumption of the consumers is known (through their gas consumption, as discussed before), and the DHW consumption has been defined, the annual energy required for space heating can be derived using the model.

The gas boiler efficiency used to estimate the annual energy consumption is 90 % of the higher heating value (35.17 $\frac{MJ}{m^3}$). This might seem on the low side given that HR104 boilers have a minimum efficiency of 94 %, and HR107 boiler of 96 % of the HHV. However, these are rated efficiencies, which are measured using return temperatures of 35 $^\circ C$. The radiators as used in Nagele typically have much higher return temperatures (which decrease the efficiency). Also, DHW production achieves much lower efficiencies than the rated efficiency. Therefore, 90 % is assumed to be a conservatively high estimate.

For the UA, an initial guess is made based on literature like Purdy & Beausoleil-Morrison [22] and van Miltenburg [31]. Subsequently, the annual energy consumption (including DHW) calculated by the model is compared to the gas-derived consumption. The UA is then adjusted accordingly. After three iterations, an error of <1% was obtained for every cluster. The obtained UA values, shown in table 5.2, remain in good accordance with literature.

Table 5.2: Obtained UA of every cluster

Cluster	UA [W/K]
1	1045
2	825
3	615
4	1210
5	970
6	1160

Heating power

For every cluster, a thermostat and heating system have been modelled. The thermostat settings vary per cluster. Appropriate thermostat settings are included in the model to replicate morning and evening peaks. When the interior temperature drops below the thermostat setting, the heating system is activated. Because the network flow is to be limited, and the ΔT between supply and return to be maximized, the system is made to have variable power (instead of an on/off system). This is done by allowing the valve on the network side of the heat exchanger to be able to partially open.

Obviously, the power of the radiators varies with inlet, outlet and ambient temperatures. This is calculated using equation 5.9 according to BS EN442. It gives the heating power of the radiators based on supply and return temperatures T_{in} & T_{ret} and P_{50}; The nominal heating power which is defined as the power during 75/65/20 operation (75 $^\circ C$ inlet, 65 $^\circ C$ outlet, 20 $^\circ C$ ambient). The radiator constant, n, is 1.33 for the standard panel radiators as installed in the Karwijhof.

$$P_{heating}(t) = P_{50} * \left(\frac{T_{in}(t) - T_{return}(t)}{ln\left(\frac{T_{in}(t) - T_{amb}(t)}{T_{return}(t) - T_{amb}(t)}\right) * 49.32}\right)^n \tag{5.9}$$

P_{50} is estimated based on equation 5.10 from BS EN442. and the assumption that for an outdoor temperature of -10 $^\circ C$, the current heating systems are able to provide sufficient heating power to

keep the dwellings at an interior temperature of 22 $^{\circ}C$, while operating on a radiator supply temperature of 70 $^{\circ}C$ and a return temperature of 50 $^{\circ}C$. The obtained values for P_{50} are shown in table 5.3. The flow over the heat exchanger is limited by the constraint that a ΔT of at least 10 K between supply and return is to be achieved. This constraint prevents consumers near the pumps from taking so much flow that consumers further from the pumps are unable to heat their homes.

$$P_{50} = (T_{room} - T_{amb}) * UA * (\frac{T_{in}(t) - T_{return}(t)}{ln(\frac{T_{in}(t)-T_{amb}(t)}{T_{return}(t)-T_{amb}(t)}) * 49.32})^{-n} \tag{5.10}$$

Table 5.3: Obtained P_{50} of every cluster

Cluster	P_{50} [W]
1	48812
2	38536
3	28727
4	56519
5	45309
6	54184

5.1.3. Validation consumer model

The consumer model is pretty straightforward. Below, some aspects of the model are considered and compared to literature in order to assess if the model obtains realistic data.

DHW consumption

The DHW consumption in $\frac{L}{year}$ is in accordance to findings by Fuentes et al. [14]. Also, the average daily energy consumption for the DHW according to the model is found to be 5.62 $\frac{kWh}{day}$ per household. This compares well with the European norm EN 16147:2011, which gives an indication of 5.85 $\frac{kWh}{day}$ for a medium sized European household.

DHW boiler electricity consumption

The electricity consumption of the boiler consists of standing heat losses, and the power delivered. For DHW concept B, the standing losses are 175 $\frac{kWh}{year}$, and the energy delivered is 32 $\frac{kWh}{year}$, which equates to about 1.6 % of the total DHW energy consumption. This seems low, but for concept B, the electric boiler only has to supply a slight amount of supplementary heat to the kitchen tapping water, which is about 12.6% of total DHW energy demand according to Yang & Svendsen [36]. Therefore, the electric boiler supplies about 13 % of the DHW tapping energy, which seems appropriate.

For concept C, the electric boiler also supplies a small part of the DHW energy for sanitary purposes. The energy consumption according to the model is 133 $\frac{kWh}{year}$, or about 6.5 % of the total DHW energy consumption. This seems reasonable since the DHW for sanitary purposes, which makes up the bulk of the energy demand, only has to be heated a couple of degrees. The standing heat losses are 307 $\frac{kWh}{year}$, which is in line with manufacturer data.

Space heating

The UA values in table 5.2 result in values per dwelling between 131 $\frac{W}{K}$ for the smaller row houses, and 243 $\frac{W}{K}$ for the larger, detached houses. These values are in agreement with values obtained by van Miltenburg [31] for the type and size of dwellings.

The nominal radiator heating powers, or P_{50}'s, according to table 5.3 vary between 6.1 kW for the smaller row houses and 15.1 kW for the larger detached houses. After a visit to Nagele, it is

concluded that these values are realistic based on the amount and sizes of radiators in the dwellings.

5.2. Solar

The system is to be designed so that almost all energy is generated by the solar collectors. There will only be a relatively small amount of electricity consumption to power the circulation and heat pumps, the auxiliary heater, and, in case of boiler implementation, some supplementary energy for DHW production.

One goal of these simulations is to find the optimum amount of solar collectors. This is done by modelling every configuration for several solar areas. The optimium sizing is then picked based on LCOH.

Hand calculations using annual yield data from the solar collector datasheet show that covering all available unshaded rooftop areas of the dwellings is not entirely sufficient to cover overall demand. Therefore, the rooftop of consumer 24 (a former school building) is used to fill the remaining demand.

5.2.1. Solar irradiance

To calculate the output of the solar collectors, solar irradiance data is needed. While ground measurement data can provide easy and reliable datasets, these are often only expressed in one term, the global horizontal irradiance (GHI). In order to calculate the output of the solar collectors, the direct normal irradiance (DNI) and diffuse horizontal irradiance (DHI) are needed. This data is obtained from satellite measurement data, specifically the SARAH dataset from PVGIS [10].

The position of the sun and the angles and power of beam radiation on the inclined surfaces have been modelled using methods described by Duffie & Beckman [7]. The amount of diffuse radiation on the surfaces is calculated using formula 5.11 by Temps & Coulson [27].

$$G_D = 0.5 * I_{DHI} * (1 + cos(\kappa)) * (1 + sin^3(\kappa/2)) * (1 + cos^2(AOI) sin^3(\phi)) \tag{5.11}$$

The solar model has been verified using PVGIS [10], a solar modelling tool developed by the European commission.

5.2.2. Solar Collectors

The solar collector output is modelled per timestep, depending on the solar irradiance and the solar collector efficiency.

The efficiency of the solar collectors is modelled according to the standard EN 12975-2, which is outlined by Kovacs [19] and Perers et al. [21]. According to Kovacs [19], EN 12975-2 has replaced all national standards in Europe, while ISO 9806 (a norm surrounding fluid heating solar collectors) is currently being revised taking into account knowledge gained during the development of EN 12975.

In EN 12975, two methods are described: The steady state method, and the quasi dynamic test method. The most important improvement of the quasi dynamic test method over the steady state method is the distinction between direct and diffuse radiation with an incidence angle modifier $K_{\theta B}(\theta_L, \theta_T)$ for direct, and $K_{\theta D}$ for diffuse irradiance. The incidence angle modifiers adjust the efficiency of the solar collector for a given incidence angle. It is defined as the efficiency at the given incidence angle divided by the efficiency at normal incidence. According to Kovacs [19], the distinction between incidence angle modifiers for direct and diffuse irradiance is quite relevant for evacuated tube collectors. Therefore, the quasi dynamic method, given by formula 5.12, is used to calculate the output of the collectors.

$$\dot{Q}/A = F'(\tau\alpha)_{en}K_{\theta B}(\theta_L,\theta_T)G_B + F'(\tau\alpha)_{en}K_{\theta D}G_D - c_6uG - c_1(T_m - T_{amb}) - c_2(T_m - T_{amb})^2 - c_3u(T_m - T_{amb}) + c_4(E_L - \sigma T_{amb}^4) - c_5 dT_m/dt \quad (5.12)$$

The solar collectors used in the project are direct flow evacuated tube collectors of the type ATON G1800 22-O from the supplier Kloben Industries. In table 5.4, the quasi dynamic performance indicators, as given by the supplier, are shown. It can be seen that both the wind speed dependence, described by c_3 and c_6, as well as the long wave irradiance dependence c_4 are zero. Scrapping these terms from equation 5.12 yields equation 5.13.

Table 5.4: Kloben Industries direct flow evacuated tube quasi dynamic performance parameters

Coefficient	Value	Unit	Description
η_0	0.641	–	*Steady state parameter for zero loss efficiency*
$K_{\theta D}$	0.972	–	*Incidence angle modifier for diffuse radiation*
c_1	0.935	$\frac{W}{(m^2K)}$	*Heat loss coefficient at* $(Tm - Ta) = 0$
c_2	0.004	$\frac{W}{(m^2K^2)}$	*Temperature dependence of heat losses*
c_3	0.000	$\frac{J}{(m^3K)}$	*Wind speed depence of heat losses*
c_4	0.000	–	*Long wave irradiance dependence on heat losses*
c_5	37.99 × 10^3	$\frac{J}{(Km^2)}$	*Effective thermal capacitance*
c_6	0.000	$\frac{s}{m}$	*Wind dependence of zero loss efficiency*

$$\dot{Q}/A = F'(\tau\alpha)_{en}K_{\theta B}(\theta_L,\theta_T)G_B + F'(\tau\alpha)_{en}K_{\theta D}G_D - c_1(T_m - T_{amb}) - c_2(T_m - T_{amb})^2 - c_5 dT_m/dt \quad (5.13)$$

$$F'(\tau\alpha)_{en} = \frac{\eta_0}{K_{\theta B}(\theta = 15°) * 0.85 + K_{\theta D} * 0.15} \quad (5.14)$$

In equation 5.13, $F'(\tau\alpha)_{en}$ is the collector efficiency factor times effective transmittance-absorptance product (the product of the cover transmittance and the absorber-plate absorptance). $F'(\tau\alpha)_{en}$ can be calculated from the steady state zero loss efficiency parameter η_0 and incidence angle modifiers using equation 5.14. It is assumed that for the testing of η_0, the direct irradiance was 85%, and the diffuse irradiance 15%. This assumption is based on findings by Kovacs [19]. On the left hand side of equation 5.13, $\dot{Q}/A$, represents the power per square meter in $\frac{W}{m^2}$, while on the right hand side, $K_{\theta D}$, c_1, c_2 and c_5 are given in table 5.4. The incidence angle modifier for direct radiation, $K_{\theta B}(\theta_L,\theta_T)$, can be calculated by multiplying the transversal ($K_{\theta T}$) and longitudinal ($K_{\theta L}$) incidence angle modifiers as given in table 5.5. G_B and G_D are the direct (beam) and diffuse irradiance on the gross area in $\frac{W}{m^2}$, respectively. With the gross area being the maximum projected area of the collector, not including connections and parts for mounting. Finally, T_{amb} is the ambient temperature in K, and T_m is the mean temperature of the collector, calculated as $T_m = \frac{T_{in}+T_{out}}{2}$, also in K.

Table 5.5: Kloben Industries direct flow evacuated tube incidence angle modifiers

Angle	10^0	20^0	30^0	40^0	50^0	60^0	70^0	80^0	90^0
$K_{\theta T}$	1.00	0.99	1.00	1.01	1.09	1.10	1.29	0.65	0.00
$K_{\theta L}$	1.00	0.99	0.97	0.95	0.90	0.81	0.66	0.33	0.00

5.2.3. Validation solar model

The solar model is validated by comparing the output and efficiency of the solar collectors in the model to ISO data from the manufacturer datasheet. First, the static output is compared to the fixed output according to the datasheet at 850 $\frac{W}{m^2}$ direct, and 150 $\frac{W}{m^2}$ diffuse radiation. Output data of the solar collector model matches within a 1 % error with datasheet numbers.

Additionally, the annual collector output at fixed mean fluid temperatures is taken as a benchmark. For the Kloben collectors, the annual output is given for the location Wurzburg facing directly south at a slope of 35 degrees. The outputs at this location are 742, 646 and 552 $\frac{kWh}{m^2}$ per year for mean fluid temperatures of 25, 50 and 75 $^\circ C$, respectively. In order account for the differences in annual irradiance between the locations, the output is compared based on efficiencies.

The datasheet outputs listed above correspond with efficiencies of 59.6, 51,9 and 44.4 % at mean fluid temperatures of 25, 50 and 75 $^\circ C$, respectively. When feeding these mean fluid temperatures into the solar model, the resulting annual efficiencies (calculated over a period of 8 years) are 57, 48.2 and 39.9 %, respectively. These slightly lower efficiencies are explained by the fact that during summer (when output is highest), ambient temperatures in Wurzburg are higher than those in Nagele.

In the complete model where the solar collectors are coupled to the consumers and the buffer, the mean collector temperatures are variable. In figure 5.2, the solar yield is shown for configuration 1-A. It can clearly be seen that the yield is highest in early summer. This is because the buffer temperatures (thus solar feed in) are low in the early summer. As the buffer temperature increases over the summer, the yield decreases. The same effect is observed for every configuration.

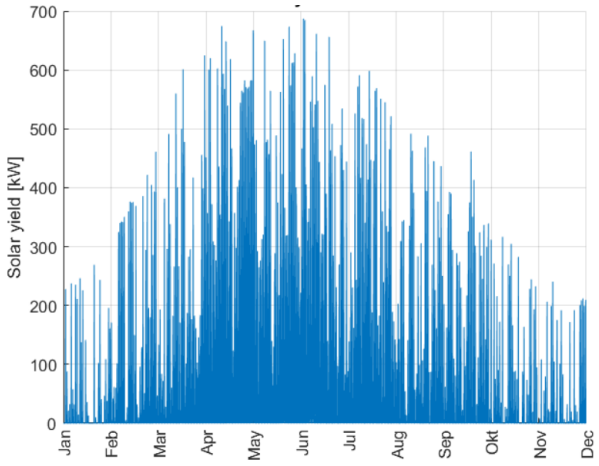

Figure 5.2: Yield of solar collectors in the system in 2008, configuration 1A, with 1000 m^2 solar area

5.3. Buffer

At the heart of the system rests the HoCoSto seasonal thermal energy storage buffer. The general shape of the buffer is shown in figure 5.3. As elaborated on in section 4.6, the height h is fixed at 3.6 m and width a at 20 m. The angle of the sides is 45 degrees, resulting in

$$a = a_1 + 2 * h$$

$$b = b_1 + 2 * h$$

Therefore, the only variable tied to the volume is b. The volume is found resulting from the volume of a simple rectangular pyramid.

$$V_{buffer} = \frac{1}{3} * a * b - \frac{1}{3} * a_1 * b_1 \tag{5.15}$$

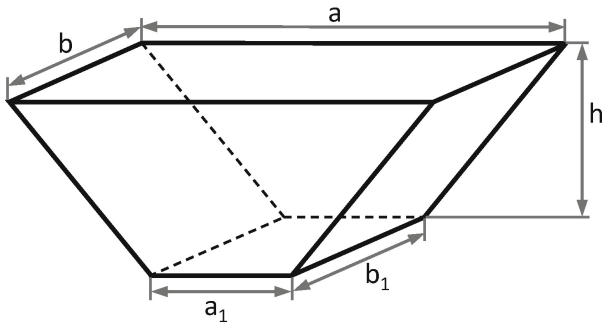

Figure 5.3: HoCoSto STES Shape

In order to be able to implement different temperature levels at various heights in the buffer, it has been divided into n nodes. For every node, an energy balance is kept. In figure 5.4, all energy and mass flows are shown. Note that no heat exchangers are used. The height of the nodes is set to be equal, resulting in different volumes for every node. Generally, the top nodes will be warmer than the lower nodes due to density differences, this is referred to as thermal stratification.

For all nodes, for every time step, the temperature of each node is updated according to formula 5.16. Note that all flows out are expressed as being positive.

$$T_{node}(t) = T_{ini} - \int_0^t \frac{P_{flow}(t) + \dot{Q}_{node}(t) + \dot{Q}_{side}(t) + \dot{Q}_{mix}(t)}{mc_{node}} dt \tag{5.16}$$

Thermal conductivity through the shell

Heat losses occur through the top, bottom and sides of the buffer. This is depicted in figure 5.4 as $\dot{Q}_{top}$, $\dot{Q}_{bot}$ and $\dot{Q}_{side}$, respectively. These losses are given by equations 5.17, 5.18 and 5.19. Details on insulation thicknesses s and their thermal conductivity, λ, are given in section 4.6. The top and bottom areas, as well as side areas of every node are calculated using simple geometry. The most complex part is finding appropriate values for T_{soil}. It is assumed that this soil temperature is equal to the undisturbed ground temperature (data taken from the KNMI [18]) plus 5 K. This seems to be a reasonable assumption based on measurements done at existing HoCoSto buffers. The resulting soil temperature directly outside of the buffer would vary between roughly 10 and 23 $^\circ C$.

$$\dot{Q}_{top}(t) = \frac{\lambda_{top}}{s_{top}} * A_{top} * (T_{top}(t-1) - T_g(t)) \tag{5.17}$$

$$\dot{Q}_{bot}(t) = \frac{\lambda_{bot}}{s_{bot}} * A_{bot} * (T_{bot}(t-1) - T_g(t)) \tag{5.18}$$

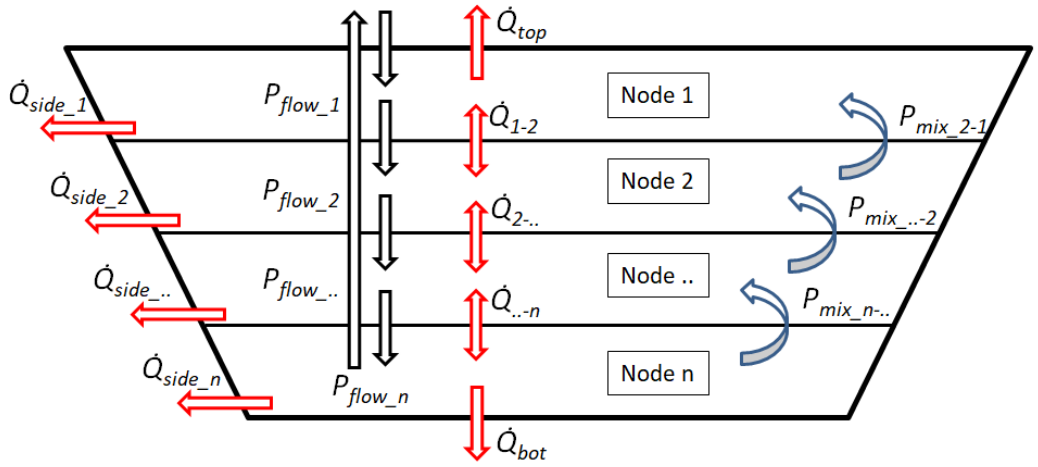

Figure 5.4: Schematic of buffer heat and mass flows

$$\dot{Q}_{side}(t) = \frac{\lambda_{side}}{s_{side}} * A_{side} * (T_{node}(t-1) - T_g(t)) \tag{5.19}$$

Conductivity between nodes

Because node temperatures will differ from each other, there will be conduction between nodes through both the water as well as through the aluminium frame. The HoCoSto buffer consists of evenly spaced aluminum rods with water in between, therefore the conductivity coefficient through the buffer can simply be calculated using the relation of cross section between water and aluminum. This relation is roughly 0.016% aluminum, 99.984% water. Assuming the thermal conductivity of the aluminum to be temperature independent 190 $\frac{W}{m*K}$, equation 5.20 can be used to calculate the resulting thermal conductivity, which is given in table 5.6.

$$\lambda_{buffer}(T) = 0.99984 * \lambda_{water} + 0.00016 * \lambda_{aluminum} \tag{5.20}$$

Table 5.6: Thermal conductivity of water and HoCoSto buffer for different temperatures

T_{water} [C]	λ_{water} [W/(m*K)]	λ_{buffer} [W/(m*K)]
0.01	0.555	0.585
20	0.598	0.628
40	0.629	0.659
60	0.651	0.681
80	0.667	0.697
99.6	0.677	0.707

Subsequently, equation 5.21 is used to calculate the conduction between the nodes. L_{nodes} is the distance between the centers of the nodes, while $A_{(n,n-1)}$ is the average area between the two nodes.

$$\dot{Q}_{(n,n-1)}(t,T) = \frac{\lambda_{buffer} * A_{(n,n-1)}}{L_{nodes}} * (T_n(t-1) - T_{(n-1)}(t-1)) \tag{5.21}$$

Buffer mixing (convection)

When a node's temperature drops below that of the node below (inverse thermocline), the differences in density will drive mixing between those nodes. It should be noted that simulations without this mixing part included in the model showed inverse thermoclines to be rare. Still, a mixing term P_{mix} has been included in the model to prevent this inverse stratification from occurring. When a node's temperature drops below that of the node below, a large mixing power will completely mix the two nodes, resulting in equal-temperature nodes.

Buffer charging and discharging

The buffer does not have a heat exchanger. When the buffer is in charging operation, there will be a draw from the bottom of the buffer, and an outlet flow to the top of the buffer. During discharging, this flow is reversed. The control of these flows is discussed in more detail in section 5.7.

When mass is subtracted from the bottom, and added to the top (or the other way around), there will be a flow through the buffer. This flow is quantified as a flow power P_{flow} in W, which obviously depends on the flow speed and temperature differences between nodes.

Frost protection

As per design of the buffer, frost has to be prevented. Because the buffer is filled with water, the minimum temperature is 0 $^{\circ}C$. Frost protection will mostly be needed towards the end of the heating season when the buffer temperature is low. This protection is implemented by the introduction of an electric auxiliary heater. It is important to recognise the fact that the buffer cannot be fully discharged by the heat pump alone. This is because the heat pump has to achieve a minimum ΔT over the evaporator in order to reach its nominal power. In the model, the ΔT over the evaporator is fixed at 8 K. Therefore, the auxiliary heater is to be activated when the inlet temperature of the evaporator $T_{evaporator_{in}}$ is lower than 8 $^{\circ}C$. When this holds, the required power of the auxiliary heater is given by equation 5.22.

$$P_{auxiliary} = \dot{m}_{evaporator} * (\Delta T_{evaporator} - T_{evaporator_{in}}) * C_p \tag{5.22}$$

Overheat protection

Overheat protection could be needed late summer and early fall when the buffer is charged and solar irradiation is high. The solar collectors cannot simply be turned off, and the buffer temperature should not exceed 100 $^{\circ}C$ since that would lead to steam formation. This issue has been mitigated by dumping energy when the buffer approaches its boiling point. The amount of dumping required varies widely between different configurations. Configurations with a small buffer and a high amount of solar collectors require a large amount of dumping, while configurations with a relatively large buffer and few solar collectors require no dumping at all.

Dumping energy can be done in various ways. A common way to dump heat is by using radiators to transmit the heat to ambient air. This method is not ideal in this scenario because it would require placing visible equipment above ground in the historic center of the town, and could also lead to noise complaints. Apart from these points, it would require additional investments. Another way is to dump hot water in the sewage system. However, dumping high temperature water is not allowed in the Netherlands, so it would need to be mixed to an allowed temperature, leading to higher fresh water consumption. The method chosen is to dump the heat using the solar collectors. The solar collectors are insulated, but the large total surface area still results in a very capable heat sink. For example, 1000 m^2 solar collectors at a mean temperature difference of 70 K (solar collectors at a mean of 95 $^{\circ}C$, ambient temperature 25 $^{\circ}C$) would result in a total heat loss of 85 kW. In the model, dumping is activated when the warmest point in the buffer (typically the top node) reaches 97 $^{\circ}C$.

5.3.1. Buffer validation

The heat losses through the sides of the buffer are simply taken as the heat transport through the insulation, assuming that the soil side equals the undisturbed soil temperature plus 5 K. The temperature at the buffer side is simply the temperature inside the buffer. Therefore, the only component which needs validation is the soil temperature. For the given method, the soil temperature outside the buffer would vary between 10 and 23 $^{\circ}C$. This temperature profile corresponds to experiences of HoCoSto. Additionally, laws in the Netherlands prohibit the warming of soil higher than 25 $^{\circ}C$. Therefore, this seems a reasonable assumption.

For the in- and outflows of heat, it is to be expected that all inflows of heat minus all outflows of heat match the energy accumulated in the buffer. This has been verified to be true for both the buffer as a whole, as well as for the individual nodes. Note that the outflow of heat includes the thermal losses.

The only remaining component of the buffer model which needs validation is the temperature gradient in the buffer. The lack of hard measurement data and expected differences between buffer size and use makes this hard to validate. Also, the buffer considered in this study is designed as an open system, while the existing HoCoSto buffers use heat exchangers. Further validation of this aspect of the buffer sub-model is recommended. However, it should be noted that the simulated temperature profiles resemble temperature profiles of existing HoCoSto buffers in both shape and range.

5.4. Circulation pumps

The 2-line DHS considered in this study is different from classic district heating networks mainly because this network is bidirectional. This is achieved by placing a fixed ΔP pump at the central location (in practice several pumps will be installed to achieve redundancy). Only a relatively low ΔP between supply and return is needed since the network size is small, and all consumers are relatively close to the central location. Therefore, pressure losses in the network are low compared to large district heating networks spanning hundreds or even thousands of consumers. The solar arrays at the consumers are outfitted with pumps on the network side which can overcome this pressure difference between return and supply. To reach the objectives of this study, exact pumping powers and pressures are not relevant. Instead, the relevant parameter regarding the pumps is the required annual electrical energy. According to findings by van Miltenburg [31], the pumping energy in modern DHS is generally slightly lower than 1 % of the consumed energy in the system. The DHS studied by van Miltenburg resembles the one in this study both in terms of network size and spacing between dwellings. Furthermore, she also incorporates solar feed-in into the network. Therefore, it has been assumed in this study that the pumping energy is equal to 1 % of the total consumed energy. Note that the impact of pumping energy on the LCOH likely is low, since the resulting pumping energy is around 6000 $\frac{kWh}{year}$, which translates into a couple hundred euros.

Validation

To validate the assumption that pumping power in the DHS will be roughly 1 % of consumed energy, a quick calculation is made to assess how much energy would be consumed to overcome a typical pressure difference in the network for the annually pumped volume. When considering the total consumed annual energy, it is easily obtained that for an average ΔT of 20 K between the supply and return of the network, the annual pumped volume $\dot{V}_{pumpedannual}$ would be roughly 50,000 $\frac{m^3}{year}$ (back and forth). When the pressure differential which is to be overcome is estimated at 200 kPa, and the pump's efficiency η_{pump} at 50 %, equation 5.23 shows that the annual pumping energy $E_{pumpedannual}$ is roughly 5560 kWh. This indicates that the pumping energy as calculated by the submodel is roughly correct. Furthermore, assuming that the pumping energy lies in this order of magnitude, it can also be concluded that the costs of pumping are an insignificantly small

factor in determining the overall costs of the system operation. Therefore, the error in the pumping energy is definitely insignificantly small.

$$E_{pumpedannual} = \frac{\dot{V}_{pumpedannual} * Head_{network} * \rho * g}{\eta_{pump}} \tag{5.23}$$

5.5. Pipelines

As laid out in section 4.5, the two-line system will use two steel-PUR-PE pipelines, while the 4-line system will use two steel-PUR-PE lines for the solar loop, and PE-twin pipelines for the heating network. The layout and sizing of the pipelines is discussed in section 4.5.

One of the most important aspects of the system, are heat losses in the network. This is presumably one of the largest downsides to the double network configuration. Therefore, the heat losses of both the separate steel pipes as well as the twin pipes have to be modelled.

According to Miltenburg [31], the overall heat transfer of common Steel-PUR-PE pipes, is given in equation 5.24

$$UA = L * \frac{1}{\frac{1}{\alpha_{water}} + \frac{1}{2\pi}(\frac{1}{\lambda_{steel}} ln\frac{d_{i,steel}}{d_{o,steel}} + \frac{1}{\lambda_{pur}} ln\frac{d_{i,PUR}}{d_{o,PUR}} + \frac{1}{\lambda_{PE}} ln\frac{d_{i,PE}}{d_{o,PE}} + \frac{1}{\lambda_{soil}} ln\frac{4*H}{d_{o,PE}})} \tag{5.24}$$

Miltenburg [31] notes that α_{water}, λ_{steel} and λ_{PE} are quite high, and therefore the quotients they are a part of can be neglected. She also notes that the insulation value of PUR degrades over time, which can cause thermal losses to increase as the DHS ages.
The governing equation for pipeline losses would then become:

$$UA = L * \frac{1}{\frac{1}{2\pi}(\frac{1}{\lambda_{PUR}} ln\frac{d_{i,PUR}}{d_{o,PUR}} + \frac{1}{\lambda_g} ln\frac{4*H}{d_{o,PE}})} \tag{5.25}$$

However, as noted by Wallenten [33], when pipes are laid in the ground close to each other their heat losses cannot be calculated independently. The problem of two pipes close to each other in the ground, as portrayed by figure 5.5, can be divided into two problems: A symmetrical and asymmetrical problem, where the symmetrical problem represents heat loss from the pipes to the surroundings and the asymmetrical problem heat transfer from one to another pipe. This concept is visualised in figure 5.6.

Steel pipelines

The heat losses from the steel pipelines can be calculated using equations 5.26 and 5.27, respectively. The total heat loss however, is only tied to the symmetrical problem as can be seen in equation 5.28. The symmetrical heat loss formula is given by formula 5.29 for two pipes. The terms h_s^{-1}, T_s and β are given by equations 5.30, 5.31 and 5.32, respectively.

$$q_{supply} = q_s + q_a \tag{5.26}$$

$$q_{return} = q_s - q_a \tag{5.27}$$

$$q_{supply} + q_{return} = 2q_s \tag{5.28}$$

$$q_s = (T_s - T_0) * 2\pi\lambda_g * h_s \tag{5.29}$$

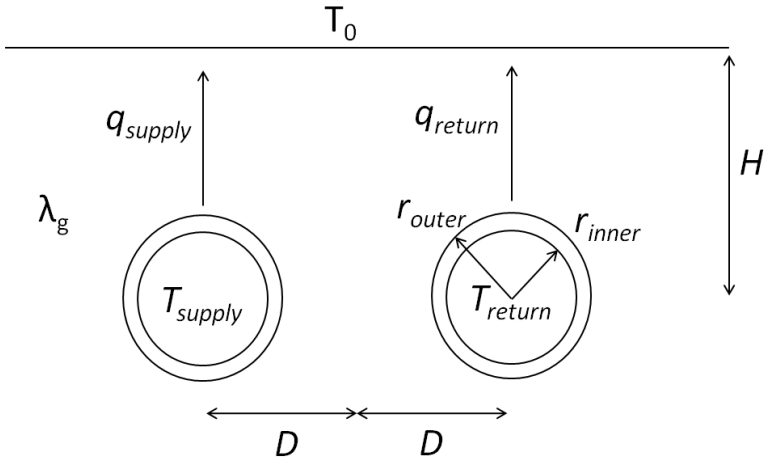

Figure 5.5: Heat loss from two pipes in the ground [33]

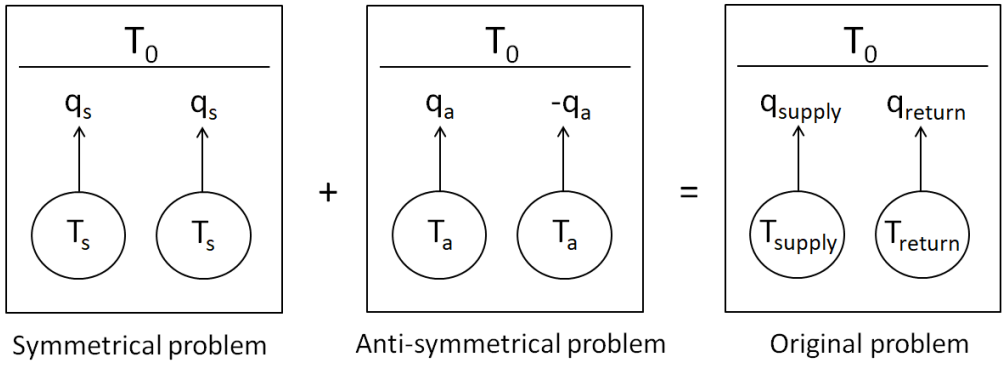

Figure 5.6: Superposition of symmetrical and anti-symmetrical problem [33]

$$h_s^{-1} = \ln\frac{2H}{r_{outer}} + \beta + \ln\sqrt{1+(\frac{H}{D})^2} \tag{5.30}$$

$$T_s = \frac{T_{supply} + T_{return}}{2} \tag{5.31}$$

$$\beta = \frac{\lambda_g}{\lambda_i}\ln\frac{r_{outer}}{r_{inner}} \tag{5.32}$$

Twin pipelines

The heating network in the 4-line network consists of twin pipelines as shown in figure 5.7. In calculating the heat losses, the same approach is taken as for the steel pipelines, however q_s and h_s^{-1} are now calculated by equations 5.33 and 5.34.

$$q_s = (T_s - T_0) * 2\pi * \lambda_i * h_s \tag{5.33}$$

$$h_s^{-1} = \ln\frac{r_{jacket}^2}{2Dr_{inner}} - \ln\frac{r_{jacket}^4}{r_{jacket}^4 - D^4} - \frac{(\frac{r_{inner}}{2D} + \frac{2r_{inner}D^3}{r_{jacket}^4 - D^4})^2}{1+(\frac{r_{inner}}{2D})^2 - (\frac{2r_{inner}r_{jacket}^2 D}{r_{jacket}^4 - D^4})^2} \tag{5.34}$$

While these equations can easily be used to calculate steady state heat losses, implementation in the model is slightly more difficult since both soil surface and fluid temperature are not constant. To

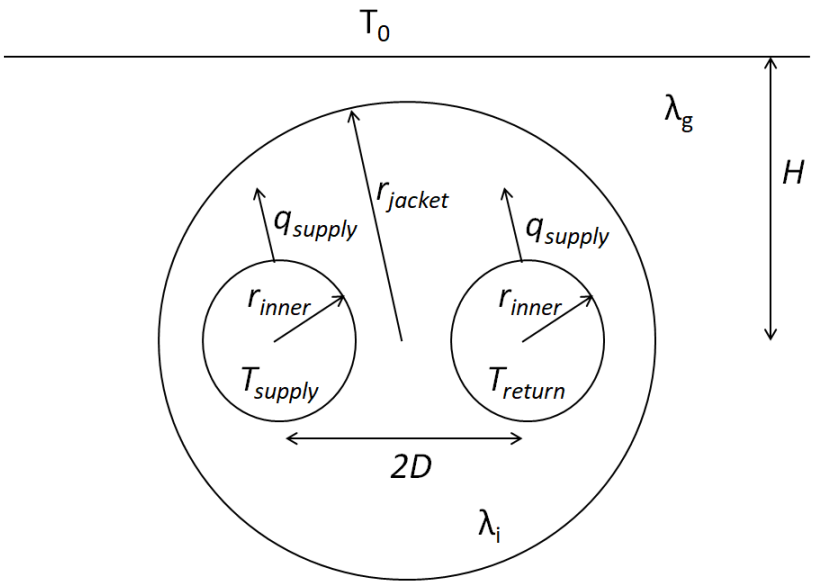

Figure 5.7: Heat loss from twin pipe in the ground [33]

overcome the varying soil temperatures, the soil temperature at a larger depth of 0.2 m is taken instead of the surface temperature. Subsequently, this distance is subtracted from H. The result is that the new T_0 is much more stable with just a gradual seasonal variation. Since the resistance over the insulation dominates over the heat resistance of the soil, the assumption that the soil temperature at a depth of 0.2 m is undisturbed seems reasonable. The effects of the variable fluid temperature are ignored, since the thermal resistance of the insulation is much higher than that of the soil. This results in minimal temperature differences of the soil.

Validation

The calculated UA values for the steel-pur-pe pipelines are 0.134, 0.160 and 0.167 $\frac{W}{K}$. The obtained values for these pipelines by van Miltenburg [31] when using the same input data are 0.136, 0.165 and 0.160 $\frac{W}{K}$ for DN20, DN25 and DN32, respectively. This indicates that the used method yields satisfactory results. Therefore, it is assumed that the UA values calculated for the twin pipelines, 0.0669, 0.0778 and 0.0916 $\frac{W}{K}$ for 25, 32 and 40 mm are also realistic. Note that the heat losses of the twin pipelines are about half of that of the steel pipelines. This corresponds well with the fact that the average insulation thickness of the twin pipes is almost twice that of the steel pipelines, and that beneficial effects are to be expected when combining two pipes into one jacket.

5.6. Heat pump

As laid out in chapter 4, a water/water heat pump will be used to provide enough exergy to the system. This heat pump has been assumed to achieve a system efficiency equal to 40% of Carnot efficiency. The coefficient of performance (COP) is calculated using either equation 5.35 or 5.36, depending on the system operation (further elaborated on in the next section). The 40% system efficiency includes the temperature differences over the heat exchangers at both sides of the heat pump.

$$COP(t) = 0.4 * COP_{Carnot} = 0.4 * \frac{\frac{T_{supply}+T_{return}}{2}}{\frac{T_{supply}+T_{return}}{2} - (T_{top} - \frac{\Delta T_{evaporator}}{2})} \tag{5.35}$$

$$COP(t) = 0.4 * COP_{Carnot} = 0.4 * \frac{\frac{T_{supply}+T_{top}}{2}}{\frac{T_{supply}+T_{top}}{2} - (T_{top} - \frac{\Delta T_{evaporator}}{2})} \tag{5.36}$$

The heat pump is only to be operated when the highest temperature level in the buffer is below the current service level supply temperature. Therefore, the heat pump will mainly be used when outdoor temperatures are low (leading to high service level temperatures), and especially toward the end of the heating season (when buffer temperatures are low).

The most important aspect of the heat pump in the model is the electricity consumption, since electricity costs for the heat pump will be a considerable part of the operational expenditures (OPEX). This research aims to find ways to lower network temperatures, one of the main reasons for that, is to lower electricity consumption of the heat pump.

Since a small buffer is used to smooth out demand spikes for the heat pump, the demand on the heat pump is averaged out over a period of 12 hours. This only has effect on the required power (in kW thermal) of the heat pump, and therefore the CAPEX. If this were not implemented, high spikes in demand (expected during cold evenings when people turn up the heat and consume a lot of DHW) would result in the need for a heat pump with a high power, pushing up required investment costs.

5.7. Control

There are various ways in which the system can operate, depending on several conditions. The logic of the control is to always minimize the current electricity consumption of the heat pump. If possible, generation from the solar collectors will directly be used to satisfy demand.

In figure 5.8, a flowchart is shown which indicates the four possible operational modes. This flowchart applies to both the 2-line network, as well as the 4-line network. Firstly, when the demand from the network (including network heat losses) is below the generation of the solar collectors ($P_{demand} < P_{solar}$) the buffer will be charging. If not, it will be discharging. Discharging can be done in two general ways: Directly, or with assistance of the heat pump. Direct discharging is always preferable since it limits electricity consumption. However, direct discharging is not possible if the temperature at the top of the buffer is lower than the service level supply temperature of the network ($T_{top} < T_{supply}$).

In case direct discharging is not possible, the heat pump is to be used to supply adequate exergy. Obviously, the buffer would then be used as a source (evaporator side), and the sink outlet would be the supply of the network. There are two possible inputs for the sink (condenser); Either the return of the heating network; or the top of the buffer. Since, as stated above, the current electricity consumption is to be minimized, the highest exergy source is to be utilized.

These four operational modes are discussed below for both the 2-line, as well as for the 4-line configuration.

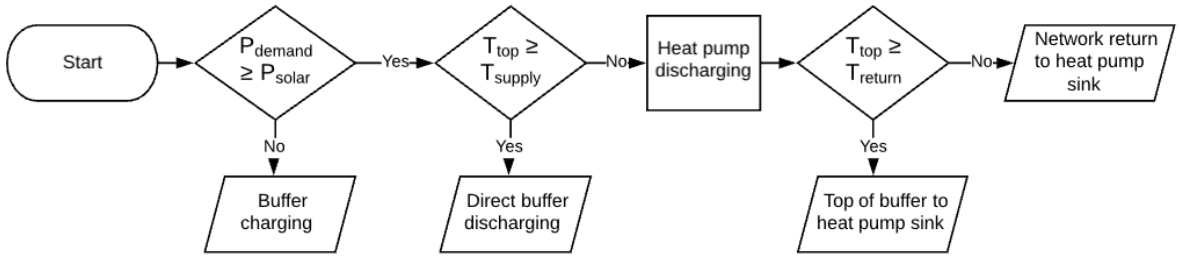

Figure 5.8: Flowchart of control

5.7.1. 2-line network

In the 2-line network, the solar collectors feed in over the heating network. Because the heating demand and solar supply flow over the same network, the power extracted from the buffer equals the demand in the network including losses minus the solar power. Therefore, the flow in the network

is bidirectional. Below, the three possible discharge modes are discussed.

Direct charge/discharge

Figure 5.9 shows the operation of the system when discharging directly. Discharging applies when the heating demand power (including network losses) is higher than the solar feed in ($P_{demand} > P_{solar}$). Discharging directly is possible when the temperature of the top of the buffer is at least as high as the service level temperature. Note that the three way valve mixes return flow with the supply flow in order to reduce the network supply temperature to exactly the service level temperature (e.g. when the top of the buffer is 70 $°C$ and the service level temperature is 65 $°C$, some colder return flow will be mixed with the 70 $°C$ in order to reach 65 $°C$). This is done to minimize the network temperature, reducing pipeline losses and maximizing solar yield. Obviously, T_{supply} can never be lower than the lowest of T_{return} or T_{top}.

In this scenario, T_{top} and T_{bottom} are known, and the supply temperature T_{supply} depends on the ambient temperature. The model of the consumer demand and network losses returns $\dot{m}_{network}$ and T_{return}. The only relevant remaining unknown, $\dot{m}_{buffer}$, is calculated using equation 5.39. This equation results from the logical massflow and power relations given by equations 5.37 and 5.38.

When discharging from the buffer, it is possible that some consumers are net producers and some are net consumers. In this case, the consumption of the net consumers is first met by the surplus production of the net producers. When the consumers collectively are net producers, $\dot{m}_{buffer}$ turns negative, and the buffer gets charged.

$$\dot{m}_{network}(t) = \dot{m}_{mix}(t) + \dot{m}_{buffer}(t) \tag{5.37}$$

$$T_{supply}(t) * \dot{m}_{network}(t) * C_p = T_{top}(t) * \dot{m}_{buffer}(t) * C_p + T_{return}(t) * \dot{m}_{mix}(t) * C_p \tag{5.38}$$

$$\dot{m}_{buffer}(t) = \dot{m}_{network}(t) * \frac{T_{return}(t) - T_{supply}(t)}{T_{return}(t) - T_{top}(t)} \tag{5.39}$$

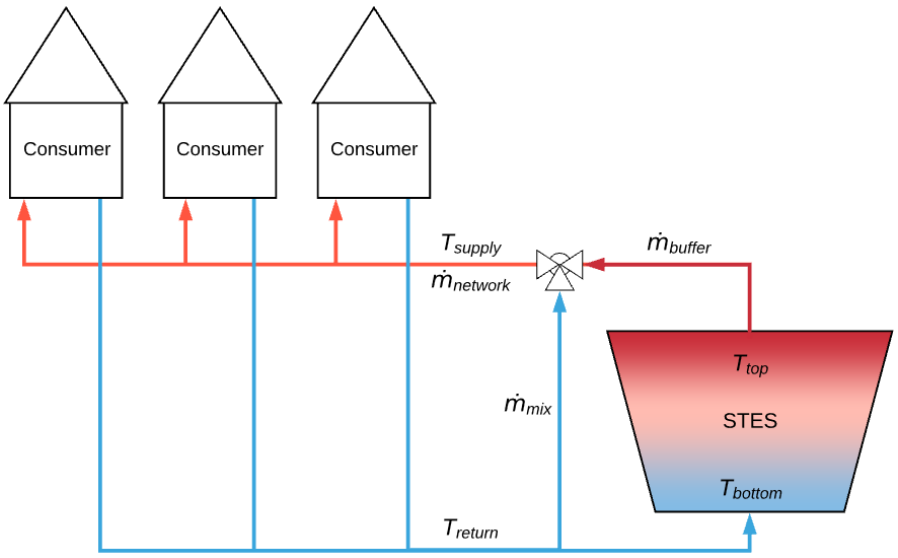

Figure 5.9: Direct discharge from buffer

Heat pump discharge

When the system is in buffer discharge operation, but not enough exergy is available in the buffer for direct discharge, the heat pump is to be used. Because the current electricity consumption is to be minimized, the heat pump will source a condenser input with maximum exergy. This can be either the top of the buffer, or the return of the network, depending on which has the highest temperature. In figure 5.10, a schematic is shown where the condenser sources from the return of the network (from here on referred to as 'closed operation'). Figure 5.11 shows a schematic where the buffer top is used as condenser input (from here on referred to as 'open operation'). Open operation results in higher mass flows through the buffer.

For these two operational modes, T_{return}, T_{supply} and $\dot{m}_{network}$ are first calculated by the network side of the model. Because the $\Delta\ T_{HP}$ of the heat pump is fixed at 8 K, the outlet temperature of the evaporator is defined as $T_{top} - 8$. The only relevant parameters which the control part of the model are to define, are $\dot{m}_{buffer}$ and the electrical power consumption of the heat pump $P_{HPelectric}$. Note that $\dot{m}_{buffer}$ is the mass flow through the buffer excluding the solar loop in case of the 4-line network.

Closed heat pump operation

When the heat pump is in "closed operation", as shown in figure 5.10, the mass flow through the buffer ($\dot{m}_{buffer}$) is calculated using equation 5.41. This equation follows from equation 5.40. The electricity consumption of the heat pump is derived simply from the coefficient of performance, and is given by equation 5.42.

$$COP(t) = \frac{P_{out}(t)}{P_{out}(t) - P_{in}(t)} = \frac{(T_{supply}(t) - T_{return}(t)) * \dot{m}_{network}(t) * C_p}{(T_{supply}(t) - T_{return}(t)) * \dot{m}_{network}(t) * C_p - \dot{m}_{buffer}(t) * C_p * \Delta T_{HP}(t)} \tag{5.40}$$

$$\dot{m}_{buffer}(t) = \frac{\dot{m}_{network}(t) * (T_{supply}(t) - T_{return}(t)) * \frac{COP(t)-1}{COP(t)}}{\Delta T_{HP}(t)} \tag{5.41}$$

$$P_{HPelectric}(t) = \frac{\dot{m}_{network}(t) * (T_{supply}(t) - T_{return}(t)) * C_p}{COP(t)} \tag{5.42}$$

Open heat pump operation

When the heat pump is in "open operation", which is shown in figure 5.11, the mass flow through the buffer is given by equation 5.44, which follows from equation 5.43. Equation 5.45 is used to calculate the electric power of the heat pump.

$$COP(t) = \frac{P_{out}(t)}{P_{out}(t) - P_{in}(t)} = \frac{(T_{supply}(t) - T_{top}(t)) * \dot{m}_{network}(t) * C_p}{(T_{supply}(t) - T_{top}(t)) * \dot{m}_{network}(t) * C_p - \dot{m}_{buffer}(t) * C_p * \Delta T_{HP}(t)} \tag{5.43}$$

$$\dot{m}_{buffer}(t) = \frac{\dot{m}_{network}(t) * (T_{supply}(t) - T_{top}(t)) * \frac{COP(t)-1}{COP(t)}}{\Delta T_{HP}(t)} \tag{5.44}$$

$$P_{HPelectric}(t) = \frac{\dot{m}_{network}(t) * (T_{supply}(t) - T_{top}(t)) * C_p}{COP(t)} \tag{5.45}$$

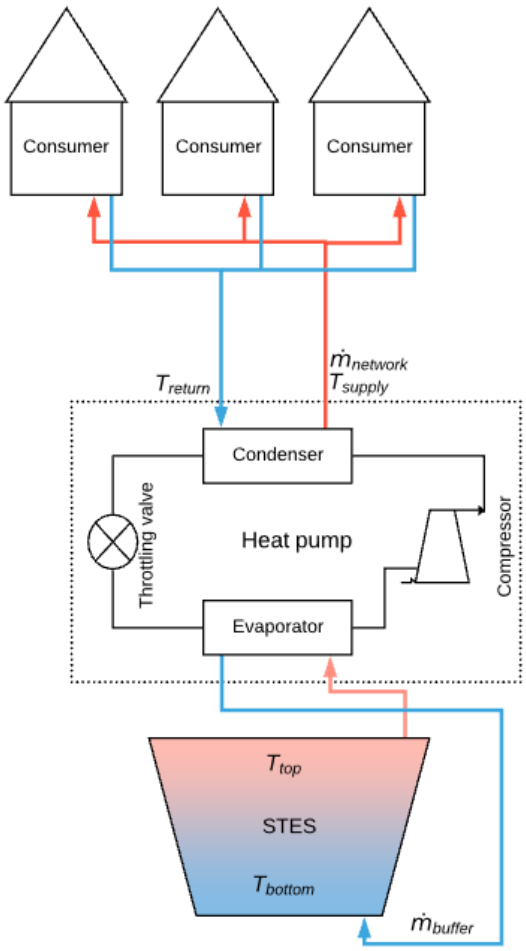

Figure 5.10: 2-line with closed heat pump operation

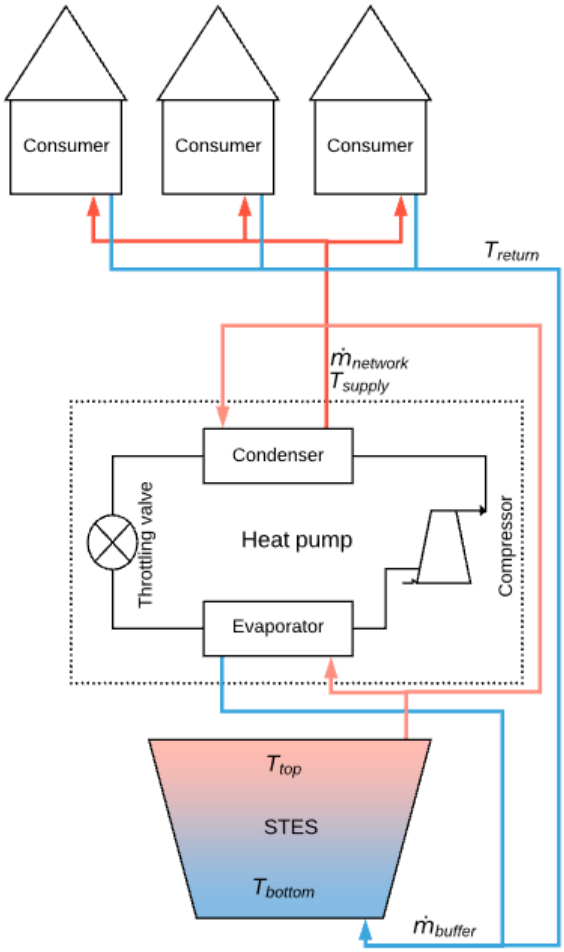

Figure 5.11: 2-line with open heat pump operation

5.7.2. 4-line network

The 4-line network is different from the 2-line network in the way that the solar collectors do not feed in over the heating network. Instead, the solar collectors are connected to the buffer through a separate network.

Direct discharge

When the temperature at the top of the buffer is higher than the required network supply temperature, the heat pump is not needed. Instead, the hot water from the buffer can be directly fed into the network. This direct discharge operation is schematically shown in figure 5.12. The operation is similar to the 2-line network direct discharge as shown in figure 5.9. Since less demand will be directly satisfied by the solar collectors, the flow through the buffer will be higher than for the 2-line network.

The mass flow from the solar collectors, $\dot{m}_{solarloop}$, and the outlet temperature of the collectors, $T_{solarloop}$ are calculated by the solar model. The remaining unknown variable, $\dot{m}_{buffer}$ is calculated using equation 5.39, the same equation as used for the 2-line network.

Heat pump discharge

Similarly to the 2-line network, in the 4-line network a heat pump is also needed at times when the temperature of the buffer is below the required supply temperature of the network. The schematics of the two possible modes of operation are shown in figures 5.13 and 5.14.

For these modes of operation, $\dot{m}_{buffer}$ and $P_{HPelectric}$ are calculated using the same equations as for the 2-line network. The only difference is that the flows on the network side will be different

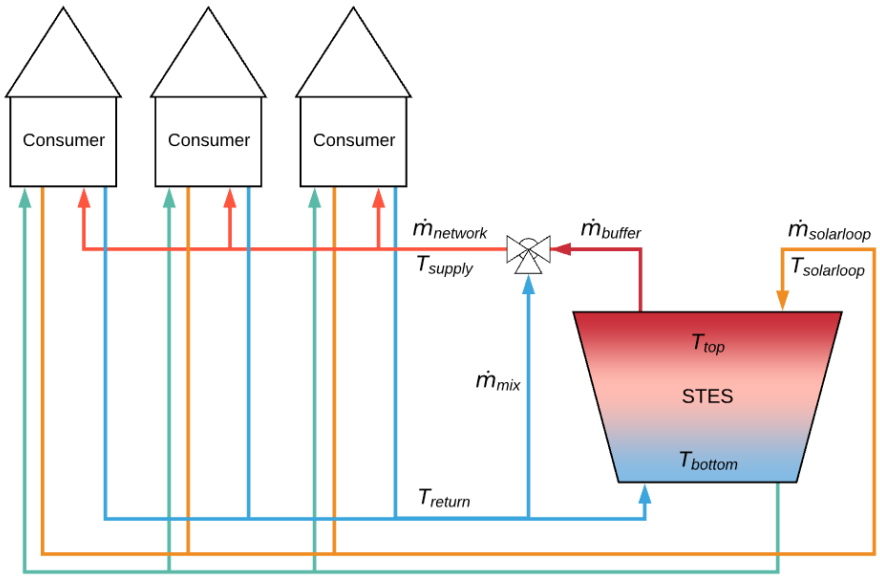

Figure 5.12: Direct discharge from buffer

due to the separation of the solar loop. However, this is handled by the network side of the model. For the control of the heat pump this doesn't change much.

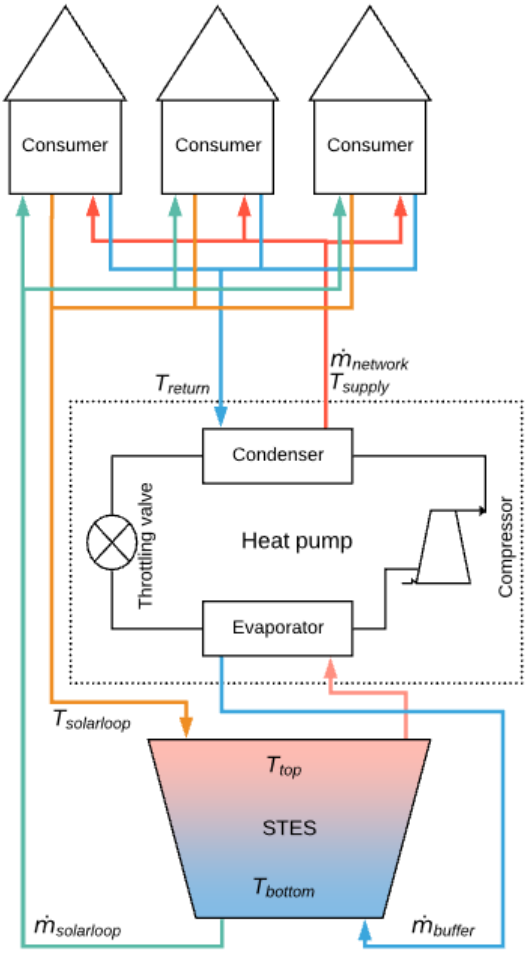

Figure 5.13: 4-line with closed heat pump operation

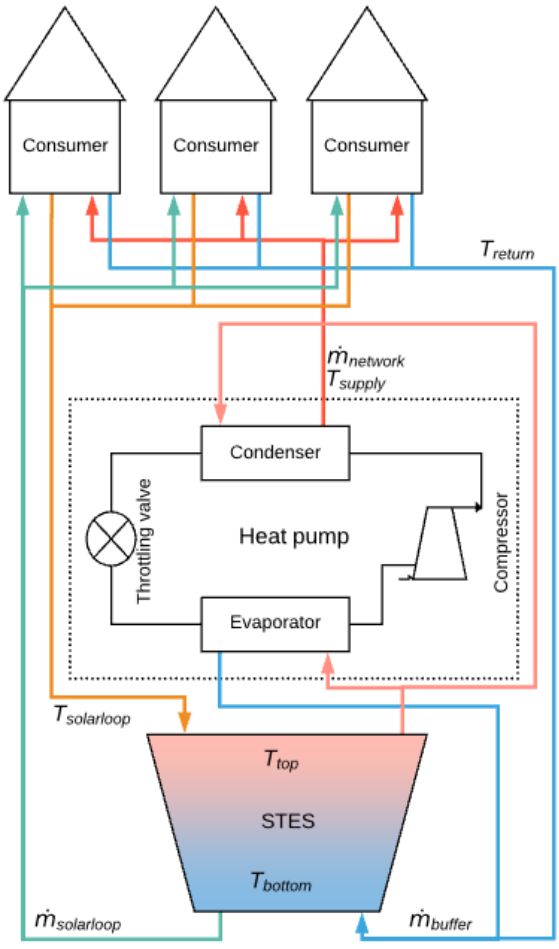

Figure 5.14: 4-line with open heat pump operation

6

Financial model

The aim of this research is to conclude which of the seven solar+storage district heating systems as described in chapter 3 can achieve the lowest LCOH and carbon footprint and how they compare to individual air to water heat pumps. Chapter 5 describes how the Matlab/Simulink models of the systems are built. This chapter goes on to explore how the obtained operational data can be translated into an LCOH.

LCOH calculation

The LCOH is given by equation 6.1, with $X(t)$ being the investment expenditures (initial CAPEX), $M(t)$ the operation & maintenance expenditures, C the electricity consumption expenditures, and $E(t)$ the consumed thermal energy at year t.

The generation and consumption are discounted for their time value using a weighed average cost of capital (WACC).

The project is regarded as a low risk green energy system. The capital costs of these systems are usually low. For this specific project, 20 % of the project finance is seen as risk-carrying with an associated cost of capital of 5 %. The remaining 80 % is a green loan with an interest rate of 1 %. The resulting WACC between these sources is 1.8 %. It is assumed that the financing period is equal to the project life, which is 30 years.

The LCOH is calculated using all expenditures of the heating system, including expenditures made inside dwellings such as delivery kits, DHW preparation devices, and electricity consumed by DHW heaters. The LCOH is calculated excluding VAT and subsidies.

$$LCOH = \frac{\text{sum of costs over lifetime}}{\text{sum of thermal energy delivered over lifetime}} = \frac{\sum_{t=1}^{n} \frac{X(t)+M(t)+C(t)}{(1+WACC)^t}}{\sum_{t=1}^{n} \frac{E(t)}{(1+WACC)^t}} \tag{6.1}$$

Investment expenditures

The investment expenditures, or CAPEX, consist of several components, all of which are shown in table 6.1. Most of the component pricing is based on HoCoSto's general knowledge and experience in the field. Every cost component concerns an 'all-in' price, including installation costs and an installer profit margin.

HoCoSto buffer

The all-in price for the HoCoSto buffer depends on the type of project. For smaller buffers, a price close to 200 $\frac{€}{m^3}$ is generally given, but for larger projects such as the one in Nagele, a price of 150 $\frac{€}{m^3}$ is reached. It is expected that the costs of the buffer will come down in the future as HoCoSto keeps innovating and improving their product.

Table 6.1: Pricing of system components

Component	Price	Unit
HoCoSto Buffer	150	[€/m^3]
Solar Collectors	450	[€/m^2]
Delivery kit	1000	[€/consumer]
Central installations	35000	[€]
Heat pump	500	[€/kW]
2-line network	180	[€/m]
4-line network	255	[€/m]
Small boiler	350	[€/consumer]
Big boiler	500	[€/consumer]

Solar collectors

The Kloben Industries solar collectors are state of the art and are unmatched in efficiency at high temperatures. They are imported from the supplier directly by HoCoSto and are installed by a third party. Based on past experiences of HoCoSto at several projects where solar collectors are applied, the price of 450 $\frac{€}{m^2}$ seems a reasonable assumption. This includes installation and all necessary components associated with installation.

Delivery kits

The price of the delivery kits of 1000 $\frac{€}{consumer}$ might seem high, but this includes installation, and more importantly, the delivery kit has to include two heat exchangers of which one (for DHW production) has to be doubly separated as per regulation.

Central installations

The central installations represent the installations at the buffer. They include pumps, valves, the control system, a small secondary buffer etc.

Heat pump

The NRGTEQ heat pump has been factored into the LCOH using a fixed cost per kW of 500 $\frac{€}{kW}$. The power required is determined in the model for every configuration, and within every configuration for every component scale option (combination of buffer m^3 and solar m^2. Since the heat pump is coupled to a small secondary buffer, the required power is averaged out over a period of 12 hours. It is assumed that the lifetime of the heat pump is 15 years.

Heating network

Two heating networks are considered in this study. The 2-line network is a steel-pur-pe network, and the 4-line network is a combination of a steel-pur-pe network and a flexible polyethylene twin network.

The 4-line network therefore consists of the costs of the 2-line network, and additionally the flexible twin network, which is assumed to be 75 $\frac{€}{m}$. The reason the surplus costs of the 4-line network is relatively low, is that there is overlap in the work required to install the two systems, such as the groundwork required. Also, the additional two lines are prefab flexible pipes, reducing the installation costs.

Boilers

The boilers are estimated to cost 350 $\frac{€}{consumer}$ for the small boilers (intended for kitchen use only), and 500 $\frac{€}{m}$ for the larger boilers, which are also to assist in DHW preparation for sanitary

purposes.

O&M and replacements

General operation and maintenance has been assumed to be a fixed percentage of 1.2 % of the investment expenditures annually. The percentage does not include energy costs and end-of-life replacements of major components.

All of the major components are expected to last the 30-year project lifetime except for the heat pump, which has an assumed life of 15 years. Hence, after 15 years, the NRGTEQ heat pump will be replaced, this has been factored in as a separate cost.

Electricity consumption expenditures

Four components in the system consume electricity: The heat pump, the electric auxiliary heater, the circulation pumps, and (when applied) the electric hot water boilers. All but the electric hot water boilers consume their electricity at the central location. The electricity costs for these components is displayed in table 6.2. It is clear that higher electricity consumption translates into lower marginal costs. This is due to the network charges and taxes on electricity which drop as more energy is consumed. At the lowest bracket, 0.125 $\frac{€}{kWh}$ is charged, dropping to 0.0883 $\frac{€}{kWh}$ in the next, and finally to 0.034 $\frac{€}{kWh}$ in the last bracket. Note that the costs in table 6.2 include not only the network charges and taxes, but also the costs of the electricity itself. It has been assumed these costs are 5 cents per kWh.

For the electric hot water boilers, it is assumed that the electricity price is 0.185 $\frac{€}{kWh}$. This is because the consumers will be in the first bracket, while paying slightly more for their wholesale electricity since they are smaller consumers.

Due to the assumption that announced reductions in taxes on electricity will offset wholesale price increases, the net electricity prices are expected to remain flat during the course of the project.

Table 6.2: Electricity prices in the first three consumption brackets

Consumption	Price	Unit
0 - 10,000	0.1750	[€/kWh]
10,001 - 50,000	0.1383	[€/kWh]
50,001 +	0.0834	[€/kWh]

7

Comparison with individual heat pumps

To compare how the system financially holds up to alternatives, it is compared to a scenario where the houses are heated by individual air to water heat pumps.

For the individual heat pump scenario, there are no system components which can be scaled. There is only one outcome, thus the COP is fixed (it is not dependent on, for instance the size of the heat pump).

As a reference, a single family dwelling is considered with the average of the gas consumption of the first 23 consumers (excluding consumer no. 24, the school). That average translates into an annual energy consumption of 19740 $\frac{kWh}{year}$ per dwelling when assuming a gas boiler efficiency of 90 %.

Because the basis of the system is that no home renovations are necessary, the same assumption holds for the individual heat pump model, this essentially means that the heat pump should be able to operate the heating system at a 70 $^{\circ}C$ inlet temperature. The heat pump chosen for the reference scenario is the LG split high temperature heat pump. Specifically, the combination of the HU161H.U32 and HN1610H.NK2 units. This combination can provide heating water up to 80 $^{\circ}C$ due to the cascade system. The cascade system consists of two heat pumps, the first using R410A as a refrigerant, and the second using R134a. The maximum power of 15 kW is sufficient for the type of consumer considered. The supply temperature of the system is shown in figure 7.1.

The DHW demand is modelled (similarly to the DHW demand in the main model) by constructing a demand profile consisting of kitchen and bathroom demand for a typical household. The space heating demand is simulated by constructing a thermal model of a dwelling. The same submodel is used as for the consumer demand in the main model. These demands are translated into electric power demands by dividing this demand by the COP of the heat pump.

The actual COP of the heat pump is assumed to be a fixed fraction of the Carnot COP. In order to make a realistic estimate of such an efficiency fraction, the COP data of the specific heat pump model in table 7.1 considered. The fraction of the Carnot COP is shown in the right column, this efficiency is calculated using equation 7.1. The data in table 7.1 is for supply temperatures of 65 $^{\circ}C$. The average supply temperature (illustrated in figure 7.1) will be lower than 65 $^{\circ}C$. Since the cascade heat pump probably achieves lower fractions of the Carnot COP at lower supply temperatures, the actual COP of the heat pump is assumed to be 40 % of the Carnot COP.

$$\eta_{heatpump} = \frac{COP}{COP_{carnot}} \tag{7.1}$$

This fraction is derived from supplier data shown in table 7.1. Since the cascade heat pump probably achieves lower fractions of the Carnot COP at lower supply temperatures, the COP is assumed to be 40 % of Carnot COP.

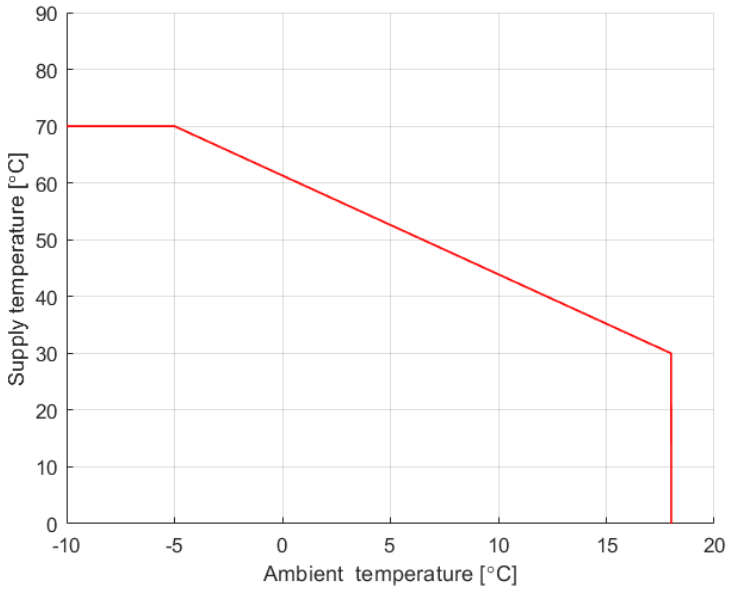

Figure 7.1: Supply temperature curve of individual air to water heat pump

Table 7.1: COP of LG heat pump at 65 $°C$ supply temperature [2]

$T_{ambient}$ [C]	COP [-]	$\eta_{heatpump}$ [-]
7	2.61	0.448
2	2.14	0.399
-2	2.25	0.446
-7	2.09	0.445

For the DHW supply, it is assumed that a large (150 L) boiler vessel is heated by the heat pump to 60 $°C$. Heating the boiler vessel to 60 $°C$ mitigates the need for legionella prevention programs. Since the boiler vessel is heated by the heat pump indirectly by means of a heat exchanger, the supply temperature of the heat pump during DHW heating is assumed to be 65 $°C$. The standing heat losses of the boiler are fixed at 45 W.

Additionally, a small 50 L buffer vessel is introduced in the heating system in order to guarantee enough heat capacity in the system to facilitate heat pump defrosting. This is required since the consumers are assumed to use classic radiators for heating, which do not contain the large amount of water needed to properly defrost. In dwellings where heating is done by radiant floors, buffer vessels are often not required.

Economic components

All-in (ex. VAT) electricity costs are fixed at 0.185 $\frac{€}{kWh}$, consisting of 6 cent energy wholesale costs and 12.5 cents in taxes and transportation. Since cheap government-sponsored green home improvement loans are available at 1.35 % interest, the WACC is set equal to that rate. In LCOH calculation, the project life is set equal to the expected heat pump life, which is assumed to be 20 years. During these years, an annual maintenance cost equal to 1% of initial CAPEX is added.

Initial CAPEX consists of several components: The price of the heat pump is 12300 €[3], additionally, the buffer and boiler vessels are priced at 200 and 450 €, respectively. Installation costs are estimated to be 3500 €.

8

Results

The objective of this research is to find ways to lower the LCOH of a solar+storage district heating system. Seven possible system configurations have been simulated, and are compared based on LCOH in this chapter. Because reducing carbon emissions is the main objective of such systems, they are not only compared based on their lowest LCOH, but also on the LCOH tied to the constraint that the minimum SCOP (seasonal coefficient of performance) is 5. As such, the conclusion includes not only which system yields the absolute lowest energy costs, but also which system is the most economical when ecological constraints are implemented. Finally, a quick comparison is given between the solar+storage DHS and a scenario in which every consumer's heating needs are met by a heat pump.

The SCOP is a measure of the total seasonal system efficiency. It is defined as the thermal energy delivered to the end consumers, divided by the total amount of electricity consumed in the system. Electricity gets consumed by the heat pump, the circulation pumps, the auxiliary heater, and (if applied) the DHW boilers. Because the majority of energy delivered to the consumers will be generated by the solar collectors, the SCOP will typically be above 1.

8.1. Sizing of configurations

Sizing of the solar and storage components greatly impacts system operation and the resulting LCOH. Generally, increasing buffer volume and/or solar area increases CAPEX, but lowers the electricity consumed by the heat pump and electric auxiliary heater.

Thus, an economic optimum is achieved for certain buffer and solar sizing. For every configuration, 5-year simulations have been run for numerous buffer volume/solar area combinations. The resulting LCOH and SCOP values are shown graphically in the sections below. At every configuration, two points are highlighted: That of the lowest absolute LCOH, and that of the lowest LCOH for a SCOP of at least 5.

Configuration 0-A

Configuration 0-A is the base scenario: A 2-line network with a fixed supply temperature of 73 $^{\circ}C$. The LCOH and SCOP of this configuration are shown in figure 8.1. It is clearly observed that an economic optimum exists, in this case for a buffer volume of 1275 m^3 buffer and 1100 m^2 solar collectors. The LCOH at this point is 0.1124 $\frac{€}{kWh}$. The lowest LCOH for an SCOP of 5 is 0.1132 $\frac{€}{kWh}$. One important observation, is that scaling the system marginally larger than the absolute economic optimum only very slightly increases LCOH, but can increase SCOP significantly. Moving from the economic optimum with an SCOP of 4.5 to the point where the SCOP is 5 leads to a decrease in electricity consumption of 10% for an increase in LCOH of 0.7 %. Note that the maximum solar area considered is 1100 m^2 due to rooftop constraints.

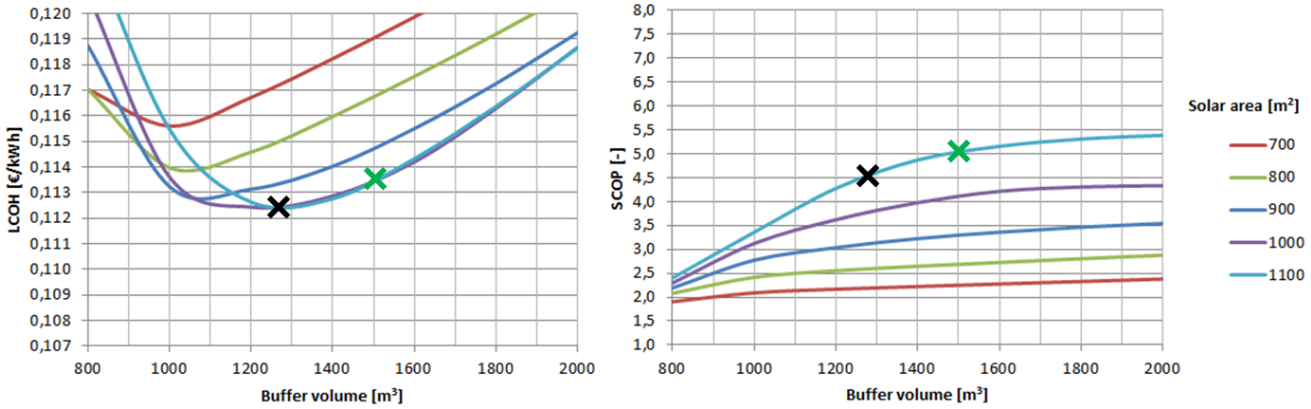

Figure 8.1: LCOH and SCOP for configuration 0-A at various buffer volumes and solar areas

Configuration 1-A

Configuration 1-A is a 2-line network which aims to improve system performance by implementing a variable supply temperature. The minimum supply temperature is restricted to 62 $^{\circ}C$ due to constraints in the DHW system. This lower supply temperature results in slightly lower pipeline losses, lower heat pump electricity consumption and higher solar collector efficiency. Since no additional costs are associated in the implementation of such a system, the LCOH is decreased compared to the base scenario, which is clearly seen in figure 8.2. At the absolute economic optimum (1000 m^2 solar and 1275 m^3 buffer), the LCOH is 0.1093 $\frac{€}{kWh}$, a 2.8 % cost reduction compared to 0.1124 $\frac{€}{kWh}$ of the base scenario. Figure 8.2 also displays the SCOP, which is seen to have increased for every system size. The lowest LCOH for a system with a minimum SCOP of 5 (at 1000 m^2 solar and 1475 m^3 buffer) is 0.1098 $\frac{€}{kWh}$, a 3% cost reduction from the base case.

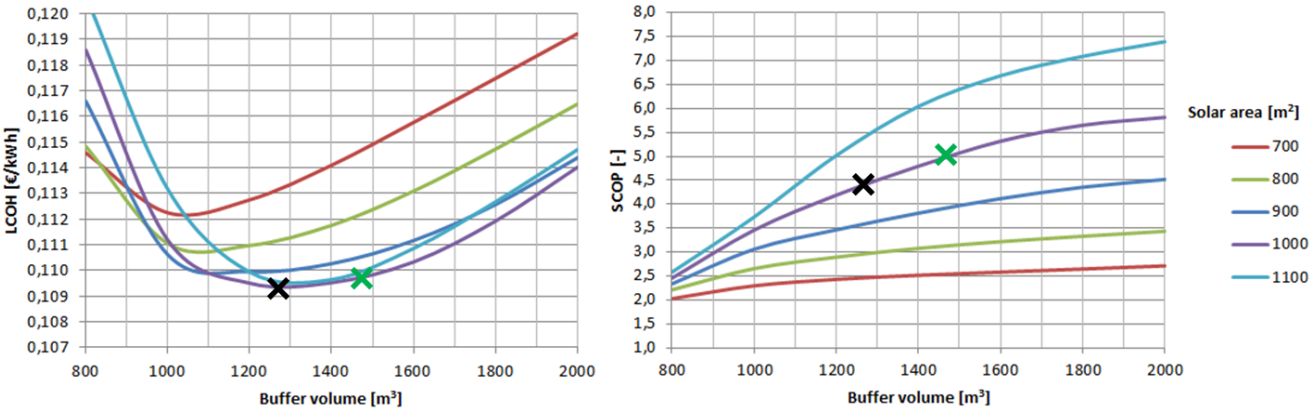

Figure 8.2: LCOH and SCOP for configuration 1-A at various buffer volumes and solar areas

Configuration 1-B

Configuration 1-B is a 2-line network with a variable supply temperature similar to configuration 1-A. However, 1-B takes it further by implementing a small DHW heater for kitchen tap water, which allows the minimum supply temperature of the network to drop from 62 to 52 $^{\circ}C$. This results in lower pipeline losses, lower heat pump electricity consumption and higher solar collector efficiency. The resulting SCOP's shown in figure 8.3 are considerably higher than those of configurations 0-A and 1-A. However, contrary to configuration 1-A, this configuration also has elements which increase the LCOH alongside the lower supply temperature which decreases LCOH compared the base case. The electric boilers result in higher CAPEX (and thus O&M), standing heat losses, and electricity consumption at decentralised locations. This is relevant because electric-

ity at decentralised locations is more expensive than at the centralised location. Even though the electricity consumption of this configuration is lower than configuration 1-A, it does not achieve a lower LCOH. The lowest optimum at 1000 m^2 solar and 1300 m^3 buffer is 0.1102 $\frac{€}{kWh}$, a 2% reduction compared to the base-case, but a 0.8% increase compared to configuration 1-A. The LCOH for an SCOP of at least 5 is 0.1103 $\frac{€}{kWh}$, achieved at 1000 m^2 solar and 1350 m^3 buffer. While being 2.6% lower than the base case, configuration 1-A reaches a 0.5% lower LCOH. This configuration fails to outperform configuration 1-A both in absolute lowest LCOH as well as in lowest LCOH at an SCOP of at least 5.

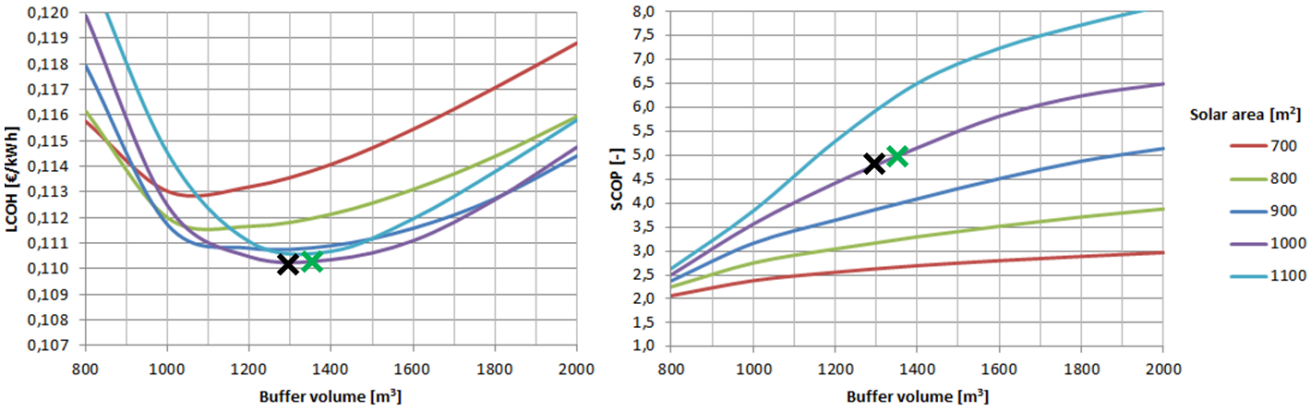

Figure 8.3: LCOH and SCOP for configuration 1-B at various buffer volumes and solar areas

Configuration 1-C

Configuration 1-C is a 2-line network with a variable supply temperature where electric DHW heaters are used for both kitchen as well as sanitary use. This allows the minimum network supply temperature to drop to 42 $°C$. LCOH and SCOP values are shown in figure 8.4. The lowest LCOH is 0.1118 $\frac{€}{kWh}$ at an SCOP of 4.9, while for a minimum SCOP of 5, the LCOH rises to 0.1119 $\frac{€}{kWh}$.

While being more economical than base-case configuration 0-A by (0.5 % for the absolute optimum and 1.1 % when the constraint of an SCOP of 5 has to be met)) , 1-C is unable to achieve lower LCOH's than 1-A and 1-B, regardless of its lower electricity consumption. The reduction in electricity consumption is not sufficient to offset the increase in costs. These cost increases result from both a higher required CAPEX for the electric DHW boilers, as well as from higher average electricity prices. The average electricity price is pushed up since more electricity is consumed through the consumer, where rates on electricity are higher.

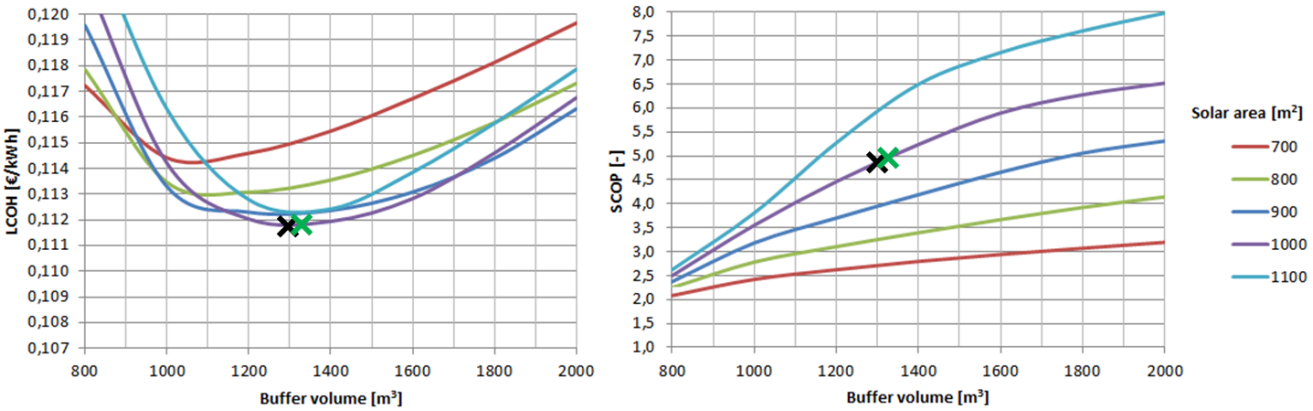

Figure 8.4: LCOH and SCOP for configuration 1-C at various buffer volumes and solar areas

Configuration 2-A

Configuration 2-B is a 4-line network where the solar collectors supply heat to the buffer through a separate network. It aims to increase solar collector efficiency by allowing them to operate at lower mean temperatures. The supply temperature of the heating network is variable, but limited to a minimum of 62 $^{\circ}C$ due to DHW production constraints. Figure 8.5 shows the LCOH and SCOP for various buffer volumes and solar areas. The lowest LCOH of 0.1073 $\frac{€}{kWh}$ is 4.5 % lower than the base scenario, while achieving a relatively high SCOP of 4.4. When the constraint of having to achieve a SCOP of 5 is to be met, the LCOH increases to 0.1081 $\frac{€}{kWh}$, which is also 4.5 % lower than its respective base scenario.

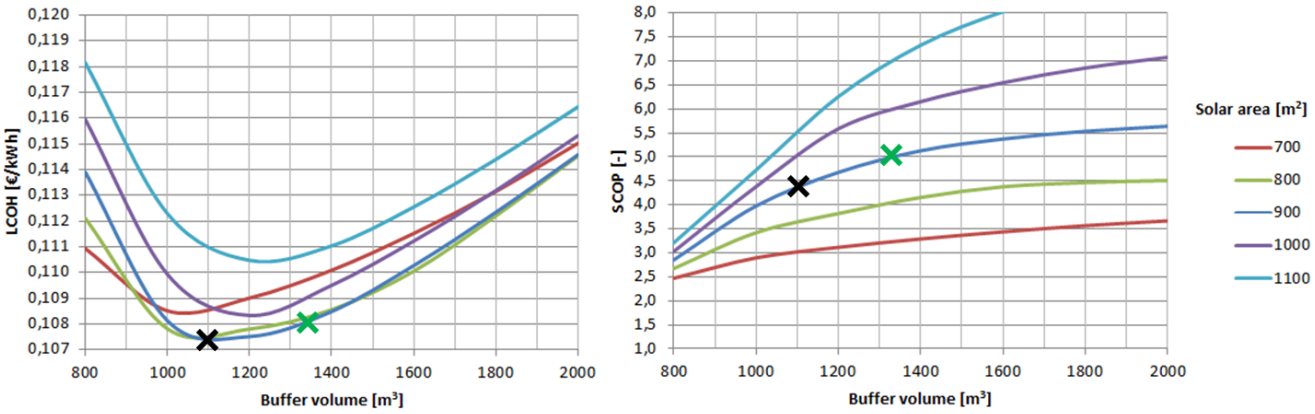

Figure 8.5: LCOH and SCOP for configuration 2-A at various buffer volumes and solar areas

Configuration 2-B

Configuration 2-B consists of a 4-line network with a variable supply temperature. Its network supply temperature is decreased from 62 to 52 $^{\circ}C$ compared to 2-A by using electric boilers to supply additional heat to kitchen tap water. In figure 8.6, the LCOH and SCOP's are displayed. The lowest LCOH is 0.109 $\frac{€}{kWh}$ at an SCOP of 4.5, which is 3 % lower than the base scenario. The LCOH when the constraint of having a SCOP of 5 is to be met is 0.1091, 3.6 % lower than the base scenario. While configuration 2-B is more cost effective than the base scenario, it fails to outperform other configurations. It appears the same holds as for 1-B, which is that the efficiency gains from lower network losses fail to recuperate the increased CAPEX, boiler heat losses, O&M costs and higher electricity rates.

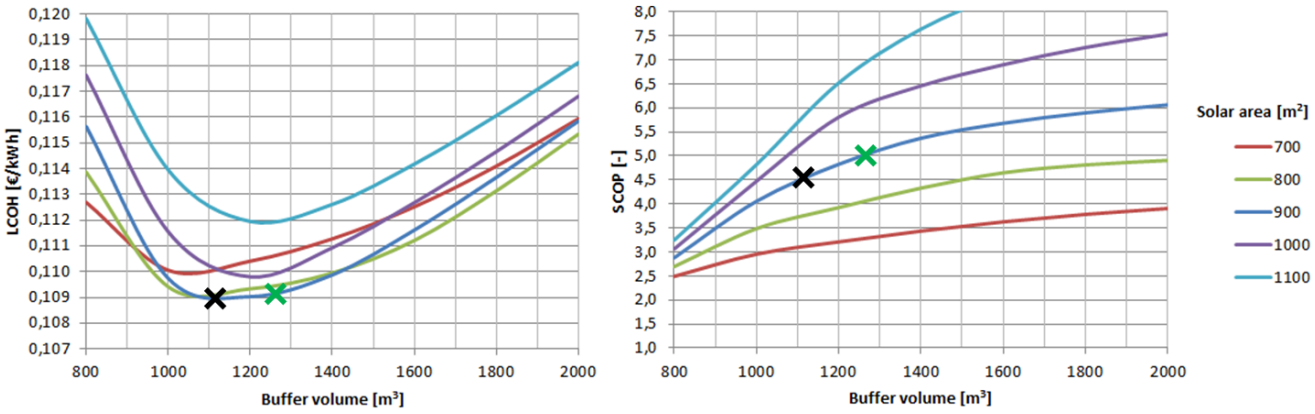

Figure 8.6: LCOH and SCOP for configuration 2-B at various buffer volumes and solar areas

Configuration 2-C

Configuration 2-C is a 4-line network with variable temperatures and electric boilers supplying additional heat to all DHW (including sanitary DHW), which allows the variable supply temperature to drop to a minimum of 42 °C. The lowest LCOH for this configuration is 0.111 $\frac{€}{kWh}$ at an SCOP of 4.4, which is a reduction in cost of 1.2 % over the base scenario. When the constraint of having to achieve an SCOP of 5 is to be met, the LCOH is 0.1113, which is 1.7 % lower than the base scenario. Similarly to configuration 1-C, 2-C fails to achieve lower LCOH's than the A configurations. Again, a reduction in electricity consumption is seen, but this is offset mainly by higher average electricity prices since more electricity is consumed through the consumer connections which pay higher rates.

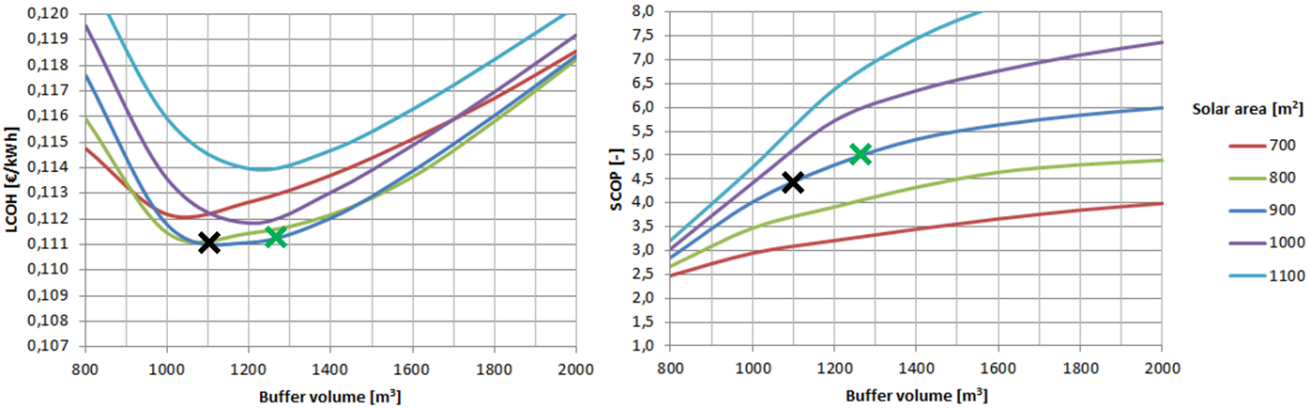

Figure 8.7: LCOH and SCOP for configuration 2-C at various buffer volumes and solar areas

8.2. Comparing configurations

Figure 8.8 shows all system costs. It shows the LCOH for every configuration for both the absolute economic optimum as well as for the situation where a SCOP of 5 has to be met.

The economically most attractive system is configuration 2-A with 1100 m^3 of buffer and 900 m^2 of solar collectors. The cost benefit however, is just 0.5 cents per kWh, or 4.5% compared to the base scenario 0-A with 1275 m^3 of buffer and 1100 m^2 of solar collectors. What can be seen in the sizing of the systems, is that sizing the buffer volume and solar area slightly larger does not increase LCOH considerably, but does increase SCOP profoundly. This is also seen in figure 8.8, where the systems with a minimum SCOP of 5 are seen to be only very slightly more expensive than systems without this constraint. For comparison, systems 0-A, 1-A, 1-B, 1-C, 2-A, 2-B and 2-C operate at SCOP's of 4.5, 4.4, 4.8, 4.9, 4.4, 4.5 and 4.4, respectively, when no constraint is implemented.

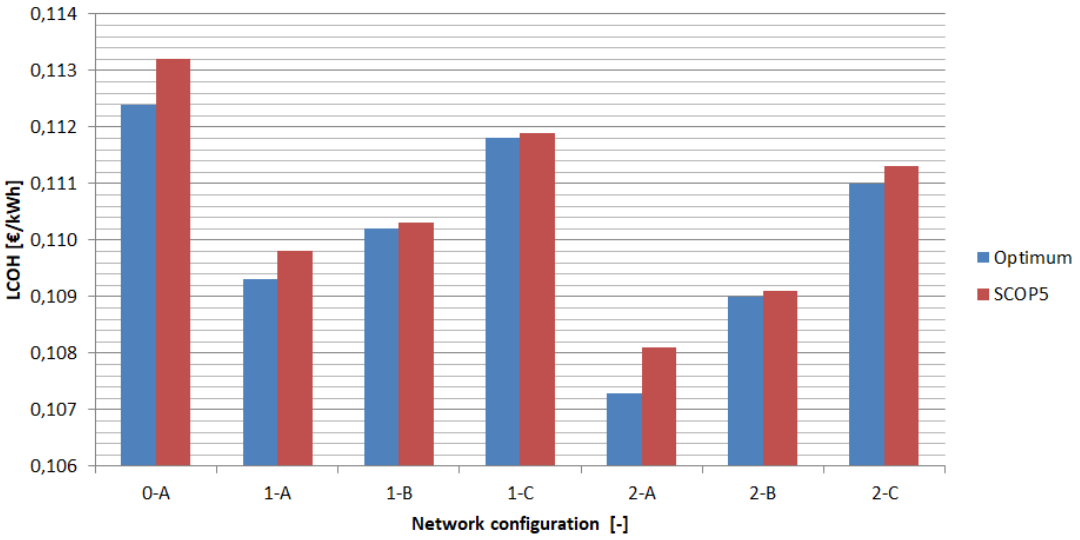

Figure 8.8: Lowest LCOH and lowest LCOH for a minimum SCOP of 5 for every system configuration

Power and COP of heat pump

Important factors in the operation of the system are the power and the COP of the heat pump. figures 8.9, 8.10, 8.11 and 8.12 show the COP and electric power of the heat pump for simulated year 2009. It is seen that the heat pump is mainly active in late winter and spring. This was to be expected since these are the periods where the buffer temperatures are low. Correspondingly, it is at these times when buffer temperatures are low that the COP is also lower. Note that the COP is capped at 10, since it is not realistic that higher COP's can be achieved. The impact of this on the results is nonetheless extremely limited since the heat pump is barely operational when higher COP's could be achieved, as can be seen in the figures.

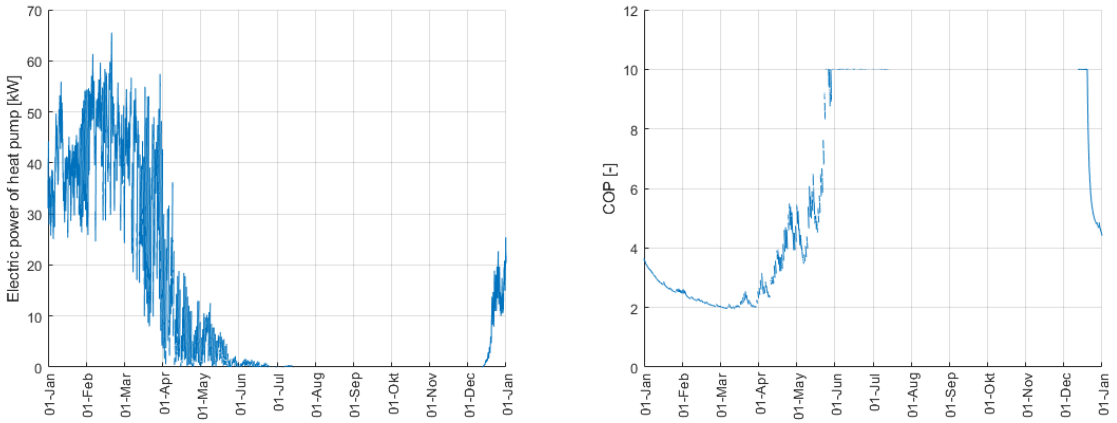

(a) Electric power of heat pump

(b) COP of heat pump

Figure 8.9: Electric power and COP of heat pump in 2009. Configuration 0-A, scaled for economic optimum. 1100 m^2 of solar collectors, 1275 m^3 of buffer.

A difference between the slightly larger scaled systems and smaller scaled systems, is that the peak electric power of the heat pump is lower for the larger scaled systems. This is because the larger scaled systems do not see their buffer temperatures drop as far as the more critically scaled ones. However, the difference is not large enough to have a meaningful impact on SCOP.

Configuration 2A, as seen in figures 8.11 and 8.12, sees lower peaks in heat pump power than configuration 0A (seen in figures 8.9 and 8.10). However, from figures 8.13 and 8.15 it can be deducted that the ultimate contribution to LCOH is only a 0.02 cents per kWh reduction in LCOH due to lower heat pump CAPEX.

Overall, it is interesting to see that the HoCoSto system can provide all heating needs till well into December without needing the heat pump.

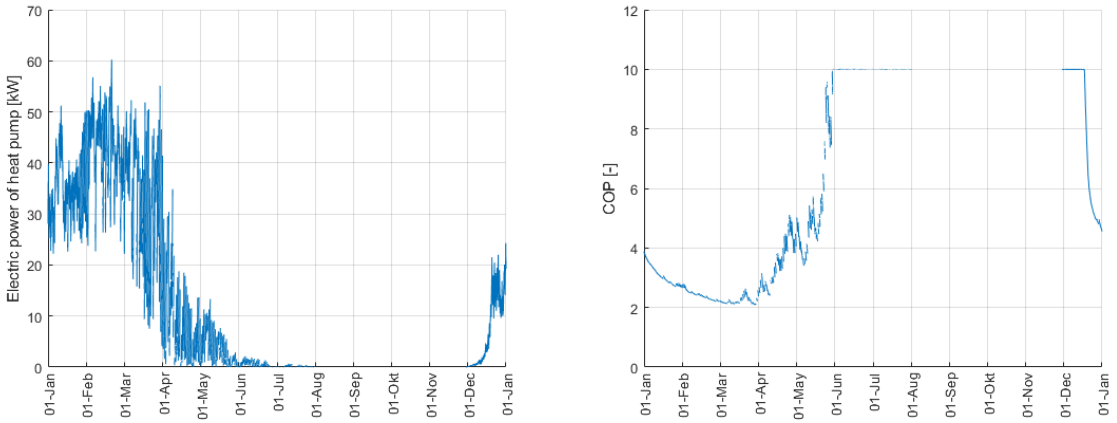

(a) Electric power of heat pump

(b) COP of heat pump

Figure 8.10: Electric power and COP of heat pump in 2009. Configuration 0-A, scaled to have a SCOP of at least 5. 1100 m^2 of solar collectors, 1500 m^3 of buffer.

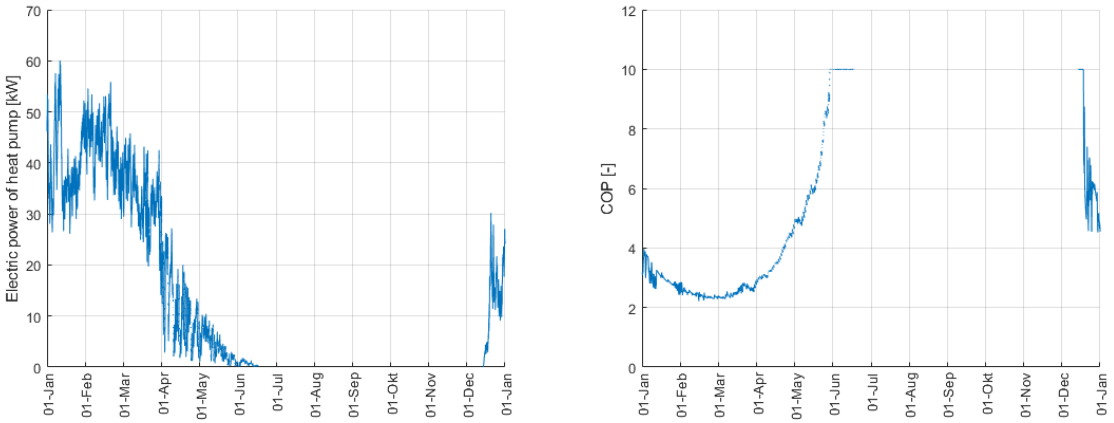

(a) Electric power of heat pump (b) COP of heat pump

Figure 8.11: Electric power and COP of heat pump in 2009. Configuration 2-A, scaled for economic optimum. 900 m^2 of solar collectors, 1100 m^3 of buffer.

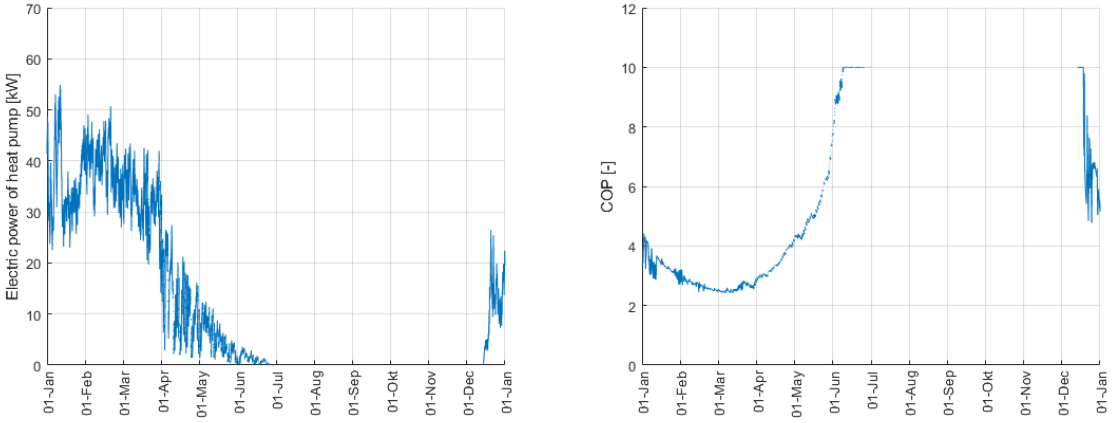

(a) Electric power of heat pump (b) COP of heat pump

Figure 8.12: Electric power and COP of heat pump in 2009. Configuration 2-A, scaled to have a SCOP of at least 5. 900 m^2 of solar collectors, 1325 m^3 of buffer.

Cost breakdown of base scenario 0-A

The cost breakdown for configuration 0-A is given in figure 8.13, sized to reach a minimum LCOH on the left, and sized to reach an SCOP of 5 on the right. The differences in costs between the two sizes of systems are small. The required reduction in electricity consumption is achieved by slightly increasing the buffer size (increasing LCOH from buffer capex by 0.19 cents and O&M by 0.06 cents). The increase in buffer size reduces the heat pump and auxiliary heater consumption, reducing the LCOH by 0.06 and 0.1 cents, respectively. The key take-away here is that slightly oversizing the system only very minimally impacts the overall LCOH, since the increased CAPEX is partly paid back in reduced consumption. Thus, allowing for a slightly higher LCOH can strongly increase SCOP.

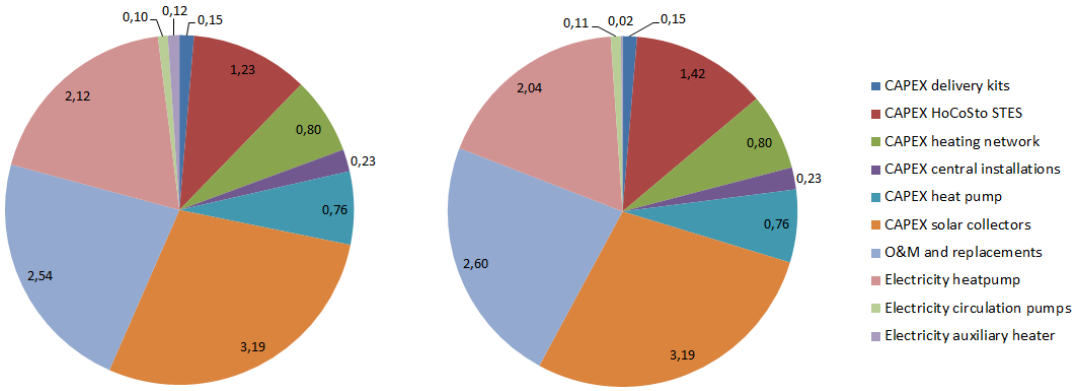

Figure 8.13: Cost breakdown for configuration 0-A in $[\frac{€cents}{kWh}]$. Sizing for lowest LCOH on the left, scaling for SCOP of 5 on the right

In figure 8.14, the buffer temperatures are shown for both sizes of configuration 0-A for a simulation period of four years. In the model, the buffer is divided into 10 nodes, but only the top and bottom node are depicted in the figure for clarity's sake.

A clear difference is observed between figures 8.14 a and 8.14 b, which is that the peak temperature is lower for the system sized for a SCOP of 5. The reason being that the buffer, and thus the heat capacity, is larger for this configuration. Another result of this larger heat capacity, is that the buffer cools down slower. This results in less need for the auxiliary heater in winter, since during those periods the bottom node stays above frost temperature.

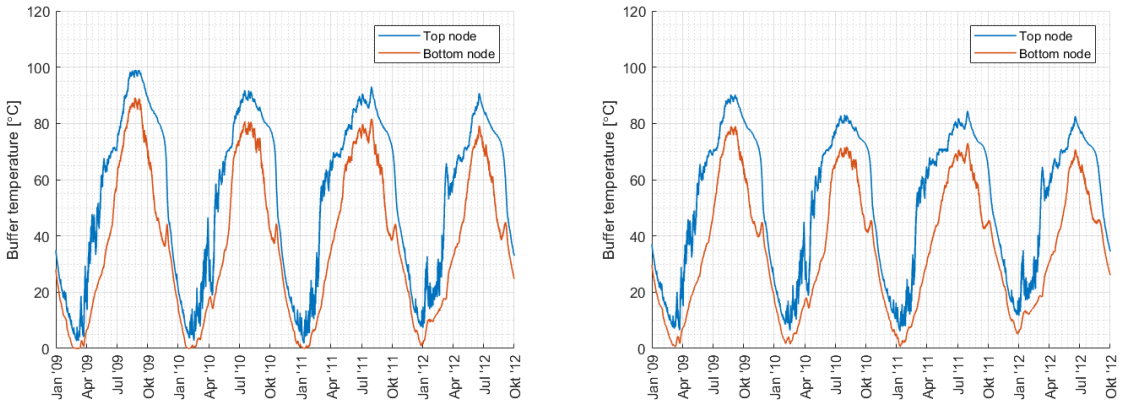

(a) Sized for lowest LCOH

(b) Sized for SCOP of 5

Figure 8.14: Buffer temperatures for configuration 0-A

Cost breakdown of configuration 2-A

Configuration 2-A achieves the lowest LCOH for both the absolute cost optimum, as well as for the scenario where a SCOP of at least 5 has to be met. Therefore, for this scenario a cost breakdown is given, and compared to that of the base scenario, 0-A.

Figure 8.15 shows a cost breakdown for configuration 2-A. Again, sized to reach a minimum LCOH on the left, and sized to reach a SCOP of 5 on the right. Between the two sizes of systems, the same is observed as for configuration 0-A. slightly oversizing the buffer reduces the electricity consumption from the auxiliary heater, but increases buffer capex and O&M. The reason for the lower auxiliary heater electricity consumption is seen in figure 8.16, which is that the buffer temperatures are not as low when the buffer is scaled slightly larger.

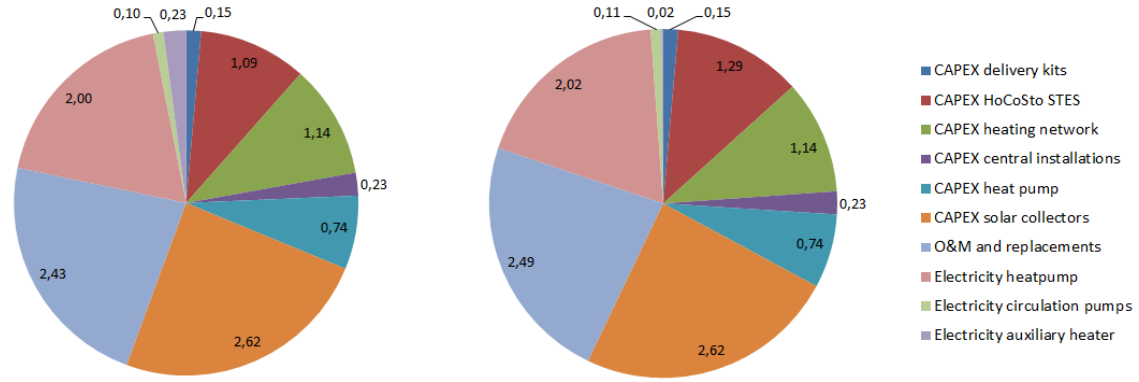

Figure 8.15: Cost breakdown for configuration 2-A in $[\frac{€cents}{kWh}]$. sizing for lowest LCOH on the left, scaling for SCOP of 5 on the right

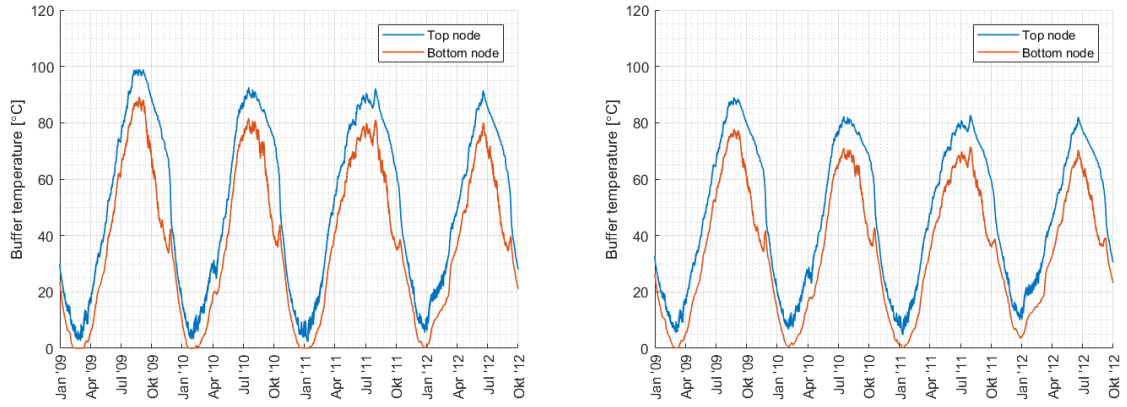

(a) Sized for lowest LCOH

(b) Sized for SCOP of 5

Figure 8.16: Buffer temperatures for configurations 0-A and 2-A, sized to have a SCOP of at least 5

Comparing configuration 2-A to base scenario 0-A

For configuration 2-A, several aspects drive the cost reduction compared to configuration 0-A. The reduced average network temperature due to the variable supply temperature reduces heat losses in the network, while also reducing the need for heat pump operation. Meanwhile, the separate solar loop allows for lower operational temperatures of the solar collectors, significantly increasing their efficiency. These efficiency gains allow for a smaller buffer and fewer solar collectors. When comparing the costs of 2-A (figure 8.15), to those of configuration 0-A (figure 8.13), this shows its value.

The reduction in LCOH for the lowest LCOH scenario mainly comes from reduced solar CAPEX (0.57 cents/kWh) and reduced buffer CAPEX (0.14 cents/kWh). As a result of lower buffer and solar CAPEX, O&M costs also drop by 0.11 cents/kWh. Even though the CAPEX drops significantly, the electricity consumption remains almost stagnant.

Comparison to air to water heat pumps

Finally, the HoCoSto system is also compared to a scenario where every house is outfitted with an individual high temperature air to water heat pump. For this scenario, the model shows the average LCOH to be 0.1273 $\frac{€}{kWh}$, consisting of 0.87 cents in O&M, 6.87 cents in electricity costs, and 4.99 cents resulting from CAPEX. The SCOP over the 5 simulated years is 2.75, which roughly aligns with claims by manufacturers.

When comparing this scenario with the solar+storage DHS, the advantages of the solar+storage system become apparent. The comparison is made with configuration 2-A, since this is both the cheapest, as well as the most efficient system. Where 2-A achieves an SCOP of 4.4 for a cost of 0.1073 $\frac{€}{kWh}$, the individual heat pump scenario is 18.6 % more expensive, and consumes 63.6 % more electricity.

Note that in this scenario an air to water heat pump would be installed at every consumer. Because these heat pumps have low COP's for low ambient temperatures (below 2), the peak load on the electricity grid would be high. This would most definitely result in the need for the grid operator to increase the local capacity of the electricity grid. These cost are not included.

An alternative option would be to rigorously renovate the houses to make them suited for low temperature heating, and implement a low temperature heating solution. However, this would not only require large investments, but it would also require the occupants to move for the duration of the renovation. Therefore, it is not seen as a comparable alternative to the HoCoSto system.

Comparison to natural gas

In order to be able to compare the overall costs of the HoCoSto system to heating with natural gas, a quick estimate is made for the LCOH of heating with natural gas.

This estimate is based on a price per m^3 of 0.67 $\frac{€}{m^3}$ for natural gas, a boiler efficiency of 90 %, 35.17 $\frac{MJ}{m^3}$ gas, annual maintenance costs of €100, initial capex of €1500, and a 20 year boiler life. It is assumed that the annual energy consumption per consumer is 18000 kWh. Again, the WACC is set at 1.8 %.

The resulting LCOH of 0.082 $\frac{€}{kWh}$ is quite a lot lower than the lowest achieved LCOH of 0.1073 $\frac{€}{m^3}$ by the HoCoSto system. However, the external costs in the form of damage to the environment are not incorporated into the natural gas heating LCOH.

9

Conclusion & Recommendations

The study shows that alterations to the network side can lead to lower overall costs of a district heating network with decentralised solar collectors and seasonal thermal energy storage.

Out of all simulated possible improvements to the base scenario, it turned out that two measures are effective; Firstly, the switch from a fixed to a variable supply temperature; Secondly, decoupling the solar collectors from the heating network by implementing a 4-line network.

The improved network configuration achieves a cost reduction of 4.5 % compared to the base scenario. In the cost breakdown, it is seen that the cutback in costs is found mainly in reduced solar collector and buffer CAPEX. This is made possible largely by a significant increase in solar collector efficiency (resulting from lower operating temperatures). An important observation is that the largest efficiency increase is seen during winter (when energy in the system carries the highest value). When the solar collectors have to feed in to the 2-line network, they are forced to operate at elevated temperatures, reducing their efficiency greatly. By connecting the solar collectors through a separate network, this issue is mitigated.

Another important observation is that additional network losses of the 4-line network compared to the 2-line network have little effect on the system. The reason being that the temperature (and thus thermal loss) of the solar loop is low when the value of heat is high (during winter). The majority of heat loss occurs when there is an abundance of solar energy.

Regardless of the choice between a 2-line or 4-line network, the switch from a fixed to a variable supply temperature is tempting since performance gains can be made with no material investment. The reduction of average network temperatures slightly reduces heat pump utilization and pipeline losses. This adjustment mainly becomes interesting for the 2-line network though, when solar collector efficiency gains can also be made.

When comparing the configurations which are scaled to achieve the absolute lowest cost with the configurations which are scaled to achieve a SCOP of at least 5, it becomes very clear that slightly oversizing solar collector area and buffer volume greatly reduces the electricity consumption of a system, without significantly adding to the costs. This is because a large part of the additional solar and storage CAPEX is earned back in lower operational costs. For the variable-temperature 4-line network, a 30 % lower electricity consumption can be achieved when a 1 % higher energy cost is accepted compared to the cheapest sizing.

It should also be noted that some network alterations proved to be ineffective in reducing the LCOH. These alterations sought to further reduce the average network temperatures by circumventing the minimum temperature constraints of DHW production. The cost benefits from a reduction in pipeline thermal losses, lower heat pump utilisation and an increase in solar collector efficiency could not recuperate the increase in costs resulting from the required measures. This increase in

costs consists of higher CAPEX, an increase in thermal losses, and a shift in electricity consumption from the centralised location to decentralised locations (where the electricity price is higher).

Finally, the comparison is made between the HoCoSto decentralised solar + seasonal energy storage concept (with the improved distribution network), and a scenario where every house is outfitted with an individual high temperature air to water heat pump. In the simulations, the HoCoSto concept is able to achieve a 15.7 % lower LCOH, while reaching a SCOP of 4.4 compared to just 2.75 for the individual heat pump scenario. This underlines how promising the HoCoSto concept is, especially when realising that many more engineering and economy of scale gains are to be made.

Recommendations

For the development of future community solar plus storage district heating systems, the implementation of the two measures is recommended. Firstly, the supply temperature should be made variable and dependent on the ambient temperature. Secondly, the solar collectors should be connected to the STES by a dedicated network instead of feeding in to the heating network. This only holds, however, if there is no existing heating network in place. Additionally, it is recommended that the buffer volume and solar collector area are slightly oversized in order to reach higher SCOP's, which reduces the electricity consumption. Large gains can be made with slight oversizing, which barely impacts LCOH. The realisation that the solar collectors should be connected through a separate network also leads to the thought that it is probably more cost effective to centralise the solar collectors, since this would mitigate the need for a solar network entirely and would simplify installation. Obviously, this is is only possible when room for a clustered solar collector field is available (this might also be a large rooftop).

Bibliography

[1] Essent, accessed on 27-08-2019. URL: https://www.essent.nl/kennisbank/energie-besparen/inzicht-in-verbruik/gemiddelde-gasverbruik.

[2] LG Therma V High Temperature, accessed on 03-12-2019. URL: https://www.lg.com/nl/hoog-temperatuur.

[3] Thermocomfort web shop, accessed on 12-12-2019. URL: https://www.thermocomfort.be/nl/product/set-hn1610h-hu161h.

[4] ARESTHO. Microflex pipelines, accessed on 10-06-2019. URL: https://www.arestho.nl/microflex-duo-geisoleerde-pe-buis-25-x-23mm.html.

[5] AVERFALK, H., AND WERNER, S. Novel low temperature heat distribution technology. *Energy 145* (2018), 526–539.

[6] DHCHOLLAND. Overzicht afleversets voor warmtelevering, accessed on 12-08-2019. URL: https://www.rvo.nl/sites/default/files/2014/11/ENG2014-010%20Overzicht%20afleversets%20voor%20warmtelevering%20(1).pdf. Tech. rep., Rijksdienst Ondernemend Nederland, 2014.

[7] DUFFIE, J., AND BECKMAN, W. *Solar Engineering of Thermal Processes*. 2013.

[8] ELMEGAARD, B., OMMEN, T., MARKUSSEN, M., AND IVERSEN, J. Integration of space heating and hot water supply in low temperature district heating. *Energy and Buildings 124* (7 2016), 255–264.

[9] ELSHENITI, M., KOTB, A., AND ELSAMNI, O. Thermal performance of a heat-pipe evacuated-tube solar collector at high inlet temperatures. *Applied Thermal Engineering 154* (5 2019), 315–325.

[10] EUROPEAN COMMISSION. PVGIS - JRC Photovoltaic Geographical Information System, accessed on 10-08-2019. URL: https://re.jrc.ec.europa.eu/pvg_tools/en/tools.html.

[11] FABRIEK, P. *Sensitivity analysis of residential building simulations model choice for specific applications and critical parameters. Delft University of Technology*. 2013.

[12] FANINGER, G. Combined solar–biomass district heating in Austria. *Solar Energy 69*, 6 (1 2000), 425–435.

[13] FLYNN, C., AND SIRÉN, K. Influence of location and design on the performance of a solar district heating system equipped with borehole seasonal storage. *Renewable Energy 81* (9 2015), 377–388.

[14] FUENTES, E., ARCE, L., AND SALOM, J. A review of domestic hot water consumption profiles for application in systems and buildings energy performance analysis. *Renewable and Sustainable Energy Reviews 81* (1 2018), 1530–1547.

[15] GUERRA SANTÍN, O. *Actual energy consumption in dwellings: The Effect of Energy Performance Regulations and Occupant Behaviour, Delft University of Technology*. 2010.

[16] HAMDHAN, I., AND CLARKE, B. Determination of Thermal Conductivity of Coarse and Fine Sand Soils. Tech. rep., 2010.

[17] KIWA. Waterwerkbladen, accessed on 18-07-2019. URL: https://www.infodwi.nl/waterwerkbladen, 2015.

[18] KONINKLIJK NEDERLANDS METEREOLOGISCH INSTITUUT. KNMI - Historic Dutch weather data. URL: https://www.knmi.nl/nederland-nu/klimatologie.

[19] KOVACS, P. Quality Assurance in solar thermal heating and cooling technology: A guide to the standard EN 12975. Tech. rep., Technical Research Institute of Sweden, 2012.

[20] LI, Y., REZGUI, Y., AND ZHU, H. District heating and cooling optimization and enhancement – Towards integration of renewables, storage and smart grid. Tech. rep., 2017.

[21] PERERS, B., KOVACS, P., OLSSON, M., PERSSON, M., AND PETTERSSON, U. A tool for standardized collector performance calculations including PVT. In *Energy Procedia* (2012), Elsevier Ltd.

[22] PURDY, J., AND BEAUSOLEIL-MORRISON, I. The Significant Factors in modeling Residential Buildings, CANMET Energy Technology Centre. Tech. rep., 2001.

[23] RÄMÄ, M., DEL HOYO ARCE, I., HERRERO LÓPEZ, S., KLOBUT, K., LÓPEZ PEREZ, S., AND FEBRES, J. Models for fast modelling of district heating and cooling networks. *Renewable and Sustainable Energy Reviews* (2017).

[24] SIBBITT, B., MCCLENAHAN, D., DJEBBAR, R., THORNTON, J., WONG, B., CARRIERE, J., AND KOKKO, J. The Performance of a High Solar Fraction Seasonal Storage District Heating System – Five Years of Operation. *Energy Procedia 30* (1 2012), 856–865.

[25] SORKNÆS, P. Simulation method for a pit seasonal thermal energy storage system with a heat pump in a district heating system. *Energy 152* (6 2018), 533–538.

[26] STEPHAN, P., AND SCHEBEK, L. Evaluation of district heating systems based on exergy analysis. University of Technology Darmstadt. Tech. rep., 2018.

[27] TEMPS, R. C., AND COULSON, K. Solar radiation incident upon slopes of different orientations. *Solar Energy 19*, 2 (1 1977), 179–184.

[28] TNO. Dinoloket, accessed on 27-06-2019. URL: https://www.dinoloket.nl/.

[29] URBANECK, T., OPPELT, T., PLATZER, B., FREY, H., UHLIG, U., GÖSCHEL, T., ZIMMERMANN, D., AND RABE, D. Solar District Heating in East Germany – Transformation in a Cogeneration Dominated City. *Energy Procedia 70* (5 2015), 587–594.

[30] VAN DER HOEVEN, P., AND LABLANS, W. Grondtemperaturen. *Koninklijk Nederlands Meteorologisch Instituut*, WR92-05 (1992).

[31] VAN MILTENBURG, R. Integration of decentralized solar collectors in Dutch district heating grids. University of Technology Delft.

[32] VAN VLIET, E., DE KEIJZER, J., SLINGERLAND, E., VAN TILBURG, J., HOFSTEENGE, W., AND HAAKSMA, V. Collectieve warmte naar lage temperatuur - Een verkenning van mogelijkheden en routes.

[33] WALLENTEN, P. Steady-state heat loss from insulated pipes. University of Technology Lund.

[34] WEMHÖNER, C., HAFNER, B., AND SCHWARZER, K. Simulation of Solar Thermal Systems with CARNOT Toolset in the Environment MATLAB ® SIMULINK ®. Tech. rep.

[35] YANG, X., LI, H., AND SVENDSEN, S. Evaluations of different domestic hot water preparing methods with ultra-low-temperature district heating. *Energy 109* (8 2016), 248–259.

[36] YANG, X., AND SVENDSEN, S. Achieving low return temperature for domestic hot water preparation by ultra-low-temperature district heating. *Energy Procedia 116* (6 2017), 426–437.